CONTROL OF LARGE SPACE STRUCTURES

by

R. Gran, M. Rossi, H.G. Moyer, and
F. Austin

April 1979

RE-589

Final Report Prepared Under Contract NAS8-32587

by

Research Department
GRUMMAN AEROSPACE CORPORATION
Bethpage, New York 11714

for

George C. Marshall Space Flight Center
NATIONAL AERONAUTICS AND SPACE ADMINISTRATION
Marshall Space Flight Center, Alabama 35812

Grumman Research Department RE-589

CONTROL OF LARGE SPACE STRUCTURES

Final Report Prepared Under Contract NAS8-32587

for

George C. Marshall Space Flight Center
National Aeronautics and Space Administration
Marshall Space Flight Center, Alabama 35812

by

R. Gran, M. Rossi, H.G. Moyer
Research Department

and

F. Austin
Structural Mechanics Section, Engineering Department

of

Grumman Aerospace Corporation
Bethpage, New York 11714

April 1979

Approved by: Richard A. Scheuing
Richard A. Scheuing
Director of Research

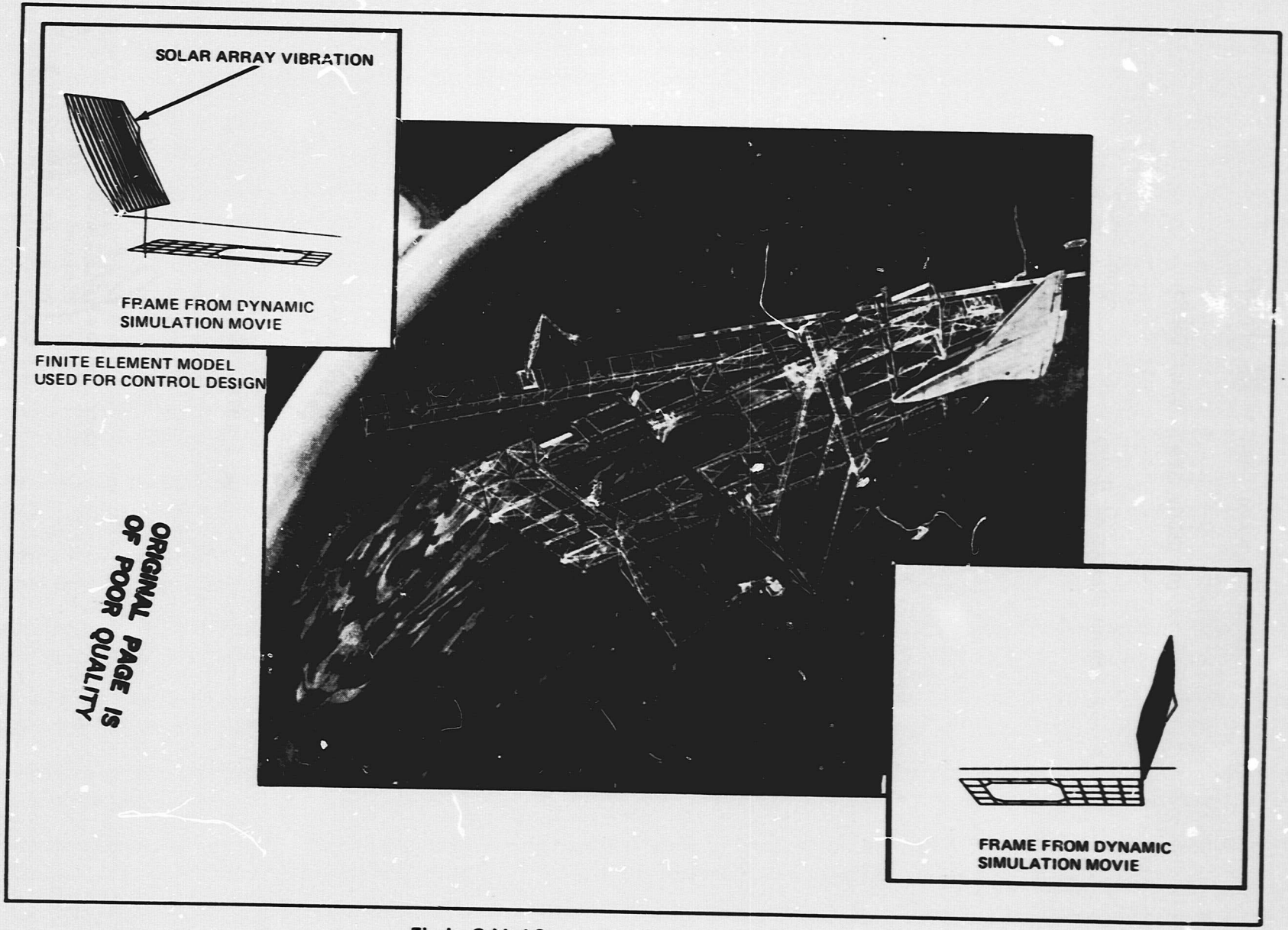

Fig. 1 Orbital Construction Demonstration Article

SUMMARY

The control of large space structures encompasses a multitude of physical phenomena. The structure itself is a complex vibrating system that is excited by internal and external forces. The external forces and torques come from aerodynamic, solar wind, and thermal excitations to geomagnetic and gravity gradient forces. Internal forces and torques are created by vibrating machinery (CMG's, gyros, etc.), by articulating structural elements and motions of astronauts. It is not surprising, then, that as the size and performance demands on structures increase the control problem looms ever larger as one of the overriding problems.

This final report describes the work that was performed by the Grumman Aerospace Corporation Research Department under contract to the Marshall Space Flight Center (Contract NAS 8-32587) which was administered by Dr. Michael Borelli. The thrust of this effort was to determine what, if any, limitations are imposed on the size of spacecraft which may be controlled using current control system design technology. The particular problems investigated were:

1. The fundamental limitations imposed by structural/control interactions, by external torques, and by the mission performance requirements for Low Earth Orbit (LEO) missions.
2. The development of control approaches for the various control tasks that are required by large space structures, i.e., as required during fabrication, assembly, pointing, shape and attitude control, etc.
3. The development of techniques for on orbit dynamic testing that will permit evaluation, during operation, of the parameters required for control design.
4. Investigate actuator requirements so that the control may be achieved with minimal use of expendable fuels.

These tasks were investigated by using a typical structure in the 35 to 70 meter size category. A control system design that used actuators that are currently available (CMG's) was designed for this structure. The amount of control power required to maintain the vehicle in a stabilized gravity gradient

pointing orientation that also damped various structural motions was determined. The moment of inertia and mass properties of this structure were varied to verify that stability and performance were maintained. This was accomplished by systematically varying the linear dimensions of the structure by a scale factor while maintaining the control gains fixed. The conclusion from this study was that the structure's size was required to change by at least a factor of two before any stability problem arose. The stability margin that was lost was due to the scaling of the gravity gradient torques (the rigid body control) and as such could easily be corrected by changing the control gains associated with the rigid body control. A secondary conclusion from this study was that the control design that accommodates the structural motions (to damp them) is a little more sensitive than the design that works on attitude control of the rigid body only. The main details of this effort are described in Section I.

The control of large structures can be considered, as the classical control system designer does, as the problem of controlling the attitude of the vehicle despite all of the disturbances that are potentially misorientating the vehicles or causing stability problems. This approach artifically divides the physical phenomena into control forces and disturbance forces. When this is done, the possibility of balancing one disturbance by a second is lost. Thus, gravity-gradient forces, which are oscillatory, might be damped by using residual aerodynamic forces to extract energy from the gravity gradient mode. To be able to achieve this goal, early in the program it was perceived that a fairly comprehensive model of the spacecraft was needed. This model (described in Section II) was used to develop a control system that uses a linear optimal control approach to:

- Achieve a stable rigid body orientation using gravity gradient forces balanced by residual aerodynamic forces
- Stabilize the interaction of rigid and flexible motion
- Increase the damping of the more important flexible modes using the same actuators that are used for rigid body control (a set of three orthogonal CMG's only)
- Be slewed, when required, from one orientation to another without adversely affecting the vibration and shape of the structure

As the control study developed, several problems emerged that were either poorly understood or that were critically lacking in theoretical basis. These were:

- A method is required for order reduction of the structural dynamics that accounts for the undamped vibration modes that are left out and also considers the effect of control bandwidth that exceeds the frequencies of the modes neglected
- A method is required that reduces the control excitation of the high frequency modes.
- A method is required that permits measurements that are not adversely corrupted by unwanted structural oscillations
- It became clear that an estimator is undesirable in the control loop because the bandwidth of the filter might easily dominate the problem. The resulting loss of gain and phase margin compared with an optimal control design is clearly undesirable. We instead have proposed that control designs be undertaken which utilize as many rate and position measurements as there are modes retained
- A method for on-orbit dynamic testing is required

In Section III, these problems are discussed and some solutions are proposed. We have shown:

- A new method for order reduction which both incorporates the closed loop dynamic characteristics and the unique problem associated with finite element modeling which ignores structural damping
- A method for control spillover reduction at higher frequencies using a low order observer
- A method for on-orbit dynamic testing which gives structural mode data and also reduces the measurement spillover problem
- A new method for synoptic control design that naturally suggests alternate actuators

ACKNOWLEDGEMENTS

An effort of the magnitude and scope of that described in this final report does not have its genesis in any one individual. Many people contributed in large and in small ways. To thank all of them would be difficult, if not impossible. However, special kudos should be given to Pat Barry and Ralph Waters of the Research Department who contributed to all phases of this effort, and to Alex Zislin and Mike Proise of the Grumman Guidance and Control Engineering Department for their efforts and patience in listening to the authors' discourses on control methods.

The pictures shown in Figs. 9, 19, and 20 are from a 16mm movie that was developed to demonstrate the effectiveness of modal control. This movie was produced directly from an Information International Inc. FR-80 computer on microfilm (COM) system. This system provides an analyst with the capability to directly produce a movie of a dynamic simulation without difficulty. We would like to thank Leroy Bell of III for the production of the movie film.

TABLE OF CONTENTS

LIST OF ILLUSTRATIONS

I. INTRODUCTION

As the size of space structures increase and the performance requirements become more severe the control problem looms larger and larger as the single most difficult problem that must be overcome. The structural size alone creates a possibility for interactions between the control system and the structural dynamics. The control performance requirements on both pointing and internal vibration (jitter) create a need for new and novel techniques for rigid body control that simultaneously achieves the desired pointing accuracy without creating structural vibration that might jitter crucial spacecraft systems (optics, antennas, etc.). The rigid body control must also be achieved in such a way that internal strain on the spacecraft structure does not change at certain desired points (points where critical optical or antenna elements are mounted must always remain at the same relative positions so that the phasing of the light or radio frequency energy does not become distorted). The achievement of this goal requires control systems with zero steady state error after a slew command. The structures that are being proposed change their size as a function of time when the structure is being fabricated in orbit. The ability to alter the control system as the dynamics change, the ability to recognize the way in which the structural and rigid body dynamics change, and the ability to sense the disturbances and the way they change are all desirable characteristics that the control system should possess.

To achieve the flexibility that all of the above requirements impose on the control system requires a fairly complex system, one which also has inherent reliability and insensitivity to variations in the structural dynamics. Also one must attempt to exploit the existing physical phenomena that cause "disturbances" on the spacecraft to control the spacecraft. Thus gravitational, geomagnetic, residual aerodynamic and solar wind forces that are normally considered as disturbances that are countered by expending reaction jet fuel, should be designed into the control system to provide the possibility of "playing one force off against another".

To achieve all of these goals a synoptic approach has been developed that attempts to design the control system for the spacecraft so that, at the outset, all of the dominant effect are modeled - the spacecraft dynamics are modeled, using

a finite element approach, with both the rigid body and flexible motion coupled in a coordinate system that does not necessarily explicitly include the rigid body - the physical forces that interact with the structure are included explicitly as distributed forces and torques acting on each of the masses (or inertias) in the finite element model -- the internal vibration sources are modeled and included to provide a measure of the jitter induced by these motions when they are deemed critical -- the slew commands are included in the dynamic description so that the best possible method for commanding the system to change its orientation can be determined -- the flexibility inherent with digital control requires that all of the modeling be done in such a way that any problems introduced by sampling can be minimized.

The study that is described in this report has developed the technology to address some of these questions and has pointed to problems where technology must be further developed. Figure 1 shows the structure that was used to develop the control technology and evaluate the effect of structural dynamics, gravity gradient dynamics and control interactions during this effor.

II. DESIGN EXAMPLE

1. INTRODUCTION

To understand the control problems for large space structures, a specific system (the Orbiting Construction Demonstration Article (OCDA)) was selected to develop a control system. The OCDA is intended to be a space base in a circular orbit 500 km above the Earth (Ref. 1). Its purpose is to facilitate the unloading, fabrication, and assembly of objects (e.g., solar power satellites, microwave power transmission satellites) ferried into orbit by the shuttle. The OCDA has four principle parts (Fig. 2): 1) the platform or rectangular truss frame, 2) the boom with traveler, 3) the array that tracks the sun and absorbs the radiation energy using elastic membranes, and 4) the mast extending on both sides of the platform holding the boom and solar array on one side and providing a docking port for the shuttle on the other

In its nominal attitude the OCDA is unstable with respect to aerodynamic drag and gravity gradient torques. These instabilities can be overcome by active control that uses momentum storage devices. Environmental effects such as the introduction of currents into the solar array to produce magnetic control torques can be effectively used to assist the control system in stabilizing these disturbances. We have studied stabilization by means of three reaction wheels with mutually orthogonal axes.

In order to calculate the control gains D in the control gain relation $u = Dx$, the systems equations $\dot{\underline{x}} = f(\underline{x},\underline{u})$ are replaced with the linear approximations

$$\dot{\underline{x}} = A\,\underline{x} + B\,\underline{u}$$

This set of equations is agumented with the cost functional

$$J = \int_0^\infty (\underline{x}^T Q \underline{x} + \underline{u}^T R \underline{u}) dt$$

where the weighting matrices Q, R are selected to reflect the critical nature of a particular node motion. The principles of optimal control then yield differential equations that can be integrated analytically.

Computational expense was reduced considerably by treating the problem in modal coordinates for both the vibration and rigid body modes. These

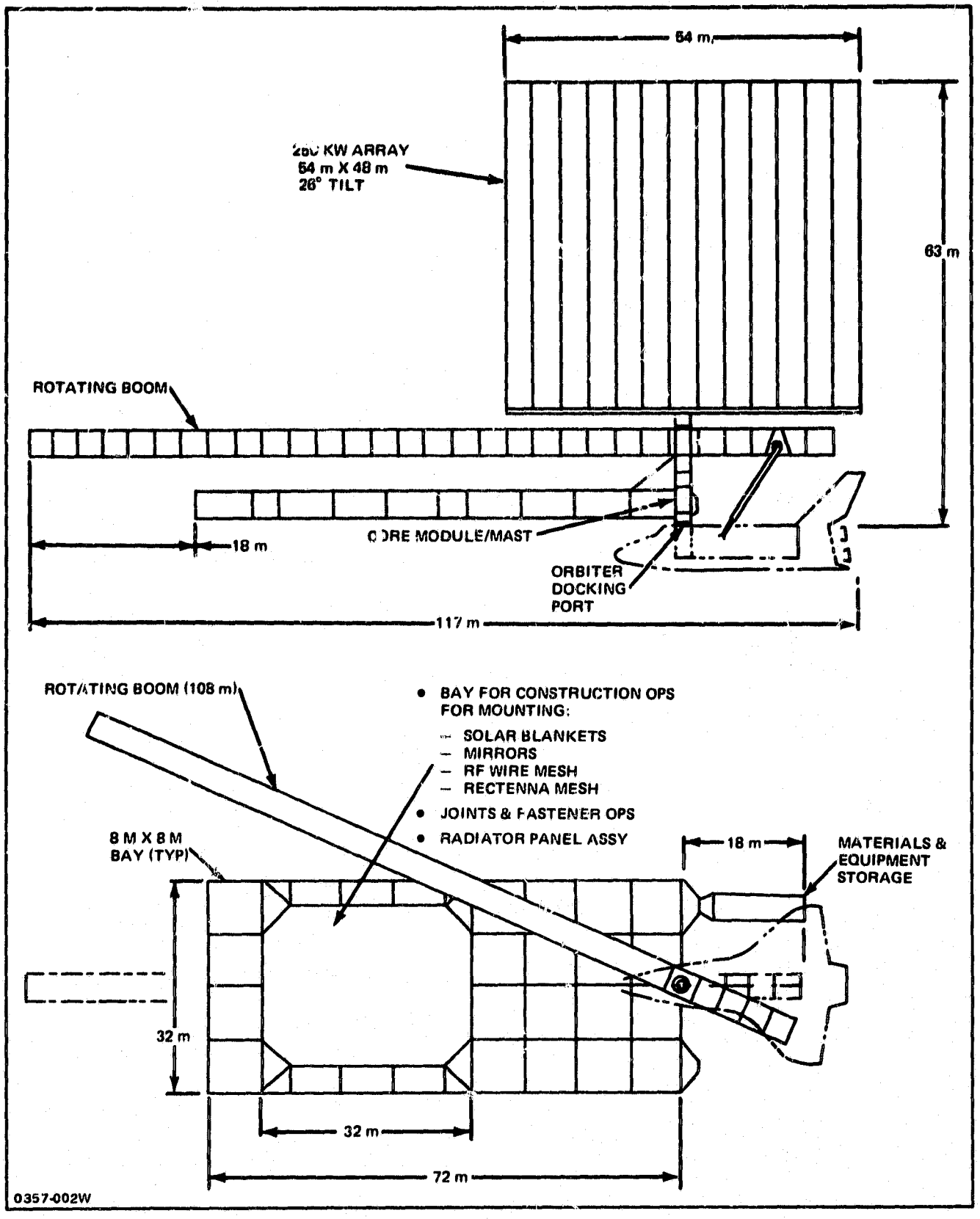

Fig. 2 Two Views of the OCDA with Shuttle. Dimensions are indicated.

were handled in a uniform rather than a hybrid manner. It was found that satisfactory results could be obtained when only a few of the modes were controlled.

In an additional study the control gains D were kept fixed while the spatial dimensions of the OCDA were scaled up until the point of instability was found.

2. CONTROL LIMITATIONS OF CURRENT TECHNOLOGY

As the size of a space structure increases, the structural frequencies become lower. Thus, for any given control system bandwidth (as determined by the dynamic requirements of the rigid body control specification) there exists a structure whose vibration frequencies fall within the control system band. If one assumes that the predominent modal frequency of such a structure is given by the first mode of a simply supported beam whose dynamics are given by the Euler-Bernoulli equation, then this mode has a frequency given by

$$\frac{\pi}{2L^2}\sqrt{\frac{EI}{m}}$$

(in hertz) where E is the modulus of elasticity, L is the length, I is the inertia and m is the mass of the beam per unit length. For a slender beam the modal frequency is given by

$$\frac{\pi}{2L^{3/2}}\sqrt{\frac{EI}{M}}$$

where M is the total mass of the beam. The result of this analysis is summarized by Fig. 3, where the first modal frequency of a slender beam is plotted as a function of beam length. By assuming that this frequency is the control system bandwidth, we can see exactly how big a structure must be for any particular control system specification before the rigid body control system might interact with the structure.

A second area where structural motion potentially impacts the control system is when open loop rotational commands are required as, for example, during a high speed slew maneuver. The usual approach to minimizing the bending interactions during these slew maneuvers is to tailor the shape and amplitude of the command pulse so that the structural modes are not excited. The optimal control

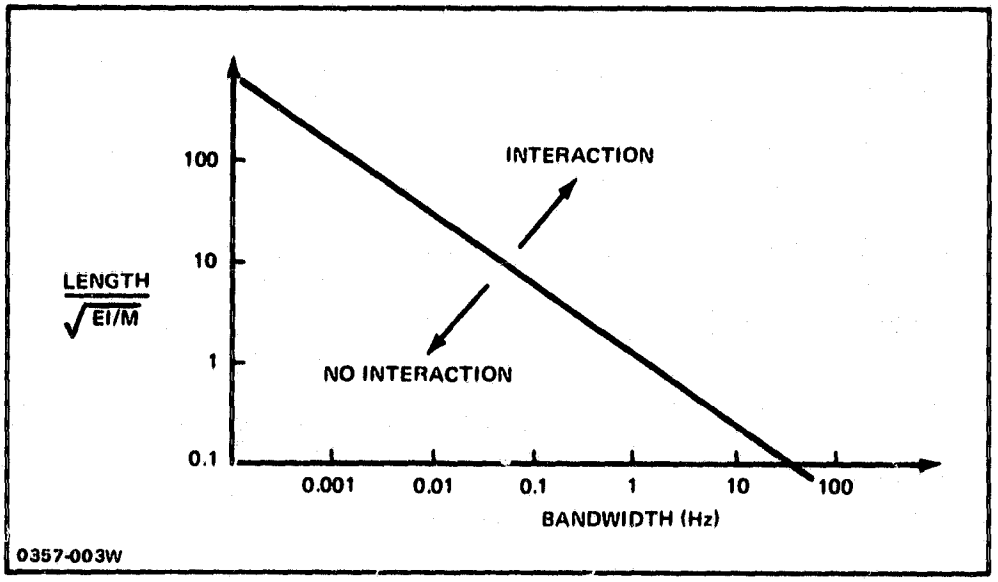

Fig. 3 Structural Size vs. Control Bandwidth. Since size of the structure determines the lowest modal frequency, the interaction of the structure and rigid body control loop is a function of the control specification (bandwidth).

approach offers a natural framework within which such minimum structural excitation by command shaping may be achieved. This is shown schematically in Fig. 4 where the command generator is shown as a linear differential equation (in this case the output of a filter with a maximally flat response) whose outputs are multiplied by "feed forward" gains. Section III-4 describes this approach in more detail. In either case, the exact size of a structure when slew maneuver/bending coupling becomes severe enough to impact performance depends on the control system pointing accuracy or figure control requirements.

The final area where structural size can impact the control system performance is in the coupling of disturbance induced structural motion into the control system. Disturbances on the spacecraft are either external--aerodynamic, gravity gradient, solar, thermal for example -- or internal as is the case with vibrations induced by rotating machinery, man motions, bearing noises due to relative motions of spacecraft elements, etc. As an example of how these disturbances may interact through the rigid body control consider the simple case where gravity gradient torques are used in low earth orbit to orient a long slender spacecraft which has a solar array mounted at one extremity (Fig. 5). In order to maintain the solar array at the correct orientation, the array must be rotated at twice the orbital rate ω_o. This will produce a periodic aerodynamic torque, due to the residual atmosphere, at the orbital period. The gravity gradient creates a torque which is proportionate to the rigid body rotation angle deviation from a line from the spacecraft to the earth center. Thus, if θ is the rigid body rotational angle, the dynamic description of this interaction is (for a single axis)

$$I\ddot{\theta} + T_G\theta = T \sin 2\omega_o t \qquad (1)$$

where

T_G = gravity gradient torque

T = magnitude of the aerodynamic torque

I = inertia (principle) of the axis considered

ω_o = frequency of an orbit

*In practice, I will be of the form $I_o + I_\delta \sin 2\omega_o t$ because of the solar array motion, and as such the design must be based on a time varying inertia.

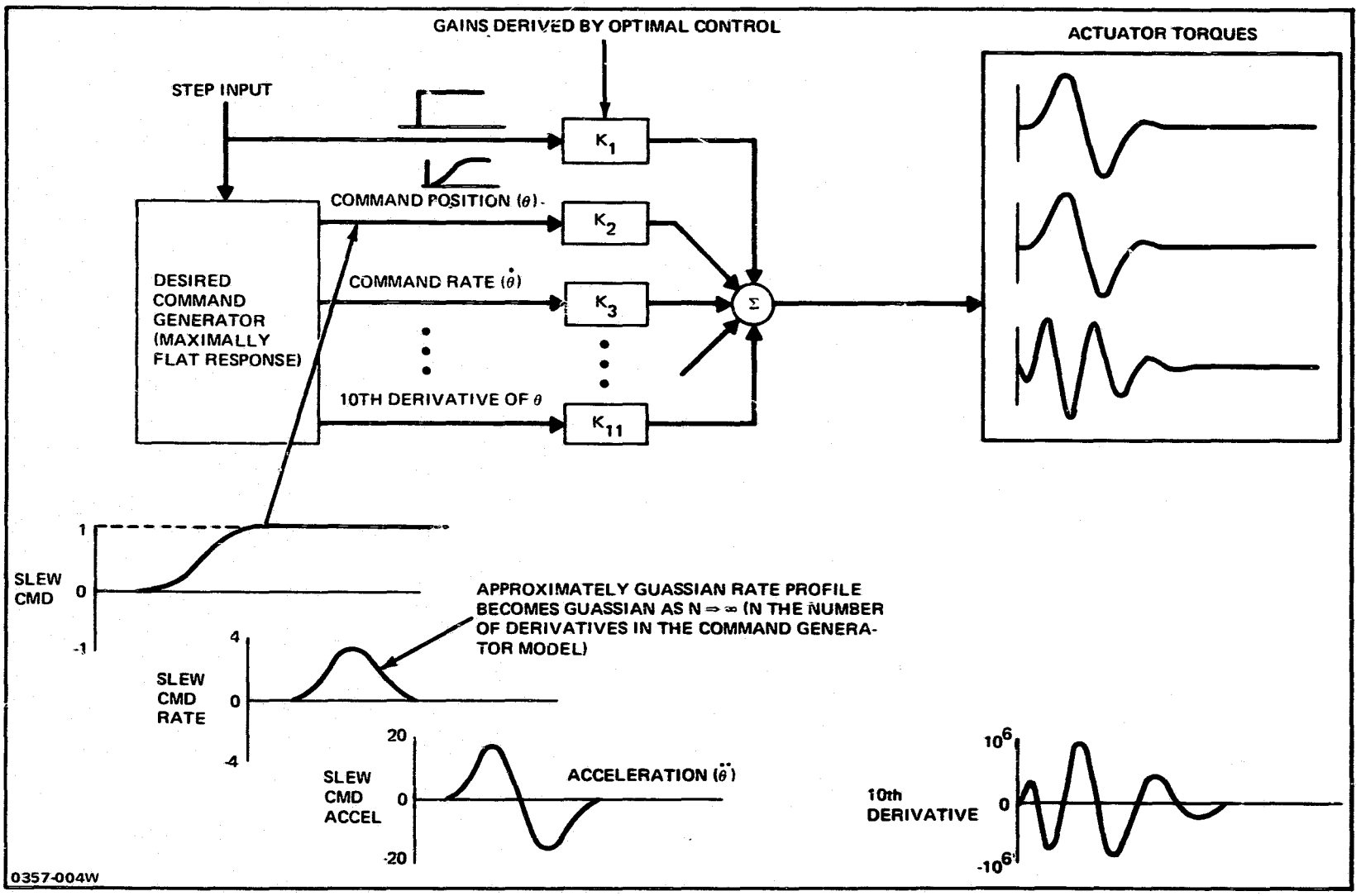

Fig. 4 Command Generator Design Using Optimal Control

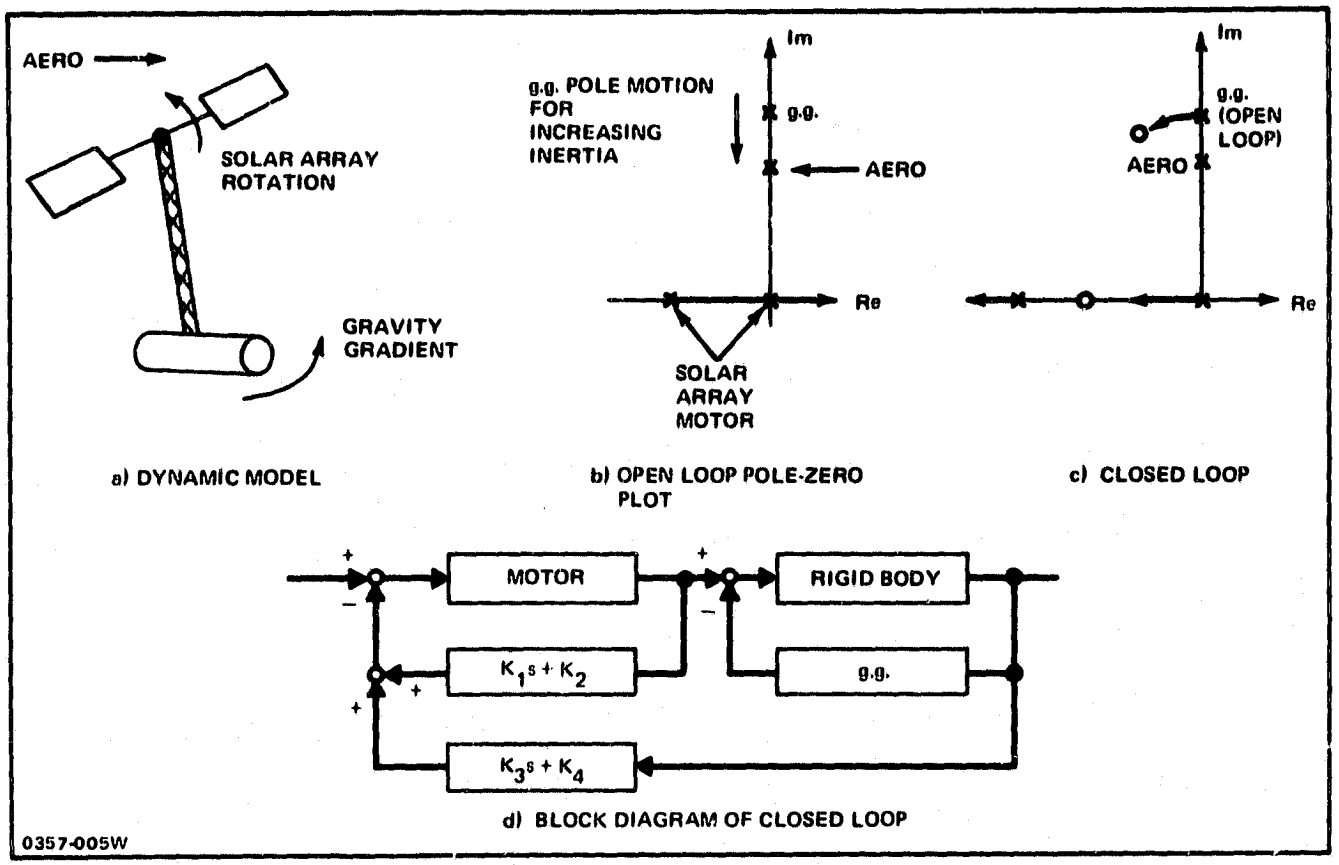

Fig. 5 Disturbance Interactions Can Cause Stability Problems as Shown by this Example

The solution to Eq. (1) is given by

$$\theta(t) = \cos\sqrt{\frac{T_G}{I}}\, t\ \dot{\theta}(o) + \sqrt{\frac{I}{T_G}}\sin\sqrt{\frac{T_G}{I}}\, t\ \theta(o) + \frac{T}{\sqrt{T_G I}}\int_o^t \sin\sqrt{\frac{T_G}{I}}\ (t-\tau)\ \sin 2\omega_o \tau\ d\tau \qquad (2)$$

Now, it is evident that if twice the orbital frequency and the gravity gradient frequencies are the same that $\theta(t)$ grows as $t \sin 2\omega_o t$. Thus an unstable interaction is possible.

For the example just described, a rather simple "fix" is possible by controlling the solar array drive motor. Thus by phasing the rotation so that the solar array alternately leads or lags the sun, the aerodynamic force may be used to extract energy from the gravity gradient and thereby damp the gravity gradient control. Figure 5 shows a root locus plot that results from this approach which shows the gravity gradient damped regardless of the orbital frequency. (This design uses full state feedback for pole placement.)

The design uses Eq. (1) with the solar array drive provided by a motor which is modeled as

$$\ddot{\theta}_m + \tau_m \dot{\theta}_m = u$$

where: θ_m is the solar array angle

$\dot{\theta}_m$ is nominally $2\omega_o$

τ_m is the motor time constant

u is the motor input (u nominally is $2\omega_o\tau_m$ and there is a perturbation Δu around that nominal which is the control)

When the solar array motor angle is substituted into the torque term on the right side of Eq. (1) we get

$$I\ddot{\theta} + T_G\theta = T \sin\theta_m$$

which, since θ_m is given by $\theta_m = \omega_o t + \Delta\theta_m$, can be written as

$$I\ddot{\theta} + T_G\theta = T\sin(\omega_o t + \Delta\theta) = T \sin\omega_o t + T\cos\omega_o t\Delta\theta)$$

Thus the dynamics of the complete open loop system (for perturbations) is given by

$$\frac{\theta(s)}{U(s)} = \frac{T/I \cos\omega_o t}{(S^2 + T_G/I)(S^2 + \tau_m S)}$$

The open loop root locus for this transfer function is shown in Fig. 5b plotted as the inertia I increases. The coupling described above occurs when the gravity gradient pole ($S = \pm j\sqrt{T_G/I}$) overlaps the aero pole ($2\omega_o$). If a control system configured is shown in Fig. 5d is used, the closed loop root locus appears as shown in Fig. 5c). The two zeros shown in Fig. 5c are the result of the feedback $K_1 S + K_2$ and $K_3 S + K_4$. Clearly, this locus is always stable independent of the gravity gradient frequency.

In general we have taken this approach for all external disturbances. When the optimal control model is formulated, any actuators that are available (the solar array drive motor for example) are included thereby allowing the "disturbances" to be used for active control.

For internal disturbances, once again the magnitudes only become crucial if the control system bandwidth or pointing requirements are severe. If these sources of vibration must be damped, the structure can be included in the optimal control model so that they may be actively isolated.

To define the limitations further, part 7 of this section describes the analysis of the OCDA large space structure controller that we designed as the structure is increased in size.

3. VIBRATION AND RIGID BODY MODES

Before a structural analysis of the OCDA can begin the orientation and tilt of the solar array must be specified. "Orientation" is defined as the angle of rotation about the mast. The "tilt" is the rotation about the beam that is closest to the platform. A zero tilt means that the mast is in the plane of the array. Unlike the orientation, the tilt does not vary continuously. It is either at plus or minus 26°, depending on the longitude of the ascending node of the orbit. The rate of orbital nodal regression is such that a flip is required every 22 days. The rate of radiation absorption is never degraded by more than 10% compared with the best tilt angle.

The particular array position used for our study is shown in Fig. 6 together with the Y, Z axes. Their origin is at the lower end of the mast (docking port). The Y axis is vertical (whether up or down is irrelevant), the X axis is out of the page and parallel to the velocity. Thus the platform and array move edgewise. Note that the shuttle - whose structure is ignored except for its moment/product of inertia - is included. Since the shuttle is over six times as heavy as the OCDA, Fig. 6 indicates that the combined center of mass is close to origin. The two points have been treated as identical in our work.

Each node (joint) of the OCDA is assigned a number and is tabulated with its coordinates and its degrees of freedom. The degrees of freedom are those translations and rotations about the three axes that are considered to be significant. Thus, up to six degrees of freedom (DOF's) can be specified for each node. The members (beams and strings) are also assigned numbers and they are tabulated with their cross sectional areas and the nodes that they join. Their lengths can then be found from the node table.

If a unit force is applied at a translation DOF or a unit torque at a rotation DOF, the displacements for the entire DOF vector can be computed. The complete set obtained by varying the unit force/torque over all the DOF's is called the flexibility matrix. Its inverse is called the stiffness matrix k.

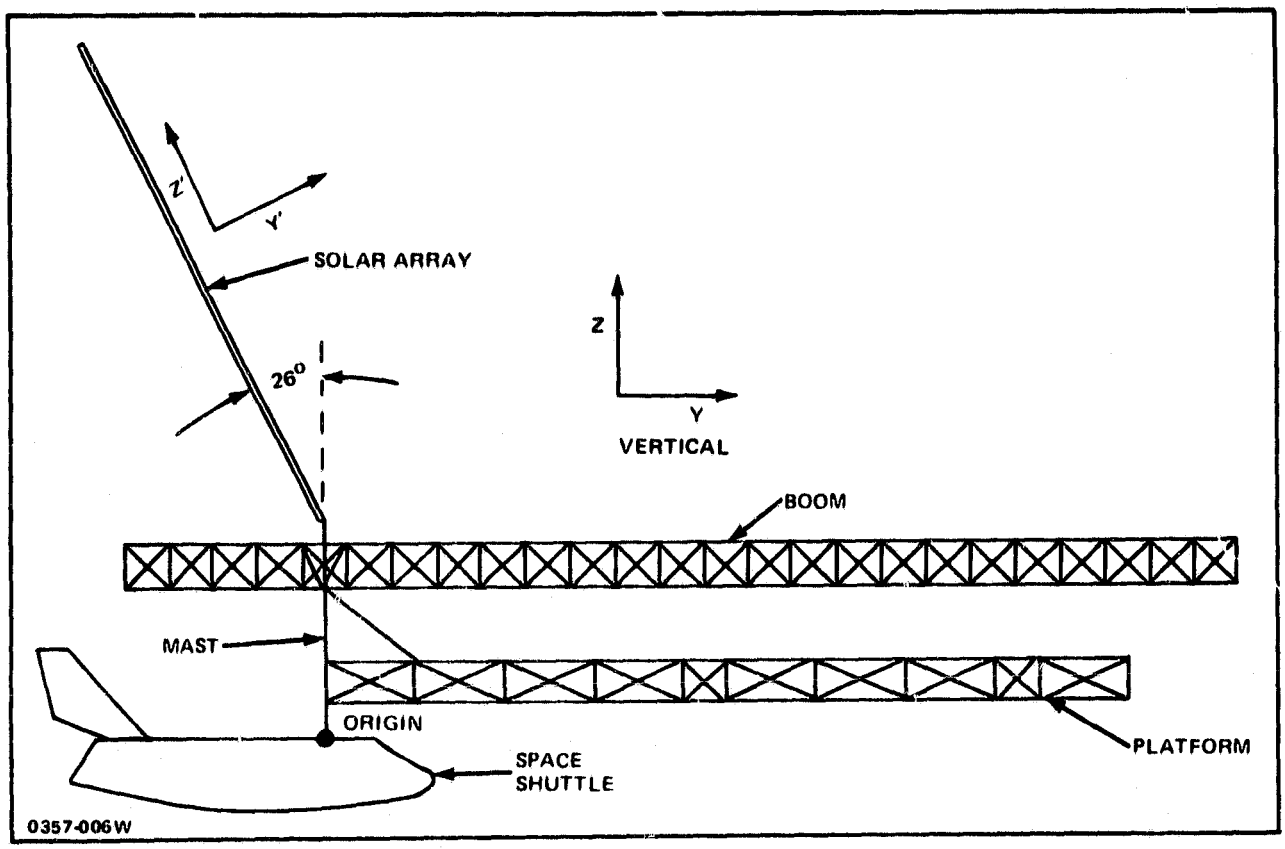

Fig. 6 Array Orientation and Tilt Chosen for the Structural Analysis (YZ and Y'Z' Axes are Shown with their Origin)

When the dimensions (and density) of a member are given, the mass and moment/products of inertia can be found from simple calculations. What is needed, however, is the inertia matrix associated with DOF's, because that is how k is defined. Recall that in general there are up to six relevant DOF's at a node that joins at least two members. If only the three translation DOF's are significant, then the 3 x 3 inertia matrix is diagonal. In the general case, whose theory is too complicated to be given here, for each node there is a 6 x 6 matrix whose elements have the dimensions of either mass, moment of mass, or product of inertia. The inertia matrix for the entire structure will be called m.

The original structural idealization had 1462 degrees of freedom. The stiffness and inertia matrices were calculated by a computer program. Computer

limitations made it desirable to have a reduced order approximation which was accomplished using a Guyan reduction. The 249 new DOF's were a subset of the old except for those of the array. There the old DOF's were translations (never rotations) along the XYZ axes. The new DOF's were directed along the X axis, normal to the array plane, and along the common normal. These directions will be called X, Y', Z', respectively (Fig. 6).

New DOF's on the array were introduced as load conditions to reduce the solar array model. These forces balance-should have been equal and opposite to the loads - this check was not satisfied at a few DOF's with the model as provided by Grumman structural engineering. Several attempts by us and the original engineer to find the source of the diffisulty failed. We therefore used the mass and stiffness matrix as provided and ignored the load balance requirement. All this does is to cause errors in the steady state forces on the structure.

If $\underline{x}$ represents the displacements of the 249 DOF's and K,M the corresponding stiffness and inertia matrices, then in the absence of external forces the Guyan model is:

$$M\ddot{\underline{x}} + C\dot{\underline{x}} + K\underline{x} = 0 \tag{3}$$

For the analysis that follows, C, the damping matrix, will be assumed to be zero. In Section III-6, this assumption will be corrected.

Let us look for solutions of the form

$$\underline{x} = \underline{\phi} \cos \omega t \tag{4}$$

where $\underline{\phi}$, ω are vector and scalar constants to be determined. After substituting and simplifying

$$\omega^2 M\underline{\phi} = K\underline{\phi} \tag{5}$$

or

$$K^{-1}M\underline{\phi} = \omega^{-2}\underline{\phi} \tag{6}$$

Thus ω^{-2} is the eigenvalue of $K^{-1}M$ with the corresponding eigenvector $\underline{\phi}$. (The solution Eq. (4) is called the vibration mode.)

If we impose the initial condition $\dot{\underline{x}}(0) = 0$ there will be a 249 vector $\underline{q}$ of arbitrary constants of integration. It will be convenient to define the generalized coordinate vector $\underline{q}$ whose elements are $q_i \cos(\omega_i t)$. The complete matrix of normalized eigenvectors $\underline{\phi}/(\underline{\phi}^T\underline{\phi})^{1/2}$ will be denoted as Φ.

The general solution of Eq. (3) is then

$$\underline{x} = \Phi\, \underline{q} \tag{7}$$

If the elements of $\underline{q}(0)$ are all zero except for $q_i(0) = 1$, then $\underline{x}(0)$ equals the i^{th} vector of Φ. $\underline{x}(t)$ will remain proportional to this vector as its elements oscillate with angular frequency ω_i. The other frequencies (modes) will not be excited.

It is perhaps surprising that the matrix of eigenvectors of $K^{-1}M$ can diagonalize simultaneously both K and M. This capability is related to the nonorthogonality of the eigenvectors of $K^{-1}M$, which in turn is due to the nonsymmetry of $K^{-1}M$.* Let $\underline{\phi}_m$ and $\underline{\phi}_n$ be eigenvectors with distinct eigenvalues. Then from Eq. (5)

$$\omega_m^2\, M\, \underline{\phi}_m = K\underline{\phi}_m \tag{8}$$

On multiplying from the left by $\underline{\phi}_n^T$

$$\omega_m^2\, \underline{\phi}_n^T M\, \underline{\phi}_m = \underline{\phi}_n^T K\, \underline{\phi}_m \tag{9}$$

If these steps are repeated with the order of $\underline{\phi}_m$, $\underline{\phi}_n$ reversed then

$$\omega_n^2\, \underline{\phi}_m^T M\underline{\phi}_n = \underline{\phi}_m^T\, K\, \underline{\phi}_n \tag{10}$$

Since K and M are symmetric, the transpose of this equation is

$$\omega_n^2\, \underline{\phi}_n\, M\, \underline{\phi}_m = \underline{\phi}_n^T\, K\, \underline{\phi}_m \tag{11}$$

On subtracting Eq. (11) from Eq. (9)

$$(\omega_m^2 - \omega_n^2)\, \underline{\phi}_n^T\, M\, \underline{\phi}_m = 0 \tag{12}$$

which shows that the off-diagonal elements of $\Phi^T M \Phi$ are zero and that M is diagonalized by Φ. To prove that K can also be diagonalized, the above steps are repeated after first dividing Eq. (8) by ω^2.

*The eigenvectors of the matrix $K^{-1}M$ are <u>not</u> orthogonal but those of K and M individually are, as shown in Eqs. (11) and (12).

The vibration modes were augmented with the 6 rigid body translations and rotations that were calculated separately. The frequencies associated with the rigid body motion are of course zero since there are no translational or rotational rigid body stiffness terms in K (until the gravity gradient is added). The symbols $\tilde{K}$, $\tilde{M}$ denote the diagonal matrices defined by

$$\tilde{K} = \Phi^T K \Phi , \qquad \tilde{M} = \Phi^T M \Phi \tag{13}$$

Note that Eq. (9) implies $\tilde{K}_{ii} = \omega_i^2 \tilde{M}_{ii}$.

The 53 vibrations modes with the highest eigenvalues (lowest frequencies) were computed (Fig. 7). Because the solar array consists of 11 semi-independent membranes, most of the modes are out-of-plane oscillations due to the first three solar array modes. Thirty of the latter were discarded by retaining only one of these membrane modes per frequency leaving 23 vibration modes. The corresponding terms of $\tilde{K}$, $\tilde{M}$ were also deleted which corresponds to reducing the order of the system by assuming the frequencies are zero. The exact mathematical statement of this "singular perturbation" is the following:

If the modal coordinate vector is denoted by q then q is partitioned into components q_1 and q_2 where, in terms of this partition

$$\begin{bmatrix} \tilde{M}_{11} & 0 \\ 0 & \tilde{M}_{22} \end{bmatrix} \begin{bmatrix} \ddot{q}_1 \\ \ddot{q}_2 \end{bmatrix} = - \begin{bmatrix} \tilde{K}_{11} & 0 \\ 0 & \tilde{K}_{22} \end{bmatrix} \begin{bmatrix} q_1 \\ q_2 \end{bmatrix}$$

where all of the matrices are diagonal (as in Eq. (13)). Now if $\tilde{M}_{22}$ has a constant ε factored out of each of its terms, then (see Ref. 2), the "reduced order" model becomes $\tilde{M}_{11} \ddot{q}_1 + \tilde{K}_{11} q_1 = 0$ as $\varepsilon \to 0$ (i.e., $q_2 \to 0$). This tacitly implies that the full 249 vector x is given by (7) with $q_2 = 0$.

That is

$$x = \begin{bmatrix} \Phi_{11} & \Phi_{12} \\ \Phi_{21} & \Phi_{22} \end{bmatrix} \begin{bmatrix} q_1 \\ 0 \end{bmatrix} = \begin{bmatrix} \Phi_{11} q_1 \\ \Phi_{21} q_1 \end{bmatrix}$$

MODE	FREQ Hz	LB, $SEC^2/IN.$	DESCRIPTION
*1	0.04766	10,653	SOLAR ARRAY – 1ST NORMAL TRANSLATION
*2	0.05538	3,913	SOLAR ARRAY – 1ST TORSION (1ST MEMBRANE)
*3	0.06008	3,822	SOLAR ARRAY – PANEL MODES (1ST MEMBRANE)
4	0.06135	3,813	SOLAR ARRAY – PANEL MODES (1ST MEMBRANE)
5	0.06176	3,475	SOLAR ARRAY – PANEL MODES (1ST MEMBRANE)
6	0.06192	3,802	SOLAR ARRAY – PANEL MODES (1ST MEMBRANE)
7	0.06201	3,711	SOLAR ARRAY – PANEL MODES (1ST MEMBRANE)
8	0.06206	3,743	SOLAR ARRAY – PANEL MODES (1ST MEMBRANE)
9	0.06209	3,647	SOLAR ARRAY – PANEL MODES (1ST MEMBRANE)
10	0.06211	3,787	SOLAR ARRAY – PANEL MODES (1ST MEMBRANE)
11	0.06212	3,697	SOLAR ARRAY – PANEL MODES (1ST MEMBRANE)
12	0.06213	3,736	SOLAR ARRAY – PANEL MODES (1ST MEMBRANE)
13	0.06214	3,676	SOLAR ARRAY – PANEL MODES (1ST MEMBRANE)
*14	0.08400	11,240	SOLAR ARRAY – 2ND NORMAL TRANSLATION
*15	0.09226	20,274	SOLAR ARRAY – SIDE BENDING (X)
*16	0.10329	5,128	SOLAR ARRAY – TORSION (2ND MEMBRANE)
*17	0.10951	28,561	HEAT TORSION – BOOM + PLATFORM AND ARRAY LOCATION
*18	0.11288	3,625	SOLAR ARRAY – PANEL MODES (2ND MEMBRANE)
19	0.11404	3,754	SOLAR ARRAY – PANEL MODES (2ND MEMBRANE)
20	0.11442	3,694	SOLAR ARRAY – PANEL MODES (2ND MEMBRANE)
21	0.11459	3,757	SOLAR ARRAY – PANEL MODES (2ND MEMBRANE)
22	0.11468	3,699	SOLAR ARRAY – PANEL MODES (2ND MEMBRANE)
23	0.11473	3,754	SOLAR ARRAY – PANEL MODES (2ND MEMBRANE)
24	0.11477	3,704	SOLAR ARRAY – PANEL MODES (2ND MEMBRANE)
25	0.11479	3,753	SOLAR ARRAY – PANEL MODES (2ND MEMBRANE)
26	0.11480	3,682	SOLAR ARRAY – PANEL MODES (2ND MEMBRANE)
27	0.11481	3,746	SOLAR ARRAY – PANEL MODES (2ND MEMBRANE)
28	0.11482	3,715	SOLAR ARRAY – PANEL MODES (2ND MEMBRANE)
*29	0.11628	26,743	VERTICAL BOOM + PLATFORM SCISSOR MODE
*30	0.12259	8,229	SOLAR ARRAY – PANEL MODES (3RD MEMBRANE)
*31	0.13057	5,362	SOLAR ARRAY – PANEL MODES (3RD MEMBRANE)
*32	0.14846	3,223	SOLAR ARRAY – PANEL MODES (3RD MEMBRANE)
33	0.14961	3,925	SOLAR ARRAY – PANEL MODES (3RD MEMBRANE)
34	0.14984	3,425	SOLAR ARRAY – PANEL MODES (3RD MEMBRANE)
35	0.14992	3,791	SOLAR ARRAY – PANEL MODES (3RD MEMBRANE)
36	0.14996	3,747	SOLAR ARRAY – PANEL MODES (3RD MEMBRANE)
37	0.14998	3,744	SOLAR ARRAY – PANEL MODES (3RD MEMBRANE)
38	0.14999	3,805	SOLAR ARRAY – PANEL MODES (3RD MEMBRANE)
39	0.15000	3,777	SOLAR ARRAY – PANEL MODES (3RD MEMBRANE)
40	0.15001	3,724	SOLAR ARRAY – PANEL MODES (3RD MEMBRANE)
41	0.15002	3,683	SOLAR ARRAY – PANEL MODES (3RD MEMBRANE)
42	0.15002	3,6033	SOLAR ARRAY – PANEL MODES (3RD MEMBRANE)
*43	0.15178	7,6922	SOLAR ARRAY – PANEL MODE
*44	0.15395	4,6886	SOLAR ARRAY – PANEL MODE
*45	0.17424	16,5774	PLATFORM NORMAL BENDING
*46	0.20019	3,24636	SOLAR ARRAY – PANEL MODE
*47	0.22621	48,6614	PLATFORM TORSION
*48	0.25980	5,6988	SOLAR ARRAY – PANEL MODE
*49	0.26885	10,4788	SOLAR ARRAY – IN-PLANE
*50	0.27068	7,5181	SOLAR ARRAY – PANEL MODE
*51	0.30673	4,1957	SOLAR ARRAY – PANEL MODE
*52	0.30795	210,487	PLATFORM LATERAL BENDING
*53	0.32406	200,3	PLATFORM BENDING

*THESE MODES HAVE BEEN RETAINED

0357-007W

Fig. 7 OCDA Vibration Modes

4. EXTERNAL FORCES AND TORQUES

If an external force/torque vector $\underline{f}$ is present, Eq. (3) generalizes to

$$M \ddot{\underline{x}} + K \underline{x} = f \tag{14}$$

Equation (7) can be used to reduce the number of equations from 249 to 29 by substituting $\underline{x} = \Phi \underline{q}$ in (14)

$$M \Phi \ddot{\underline{q}} + K \Phi \underline{q} = \underline{f} \tag{15}$$

Multiplying on the left by Φ^T and using Eq. (13)

$$\tilde{M} \ddot{\underline{q}} + \tilde{K} \underline{q} = \Phi^T f \tag{16}$$

This equation is exact although $\underline{x}$ as calculated from Eq. (7) is approximate.

The complete orthogonalization procedure described above follows the classical structural analysis techniques. A more general approach utilizes the linear algebra of symmetric matrices. Thus (14) can be rewritten as follows:

- Let M be written as a product of a lower and upper triangular factor as

$$M = LL^T \tag{17}$$

  This "Cholesky" factorization may always be performed since M will always be symmetric and positive definite.

- Define a new vector $\underline{z}$ as

$$\underline{z} = L^T \underline{x} \tag{18}$$

- With $\underline{z}$ replacing $\underline{x}$ in Eq. (14) we get

$$\ddot{\underline{z}} = -L^{-1} K L^{-T} \underline{z} + L^{-1} \underline{f} \tag{19}$$

- Modal Transformation: Since K was symmetric $L^{-1}KL^{-T}$ remains symmetric and the following results from linear algebra may be used to diagonalize it.

- Lemma (Ref. 3): A real symmetric matrix can always be diagonalized by an orthogonal transformation and its eigenvalues are always real. Thus, let $\underline{z} = \Phi' \underline{q}'$ where Φ' is orthornormal ($\Phi' \Phi'^T = \Phi'^T \Phi' = I$) so that

$$\ddot{q}' = - \Phi^T L^{-1} K L^{-T} \Phi' \, q' + \Phi^T L^{-1} f \qquad (20)$$

where

$$\Phi^T L^{-1} K L^{-T} \Phi' = \Omega^2 = \begin{bmatrix} \omega_1^2 & 0 & \cdots & 0 \\ 0 & \omega_2^2 & \cdots & 0 \\ 0 & 0 & \cdots & \omega_n^2 \end{bmatrix}$$

and we assume $\omega_1^2 \leq \omega_2^2 \leq \cdots \leq \omega_n^2$.

Notice that the q' defined in Eq. (20) and the q from Eq. (16) are not identical since M in Eq. (16) is not the identity matrix. In fact $q' = \tilde{M}^{\frac{1}{2}} q$ and $\Phi = \tilde{M}^{\frac{1}{2}} \Phi'$ where

$$\tilde{M}^{\frac{1}{2}} = \begin{bmatrix} \tilde{M}_{11}^{\frac{1}{2}} & 0 & \cdots & 0 \\ 0 & \tilde{M}_{22}^{\frac{1}{2}} & \cdots & 0 \\ & \cdots & & \\ 0 & 0 & \cdots & \tilde{M}_{nn}^{\frac{1}{2}} \end{bmatrix}$$

The only external generalized forces considered were the aerodynamic drag acting on the solar array and the external torques due to the gravity gradient and the momentum wheels.

Before discussing the drag we digress to recall that the axes used for the earlier computer work that was taken over for the present investigation were those of Fig. 6. However, the earlier report (Ref. 1) followed the more conventional usage and interchanged the labels for the Y and Z axes. When the solar array has the orientation shown in Fig. 6 it is moving edgewise and there is no aerodynamic drag. We used the axes of Ref. 1, but in order to investigate stabilization in the presence of drag we rotated the OCDA so that the array moved nearly facewise (Fig. 8). Note that motion is along the Z axis and the X axis is vertical.

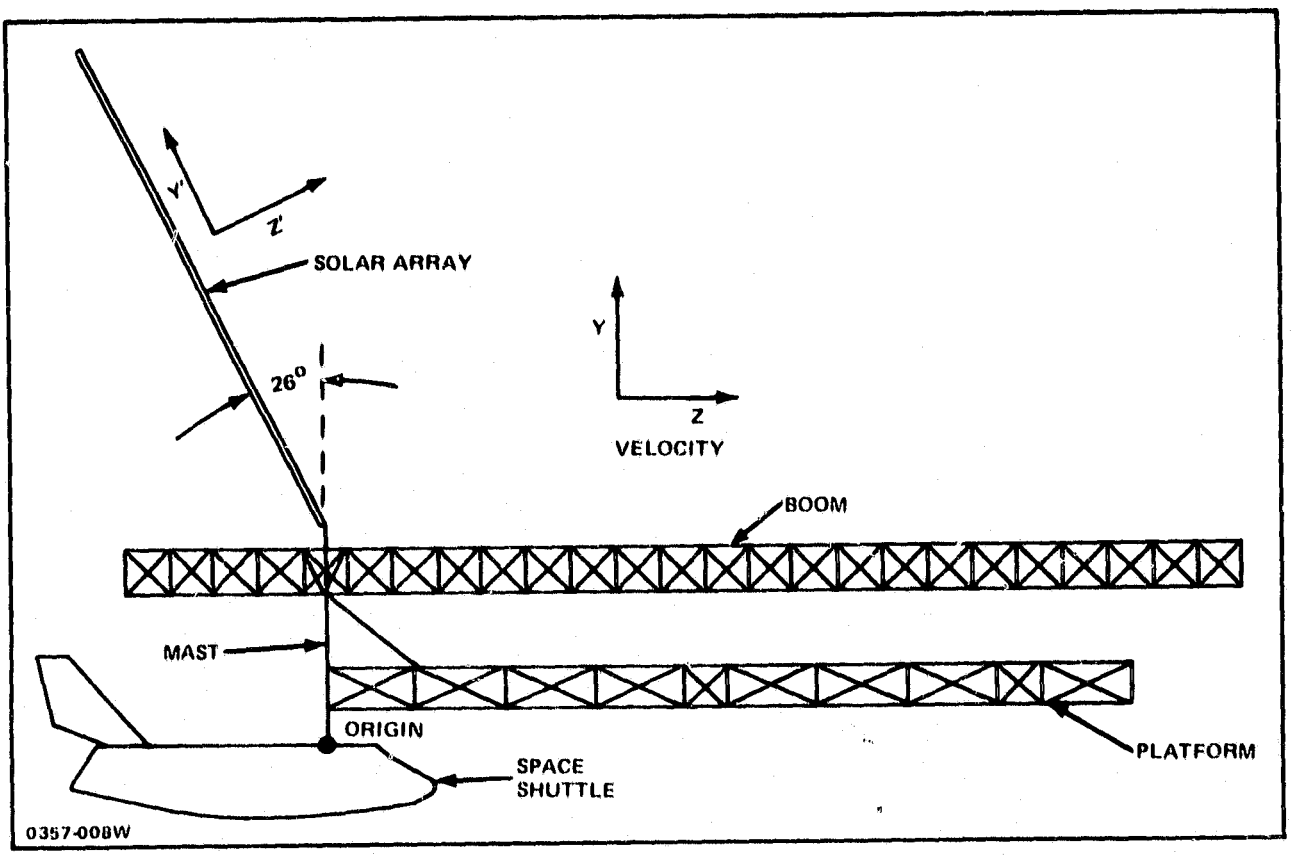

Fig. 8 Axes Used for the Present Investigation. (X is vertical.)

Since the drag was distributed over the solar array membranes, it was necessary to find lumped values at the nodes. The drag at a corner was assumed to be one-fourth that of an interior node. The drag at other edge points was one-half that at interior nodes. The forces were assumed to be in the direction normal to the array (-Z', Fig. 8) rather than opposed to the velocity as they should have been. It was impossible to give the drag the latter direction because the Y' and Z' DOF's were not selected in pairs at each membrane node. Indeed the latter were always selected but never the former.

These remarks will become clearer if we look at Φ in more detail. It has the form

$$\Phi = \begin{bmatrix} \Phi_{11} & \Phi_{12} & \Phi_{13} \\ \Phi_{21} & I & 0 \\ \Phi_{31} & 0 & I \end{bmatrix} \tag{21}$$

where in this representation the first column stands for the 23 vibration modes, the second the three rigid body translation modes, and the third the three rotation modes. The 3 x 3 unit and null matrices are denoted by I and 0, respectively. The matrices $\tilde{M}$, $\tilde{K}$ and the vectors $\underline{f}$ and $\underline{q}$ can be decomposed similarly into

$$\begin{aligned} &\tilde{M}_1 = \text{diag}\,[\tilde{M}_{1,1} \cdots \tilde{M}_{22,23}], \quad \tilde{M}_2 = \text{diag}\,[\tilde{M}_{24,24} \cdots \tilde{M}_{26,26}] \\ &\tilde{M}_3 = \text{diag}\,[\tilde{M}_{27,27} \cdots \tilde{M}_{29,29}], \quad \tilde{K}_1 = \text{diag}\,[\tilde{K}_{1,1} \cdots \tilde{K}_{23,23}] \\ &K_2 = K_3 = 0 \quad , \quad \underline{f}^T = [\underline{f}_1^T, \underline{f}_2^T, \underline{f}_3^T] \\ &\underline{q}^T = [\underline{q}_1^T, \underline{q}_2^T, \underline{q}_3^T], \ \underline{q}_1 \text{ is of dim. 25 and } \underline{q}_2 \text{ and } \underline{q}_3 \text{ are each of dim. 3.} \end{aligned} \tag{22}$$

The nonzero elements of the 243-vector $\underline{f}_1$ are the drag terms discussed above, the three-vector $\underline{f}_2$ is null. The three-vector $\underline{f}_3$ of gravity gradient and momentum wheel torques will be discussed in detail below. Equation (16) can now be written as the three equations

$$\tilde{M}_1 \ddot{q}_1 + .002(\tilde{M}_1\tilde{K}_1)^{\frac{1}{2}} \dot{q}_1 + \tilde{K}_1 q_1 = \Phi_{11}^T \underline{f}_1 + \Phi_{31}^T \underline{f}_3$$

$$\tilde{M}_2 \ddot{q}_2 = \Phi_{12}^T \underline{f}_1 \quad , \quad \tilde{M}_3 \ddot{q}_3 = \Phi_{13}^T \underline{f}_1 + \underline{f}_3 \tag{23}$$

Note that a modal structural damping term has been introduced into the vibration modes. This term changes the solutions of the homogeneous equation (Eq. (3)) by a factor $\exp(-.001\omega t)$. It also has a major effect on the modes which were reduced out of the dynamics as will be discussed in Section III-6.

The second of Eqs. (23) represents the three equations

$$\bar{M}_2 \ddot{\bar{x}} = \underline{\phi}_{24}^1 \underline{f}_1 \quad , \quad \bar{M}_2 \ddot{\bar{y}} = \underline{\phi}_{25}^1 \underline{f}_1 \quad , \quad \bar{M}_2 \ddot{\bar{z}} = \underline{\phi}_{26}^1 \underline{f}_1 \tag{24}$$

where $\bar{M}_2 = M_{24,24} = M_{25,25} = M_{26,26}$; $\bar{x}$, $\bar{y}$, $\bar{z}$ are the coordinates of the center mass; and $\underline{\phi}_i^1$ (i = 24, 25, 26) is a 243-row vector whose elements equal the first 243 elements of the i^{th} vector of Φ. The terms of the scalar product $\underline{\phi}_{24}^1 \underline{f}_1$ are all zero because the nonzero terms of $\underline{\phi}_{24}^1$ and $\underline{f}_1$ never coincide. The terms of $\underline{\phi}_{25}^1$ that coincide are all equal to (using the axes of Fig. 3) $\cos(Y,Z') = \sin 26°$, the corresponding terms of $\underline{\phi}_{26}^1$ are $\cos(Z,Z') = \cos 26°$. The acceleration in the Y direction does not vanish although it is normal to the velocity. There is no way to correct this qualitative error because no Y' DOF's were selected for the array membranes.

Reference 1 states that the momentum wheels are located in the mast midway between the platform and the boom. However, they were placed at the docking port (origin) for the present study. We have retained the latter position and assumed that the angular momenta $h_{\omega x}, h_{\omega y}, h_{\omega z}$ of the three wheels have fixed directions along the coordinate axes. Small control torques $u_x = \dot{h}_{\omega x}$, $u_y = \dot{h}_{\omega y}$, $u_z = \dot{h}_{\omega z}$ are obtained by changing the magnitudes of the angular momenta. In accordance with conservation laws, an increase in the angular momentum of a wheel produces a decrease in the angular momentum of the OCDA.

The rigid body yaw about the X axis (Fig. 6), pitch about the Y axis, and roll about the Z axis will be denoted by $\alpha = q_{27}$, $\beta = q_{28}$, $\gamma = q_{29}$, respectively. The corresponding moments of inertia are $A = M_{27,27}$, $B = M_{28,28}$, $C = M_{29,29}$. Linearized gravity gradient torques are given in Ref. 4, p. 244 and appendix 1. Thus the detailed expressions for the last of Eqs. (23) are

$$
\begin{aligned}
A\ddot{\alpha} &= \phi_{27}^{1}\underline{f}_1 + c\alpha - b\dot{\gamma} - \omega_z h_{\omega y} + \omega_y h_{\omega z} - u_x \\
B\ddot{\beta} &= \phi_{28}^{1}\underline{f}_1 + e\beta - \omega_x h_{\omega z} + \omega_z h_{\omega x} - u_y \\
C\ddot{\gamma} &= \phi_{29}^{1}\underline{f}_1 + a\gamma + b\dot{\alpha} - \omega_y h_{\omega x} + \omega_x h_{\omega y} - u_z
\end{aligned}
\tag{25}
$$

These equations use the following abbreviations: ω_o is the angular frequency corresponding to the 90 minute orbital period,

$$
\begin{aligned}
a &= 4\omega_o^2(A-B), & b &= \omega_o(A-B+C) \\
c &= \omega_o^2(C-B), & e &= 3\omega_o^2(A-C)
\end{aligned}
\tag{26}
$$

$$
\omega_x = \dot{\alpha} + \omega_o\gamma, \qquad \omega_y = \dot{\beta} - \omega_o, \qquad \omega_z = \dot{\gamma} - \omega_o\alpha .
$$

The scalar products $\phi_{28}^{1}\underline{f}_1$, $\phi_{29}^{1}\underline{f}_1$ evaluate to zero. This occurs because DOF's were selected in a symmetric manner over the array so that there is a negative term to cancel every positive term. Thus defining the drag to be in the Z' rather than the -Z direction does not introduce qualitative errors in the torques as it does in the forces on the center of mass. The quantitative error for the torque about the X axis tends to cancel out when summing over all the DOF's of the array. That is, the moment arm is smaller for Z' forces than it is for -Z forces at nodes near the platform and larger at nodes far from the platform. Note that another non-homogeneous term enters through ω_y.

Equations (23) with initial conditions $\underline{q}(0) = \dot{\underline{q}}(0) = 0$ describe a step disturbance - the drag is zero when $t < 0$ and jumps to its full value when $t = 0$. It is also interesting to study an impulsive disturbance occurring at $t = 0$. In this case the non-homogeneous terms are removed from Eq. (23) and the initial conditions $\dot{\underline{q}}(0)$ are set equal to them.

5. STATE VARIABLE MODEL FOR CONTROL DESIGN

The optimal control model we are developing uses 23 modes by leaving out the less important vibration modes through order reduction in modal coordinates. The force vector $\underline{f}$ consists of a distributed aerodynamic load on the solar array and the gravity gradient torques on the rigid body (we assume that the gravity forces are distributed as described in Appendix I). Thus the force vector $\underline{f}$ becomes

$$\underline{f} = \begin{bmatrix} \underline{f}_1 \\ \underline{0} \\ \underline{f}_3 \end{bmatrix} \quad \begin{matrix} \leftarrow \text{243 vector of aerodynamic forces distributed into the structure} \\ \\ \leftarrow \text{3 vector of gravity gradient torques and control torques} \end{matrix} \tag{27}$$

where

$\underline{f}_3 = T_{G_1}\,\underline{x}_3 + T_{G_2}\,\dot{\underline{x}}_3 + H\,\underline{u} + H_o$ as in Eq. (25)

$H\underline{u}$ = control forces; $H_o = \begin{bmatrix} -\omega_o h_{\omega z} \\ 0 \\ \omega_o h_{\omega x} \end{bmatrix}$ is the non-homogeneous forcing function.

T_{G_1} = gravity gradient torques induced by rigid body rotations

T_{G_2} = gravity gradient torques induced by rigid body rotational rates.

Following Eq. (25) T_{G_1} and T_{G_2} are given by

$$T_{G_1} = \begin{bmatrix} \omega_o^2\,(C - B) & 0 & 0 \\ 0 & 3\omega_o^2\,(A - C) & 0 \\ 0 & 0 & 4\omega_o^2\,(A - B) \end{bmatrix} \tag{28}$$

$$T_{G_2} = \begin{bmatrix} 0 & 0 & -\omega_o(A-B+C) \\ 0 & 0 & 0 \\ \omega_o(A-B+C) & 0 & 0 \end{bmatrix} \tag{29}$$

$$H\underline{u} = \begin{bmatrix} 0 & -\omega_z & \omega_y & 0 \\ \omega_z & 0 & -\omega_x & 0 \\ -\omega_y & \omega_x & 0 & \ell D \end{bmatrix} \begin{bmatrix} h_{\omega x} \\ h_{\omega y} \\ h_{\omega z} \\ \delta_{Array} \end{bmatrix} \tag{30}$$

$h_{\omega x,y,z}$ - angular momentum of the controller about the principle axes

$\ell D\delta$ Array - torque produced by the solar array angle δ_{Array} and ℓ is the lever arm of the drag force D. When D is non-zero $\underline{f}_1$ is zero and vice versa

As can be seen the formulation of the control terms Eq. (30) allows the simultaneous incorporation of the gravity gradient, aerodynamic drag and control momentum exchange devices. To distribute the terms from Eq. (25) into the structural mode model Eq. (16) we let $\underline{f}$ be given by Eq. (27) in Eq. (16) and get

$$\begin{bmatrix} \tilde{M}_1 & 0 & 0 \\ 0 & \tilde{M}_2 & 0 \\ 0 & 0 & \tilde{M}_3 \end{bmatrix} \left\{ \begin{bmatrix} \ddot{q}_1 \\ \ddot{q}_2 \\ \ddot{q}_3 \end{bmatrix} + \begin{bmatrix} \Omega_1^2 & 0 & 0 \\ 0 & 0 & 0 \\ 0 & 0 & 0 \end{bmatrix} \begin{bmatrix} q_1 \\ q_2 \\ q_3 \end{bmatrix} \right\}$$

$$= \begin{bmatrix} \Phi_{31}^T \\ \Phi_{32}^T \\ \Phi_{33}^T \end{bmatrix} \left\{ T_{G_1}[\Phi_{31}\Phi_{32}\Phi_{33}]\, q + T_{G_2}\,[\Phi_{31}\Phi_{32}\Phi_{33}]\, \dot{q} + H\underline{u} + H_o \right\} \tag{31}$$

which may be reduced to give

$$\ddot{\underline{q}} = \underbrace{\begin{bmatrix} -\Omega_1^2 + M^{-1}\Phi_{31}{}^T G_1 \Phi_{31} & M_1^{-1}\Phi_{31}{}^T G_1 \Phi_{32} & M_1^{-1}\Phi_{31}{}^T G_1 \Phi_{33} \\ M_2^{-1}\Phi_{32}^T G_1 \Phi_{31} & M_2^{-1}\Phi_{32}^T G_1 \Phi_{32} & M_2^{-1}\Phi_{32}^T G_1 \Phi_{33} \\ M_3^{-1}\Phi_{33}^T G_1 \Phi_{31} & M_3^{-1}\Phi_{33}^T G_1 \Phi_{32} & M_3^{-1}\Phi_{33}^T G_1 \Phi_{33} \end{bmatrix}}_{S} \underline{q}$$

$$+ \underbrace{\begin{bmatrix} M_1^{-1}\Phi_{31}^T G_1 \Phi_{31} & \cdots & M_1^{-1}\Phi_{31}^T G_1 \Phi_{33} \\ M_2^{-1}\Phi_{32}^T G_1 \Phi_{31} & \cdots & M_2^{-1}\Phi_{32}^T G_1 \Phi_{33} \\ M_3^{-1}\Phi_{33}^T G_1 \Phi_{31} & \cdots & M_3^{-1}\Phi_{33}^T G_1 \Phi_{33} \end{bmatrix}}_{T} \dot{\underline{q}} + \begin{bmatrix} M_1^{-1}\Phi_{31}^T \\ M_2^{-1}\Phi_{32}^T \\ M_3^{-1}\Phi_{33}^T \end{bmatrix} H\underline{u} + M^{-1}H_o \qquad (32)$$

and finally, by defining the state vector $\underline{z}$ as $\underline{z}^T = (\underline{q}^T : \dot{\underline{q}}^T)$ the model used for designing the optimal control system becomes:

$$\dot{\underline{z}} = \begin{bmatrix} 0 & 0 & 0 & U_{23} & 0 & 0 \\ 0 & 0 & 0 & 0 & U_3 & 0 \\ 0 & 0 & 0 & 0 & 0 & U_3 \\ S_{11} & S_{12} & S_{13} & T_{11} & T_{12} & T_{13} \\ S_{21} & S_{22} & S_{23} & T_{21} & T_{22} & T_{23} \\ S_{31} & S_{32} & S_{33} & T_{31} & T_{32} & T_{33} \end{bmatrix} \underline{z} + \begin{bmatrix} 0 \\ 0 \\ 0 \\ M_1^{-1}\Phi_{31}^T H \\ M_2^{-1}\Phi_{32}^T H \\ M_3^{-1}\Phi_{33}^T H \end{bmatrix} \underline{u} + \begin{bmatrix} 0 \\ 0 \\ 0 \\ M^{-1}H_o \end{bmatrix} \qquad (33)$$

or neglecting the $M^{-1}H_o$ term

$$\dot{\underline{z}} = A\underline{z} + B\underline{u} \qquad (34)$$

where

$\underline{z}$ is now a 58 vector (46 states for the structural dynamics and 12 rigid body states)

S and T are defined implicitly by Eq. (33)

U_n is the n x n identity matrix.

The nominal solar array angle is 23° so that the last component of $\underline{u}$ acts as a disturbance on the structure through the $M_1^{-1}\Phi_{31}^T H$ component of the matrix B in Eq. (34). Thus, the uncontrolled motion of the spacecraft can be developed and used as a reference to compare the controlled motion. The open loop dynamic response at various times are shown in Fig. 9. For the control system design in the next section, the rigid body tranlation modes have been deleted so the control vector $\underline{z}$ is reduced in order to 52.

Notice in the formulation of the dynamic model leading to Eq. (33) that the rigid body modes are retained in the same coordinates as the structural modes. This is distinct from Likens et al. (Ref. 5) where a hybrid coordinate system is used.

6. OPTIMAL DIGITAL CONTROL FOR OCDA

It is not the main point of this report to present the theory of linear discrete-time optimal control. Therefore, we will briefly outline here the major assumptions made in designing optimal discrete systems. For further details the reader is referred to the excellent tutorial paper by Dorato and Levis, Ref. 6.

The continuous model of the spacecraft in state variable form (where all matrices are constant) is given by Eq. (34)*

$$\dot{\underline{x}} = A\underline{x} + B\underline{u} + C\underline{w}$$

$$\underline{y} = M\underline{x} + \underline{\nu} \qquad (34)$$

---

* The usual notation in the control literature is to use $\underline{x}$ as the state vector. This convention is used here thus the original version of Eq. (34) (on page 25) is modified (in the original formulation $\underline{x}$ was the physical motions of the finite element degrees of freedom).

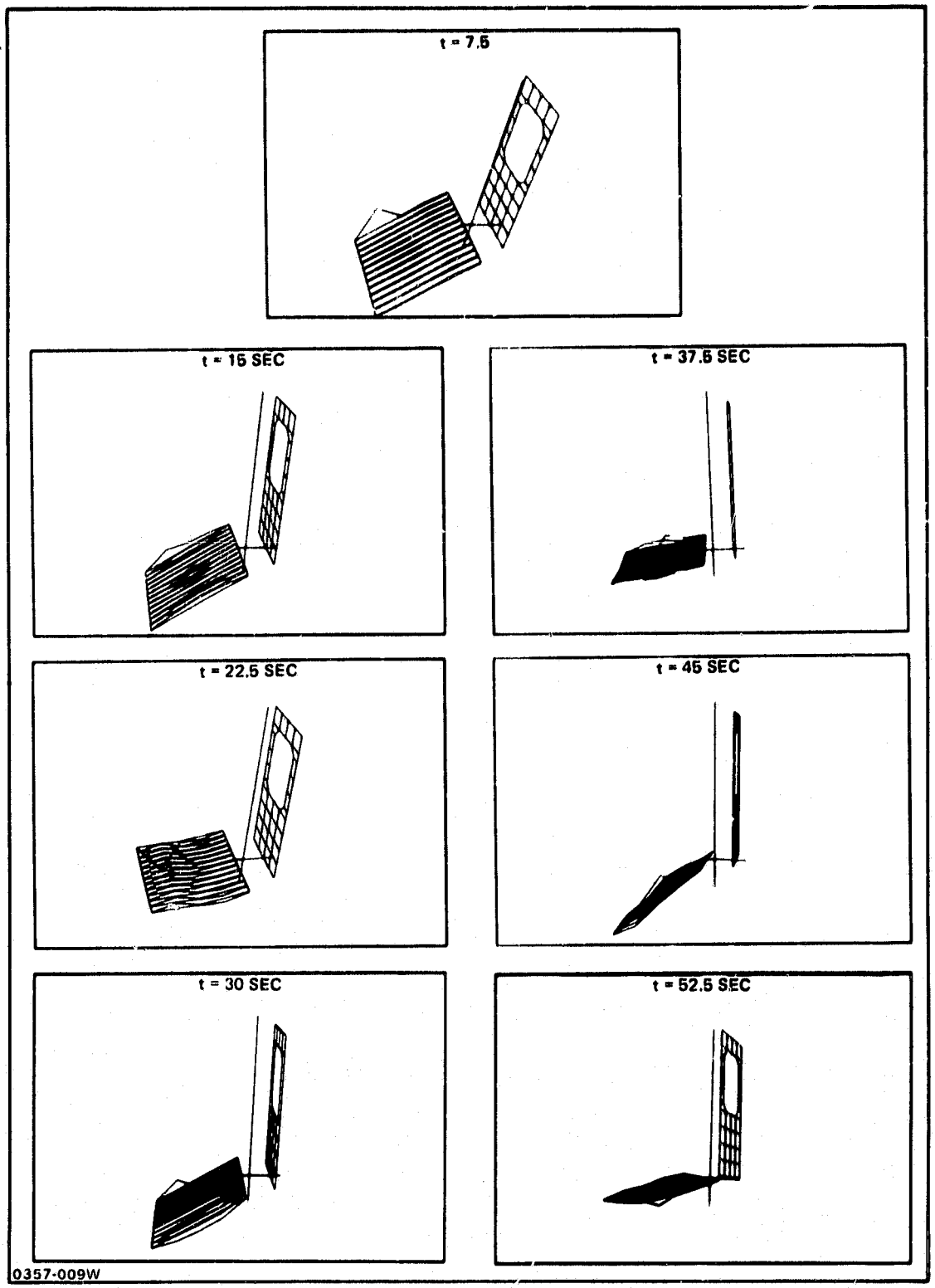

Fig. 9 Uncontrolled, Open Loop, Response of the OCDA – Impulse Loading of the Solar Array as the Driving Force

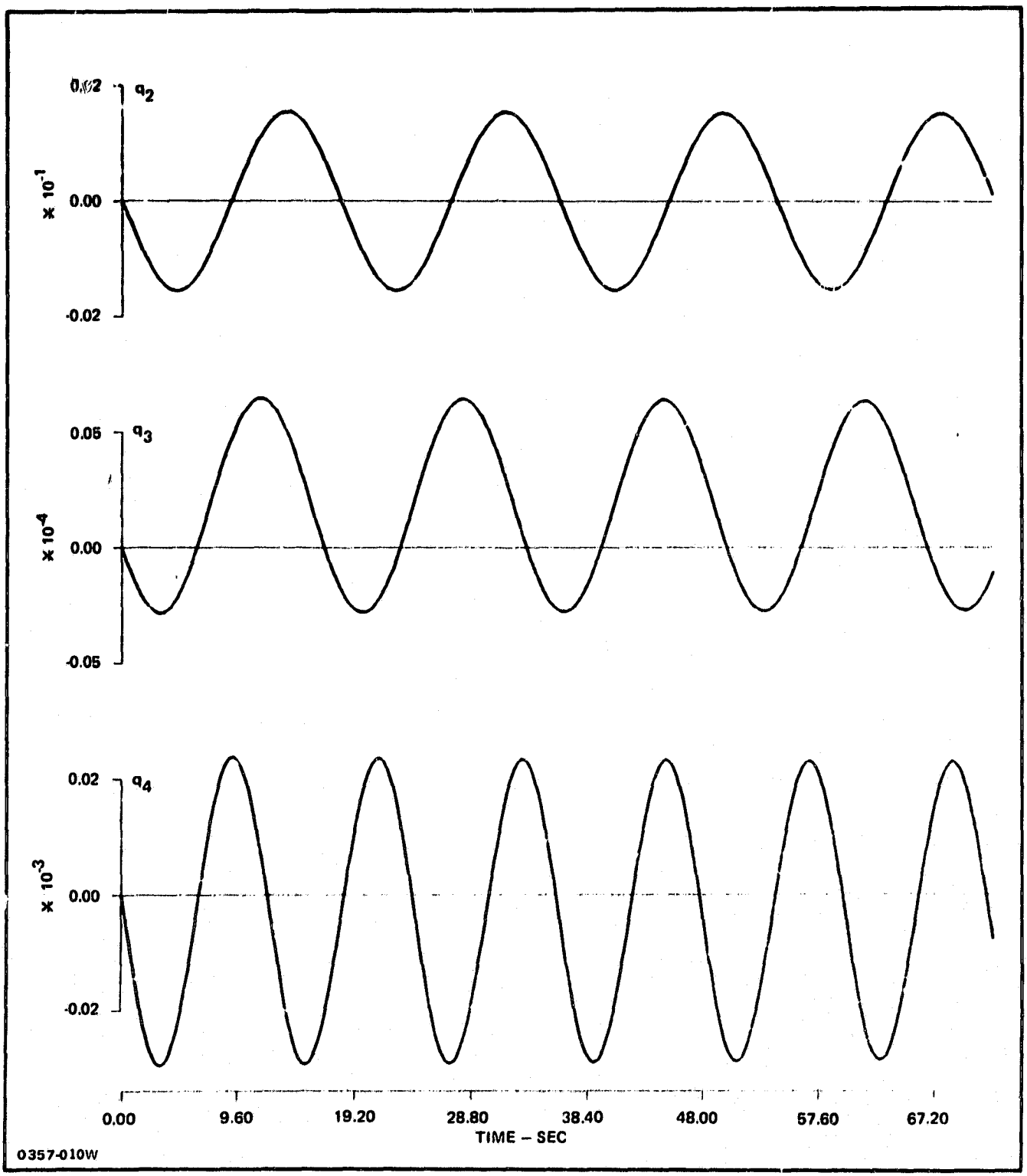

Fig. 10 Orbiting Construction Base – No Control – Modal Motion of Modes 2, 3 and 4 (Inches)

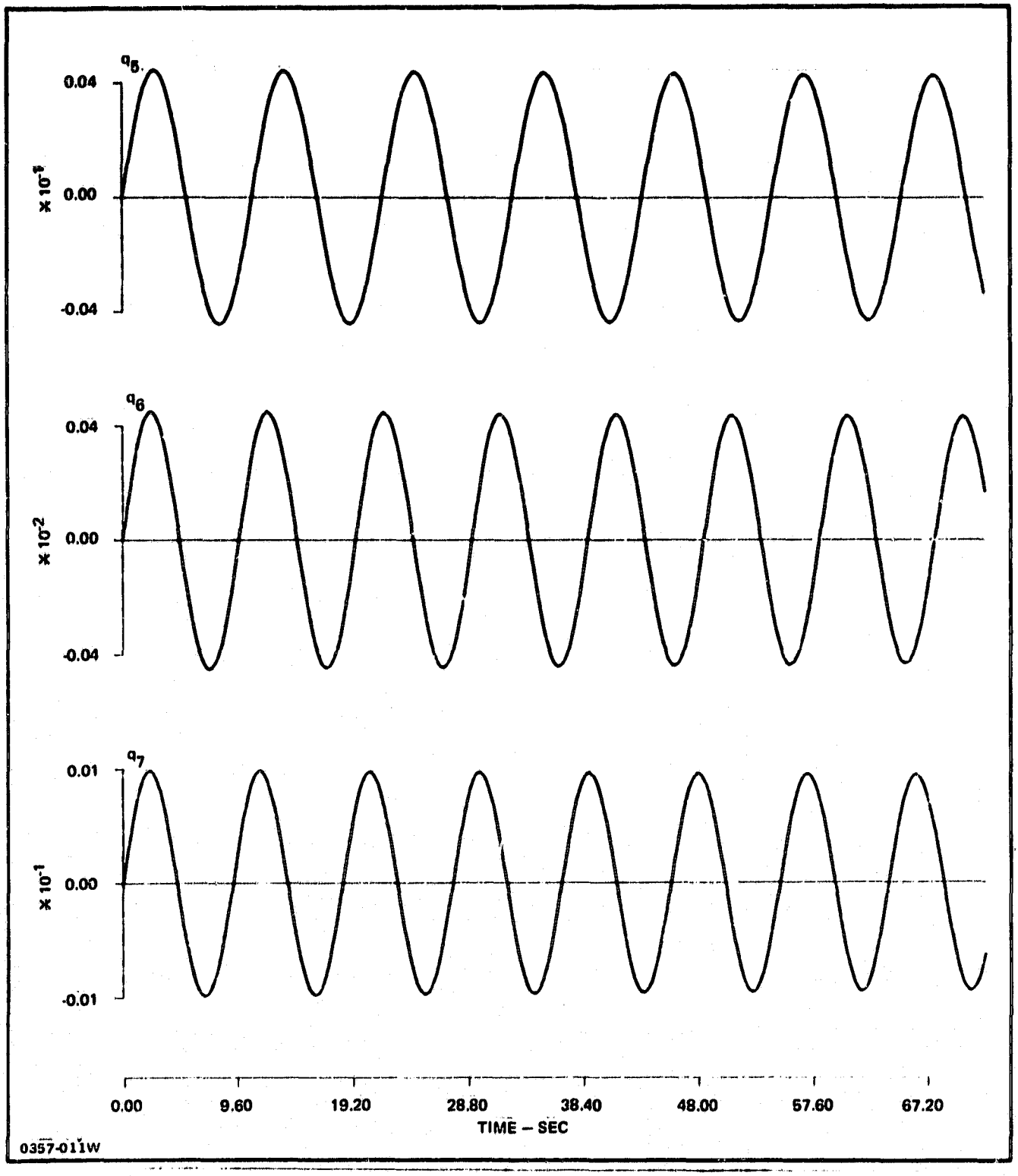

Fig. 11 Orbiting Constant Base – No Control – Modes 5, 6 and 7 (Inches)

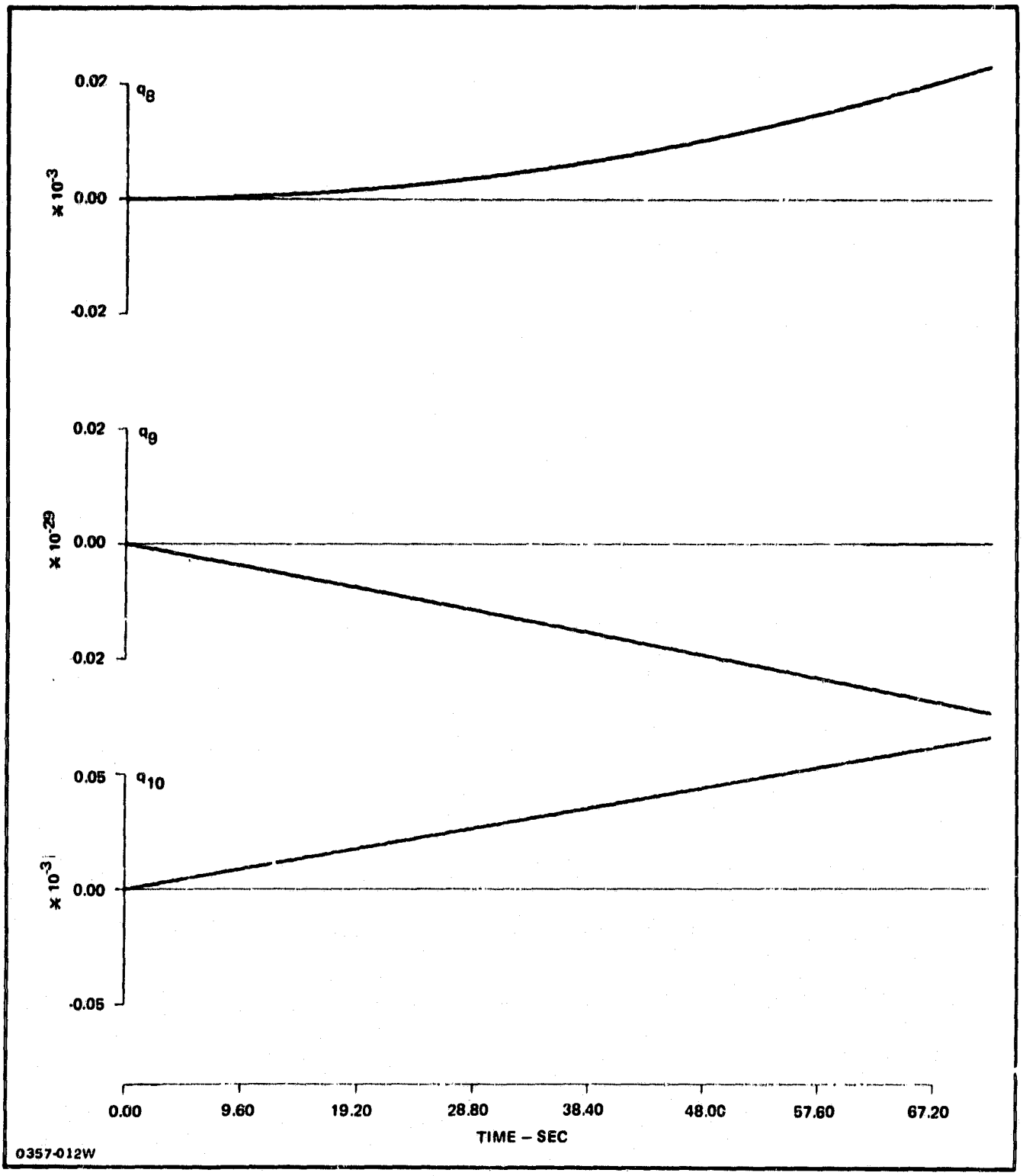

Fig. 12 Orbiting Constant Base – Open Loop Rigid Body Rotation Modes (Radians)

where $\underline{x}$ is the 52 vector of spacecraft states and any augmented noise states (which are not included) $\underline{u}$ is a 4 vector control; $\underline{w}$ would be a m_1 vector noise process (which is assumed to be a white process); $\underline{y}$ is the vector measurement which we are assuming is $\underline{x}$; and $\underline{\nu}$ is an m_2 vector white measurement noise. The discrete-time version of Eq. (34) is given by

$$\underline{x}_{K+1} = \Phi(\Delta t)\ \underline{x}_K + \Gamma(\Delta t)\ \underline{u}_K + G(\Delta t)\ \underline{w}_K$$

$$\underline{y}_K = M\underline{x}_K + \underline{\nu}_K$$

Δt = the sample time

$\Phi(\Delta t)$ = the transition matrix evaluated at Δt (i.e., $e^{A\Delta t}$)

$\Gamma(\Delta t) = \int_0^{\Delta t} \Phi(\Delta t - \tau) B\, d\tau$

(i.e., $\dot{\Gamma} = A\Gamma + B$, $\Gamma(0) = 0 \rightarrow \Gamma(\Delta t) = \int_0^{\Delta t} e^{A\tau} B d\tau$)

$G(\Delta t)$ = a matrix which satisfies $G(\Delta t)G^T(\Delta t) = P(\Delta t)$ where

$P(\Delta t)$ is the covariance of matrix of $\underline{x}$ from Eq. (34) at $t = \Delta t$.

In general, one would like to solve the following problem: "Given a quadratic performance index of the form

$$J = \int_{t_o}^{T} (\underline{x}^T Q \underline{x} + \underline{u}^T R \underline{u})\, dt \tag{35}$$

find the control which minimizes J subject to the constraint of the differential Eq. (34)."

The discrete version of Eq. (35) is obtained from Eq. (35) and the fact that the controls are held fixed over the sample interval Δt. This discretization of Eq. (35) is necessary to be able to compare the discrete design with the continuous design. It is generally better to use the performance index for the discrete system which matches the continuous system also to determine the effect of increasing sample time. Thus, the performance measure Eq. (35) becomes

$$J = \sum_{K=1}^{N} \underline{x}_K^T \tilde{Q}\ \underline{x}_K + 2\ \underline{u}_K^T \tilde{S}\ \underline{x}_K + \underline{u}_K^T \tilde{R}\ \underline{u}_K \tag{36}$$

where

$$\tilde{Q} = \int_0^{\Delta t} \Phi^T(\tau)\, Q\, \Phi(\tau)\, d\tau$$

$$\tilde{S} = \int_0^{\Delta t} \Gamma^T(\tau)\, Q\, \Phi(\tau)\, d\tau \qquad *$$

$$\tilde{R} = \int_0^{\Delta t} \{R + \Gamma^T(\tau)\, Q\Gamma(\tau)\}\, d\tau$$

The computation of $\tilde{Q}$, $\tilde{S}$ and $\tilde{R}$ uses an eigenvalue-eigenvector approach where the transition matrix $\Phi(t)$ is written as $Te^{\Lambda t}T^{-1}$ with Λ as the diagonal matrix obtained by diagonalizing the matrix A.

The discrete-time control problem is solved by using either the discrete maximum principle or dynamic programming. In either case the ultimate solution is that $\underline{u}_K$ is a linear function of the states of the system where the gain matrix K_k satisfies

$$K_k = -(\tilde{R} + \Gamma^T P_K \Gamma)^{-1}(\Gamma^T P_K \Phi + \tilde{S}) \tag{37}$$

and P_k is the solution of the discrete matrix Ricatti equation

$$P_k = (\Phi^T P_{k+1} \Phi + \tilde{Q}) - (\Gamma^T P_{k+1} \Phi + \tilde{S})^T (\tilde{R} + \Gamma^T P_{k+1} \Gamma)^{-1} (\Gamma^T P_{k+1} \Phi + \tilde{S}) \tag{38}$$

with $P_N = [0]$.

If, as is generally assumed, the steady-state (constant) gain matrix is desired, we have found that the best way to solve for the gain, Eq. (37), is to use Potter's technique (Ref. 7) of evaluating the eigenvalues and eigenvectors of the 2n x 2n matrix which results from the application of the discrete maximum principle. Problems such as the OCDA control which are high order and with significant differences in time constants are as easily solved as low-order problems when using a numerical eigenvalue, eigenvector technique. If such

*The matrix $\Gamma(t)$ is defined after Eq. (35); also it is significant that the discrete performance index contains a nonzero matrix S even though Eq. (35) does not.

problems were solved using iteration, the computer time required would be exorbitant. This matrix, for the performance index Eq. (36) is given by

$$H = \left[\begin{array}{c|c} H_{11} & H_{12} \\ \hline H_{21} & H_{22} \end{array}\right]$$

where

$$H_{11} = (\Phi - \Gamma\tilde{R}^{-1}\tilde{S})^{-1}$$

$$H_{12} = (\Phi - \Gamma R^{-1}\tilde{S})^{-1}\Gamma\tilde{R}^{-1}\Gamma^{T}$$

$$H_{21} = (\tilde{Q} - \tilde{S}^{T}R^{-1}\tilde{S})(\Phi - \Gamma\tilde{R}^{-1}\tilde{S})^{-1}$$

$$H_{22} = (\Phi^{T} - \tilde{S}^{T}\tilde{R}^{-1}\Gamma^{T}) + (\tilde{Q} - \tilde{S}^{T}\tilde{R}^{-1}\tilde{S})(\Phi - \Gamma\tilde{R}^{-1}\tilde{S})^{-1}\Gamma\tilde{R}^{-1}\Gamma^{T} \qquad (39)$$

H has the property that its eigenvalues are the n poles of the closed-loop system and their reciprocals (there are 2n eigenvalues, n stable and n unstable). The steady-state gain is given by the Potter algorithm as follows:

Let W be the matrix of eigenvectors, then

$$W^{-1}HW = \begin{bmatrix} \Lambda & 0 \\ 0 & \Lambda^{-1} \end{bmatrix}$$

where Λ represents the eigenvalues outside the unit circle. Then if W is partitioned as

$$\left[\begin{array}{c|c} W_{11} & W_{12} \\ \hline W_{21} & W_{22} \end{array}\right], \quad W_{ij} \text{ is } n \times n$$

the steady-state cost P_o is given by

$$P_o = W_{21}W_{11}^{-1} \qquad (40)$$

The program that is used to derive the optimal controls uses this technique to obtain the optimal gains. The Q - R algorithm is used to determine the eigenvector matrix W. Potter's technique applies to both continuous and discrete systems; however, in the continuous version the eigenvalues of the 2n x 2n matrix H have symmetry about the imaginary axis (rather than radial symmetry). Since we use the continuous optimal design as a reference, the Potter solution for the continuous design existed first. To take advantage of this existing program we map the roots of the matrix H using the bilinear transformation

$$w = (1 - z)/(1 + z)$$

This allows the roots inside and outside the unit circle to be selected based on their locations in the left-half or right-half w-plane.

The last point we have to consider is how one selects the sample time Δt. This has already been discussed in a former paper by the authors (Ref. 8), but a brief outline is in order here. The selection of a fundamental sample time uses the fact that between samples the system is essentially open-loop. Therefore, if perfect control at the sample times were achieved, between samples the uncertainty would propagate via the covariance matrix differential equation

$$\dot{P} = AP + PA^T + CC^T$$

$$P(0) = [0]. \qquad (41)$$

At the first time t that the uncertainty due to this open-loop propagation exceeds a bound specified by the control specifications, there must be a sample to lower this uncertainty. Since we are neglecting uncertainties that are due to the control (feedback) and the state estimation in doing the propagation of Eq. (41) (i.e., P(0) is really not [0]), the actual sample rate should be modified based on the closed-loop noise response. As we will see the existence of computer aided design programs allows all of the above steps to be implemented. To show all of the output of the computer computations for the OCDA example would not be very instructive; we therefore have shown in Section IV an exercise for a simplified example. Reference 9 shows more details of this analysis.

Many times it is necessary to provide a constant force to provide the desired steady state position. To guarantee that this force does not cause an undesirable

deviation at some position on the structure, the control is assumed to be applied through a set of integrators. Thus $\underline{f} = B\underline{u}'$, where B distrubutes the control forces $\underline{u}'$ through the structure. $\underline{u}'$ is integrated control, i.e.,

$$\underline{u}' = \int_o^t \underline{u}\ dt$$

or

$$\frac{d\underline{u}'}{dt} = \underline{u}$$

The dynamic state of Eq. (34) is modified as follows:

$$\underline{y} = \begin{bmatrix} \underline{q}_1 \\ \dot{\underline{q}}_1 \\ \underline{u}' \end{bmatrix}$$

so

$$\dot{\underline{y}} = \begin{bmatrix} 0 & I_m & 0 \\ -\Omega_1^2 & 0 & [\Phi_{11}^T \Phi_{21}^T]L^{-1}B \\ 0 & 0 & 0 \end{bmatrix} \underline{y} + \begin{bmatrix} 0 \\ 0 \\ I_p \end{bmatrix} \underline{u} \qquad (42)$$

is the "state variable" model of the structure which is used to design the control system. $\underline{y}$ has dimension 52 + p where p is the dimension of $\underline{u}$ (the control).

The optimal control design based on the model Eq. (34) uses the performance measure Eq. (35). But Eq. (35) is really based on the actual full 243 degrees of freedom and through the order reduction, Eq. (35) becomes

$$J = \int_0^\infty \left(\left\{ L^{-1} \begin{bmatrix} \Phi & \underline{q} \\ \Phi & \dot{\underline{q}} \end{bmatrix} \right\}^T \begin{bmatrix} Q_{11} & Q_{12} \\ Q_{12} & Q_{22} \end{bmatrix} L^{-1} \begin{bmatrix} \Phi & \underline{q} \\ \Phi & \dot{\underline{q}} \end{bmatrix} + \underline{u}^T R \, \underline{u} \right) dt$$

$$= \int_0^\infty \left\{ L^{-1} \begin{bmatrix} \Phi_{11} \, \underline{q}_1 & \Phi_{12}(\Omega_2^2)^{-1} \, [\Phi_{11}^T \Phi_{22}^T] L^{-1} B_2 \underline{u}' \\ \Phi_{11} \, \dot{\underline{q}}_1 + & \Phi_{12}(\Omega_2^2)^{-1} \, [\Phi_{11}^T \Phi_{22}^T] L^{-1} B_2 \underline{u}' \end{bmatrix} \right\}^T$$

$$Q \left\{ L^{-1} \begin{bmatrix} \Phi_{11} \, \underline{q}_1 & \Phi_{12}(\Omega_2^2)^{-1} \, [\Phi_{11}^T \Phi_{22}^T] L^{-1} B_2 \underline{u}' \\ \Phi_{11} \, \dot{\underline{q}}_1 + & \Phi_{12}(\Omega_2^2)^{-1} \, [\Phi_{11}^T \Phi_{22}^T] L^{-1} B_2 \underline{u}' \end{bmatrix} \right\} + \underline{u}^T R \, \underline{u} \; dt$$

The resulting performance measure is therefore of the form

$$J = \int_0^\infty \left\{ \begin{bmatrix} \underline{q}_1 \\ \dot{\underline{q}}_1 \end{bmatrix}^T \hat{Q} \begin{bmatrix} \underline{q}_1 \\ \dot{\underline{q}}_1 \end{bmatrix} + \begin{bmatrix} \underline{q}_1 \\ \dot{\underline{q}}_1 \end{bmatrix}^T \hat{S} \, \underline{u} + \underline{u}^T \hat{R} \, \underline{u} \right\} dt \qquad (43)$$

Equation (43) must be used instead of Eq. (35) to develop the discrete control performance measure Eq. (36).

As can be seen a cross product between $\underline{q}_1$ and $\underline{u}$ is now explicitly included in the performance measure. Furthermore, even though $\underline{q}_1$ is a reduced state, its order is still quite large. The solution of Eq. (43) as an optimal control problem requires extremely accurate numerical techniques. Furthermore when the solution has been achieved, there is still the problem of the control exciting the higher frequency modes. Notice that this design will require full state feedback (i.e., $\underline{q}_1$, $\dot{\underline{q}}_1$). This implies using measurements of m physical degrees of freedom, $\underline{x}^m$ and $\dot{\underline{x}}^m$. Then since

$$\begin{aligned} \underline{q} &= \Phi^T L \, \underline{x} \\ \underline{q}_1 &= [L_m] \, \underline{x}^m + F_m \underline{f} \end{aligned} \qquad (44)$$

where L_m denotes the restriction of the matrix $\phi^T L$ to an mxm matrix corresponding to those nodes $\underline{x}^m$ measured. No Kalman filter or observer is introduced by implementing this pseudo-full state measurement scheme.

The determination of L_m requires some explanation. In the order reduction described in Section II-3, the fact that the "fast" states (denoted by $\underline{q}_2$) were zero meant that

$$\underline{x} = \begin{bmatrix} \Phi_{11} & \underline{q}_1 \\ \Phi_{21} & \underline{q}_1 \end{bmatrix} \tag{45}$$

where $\underline{q}_1$ was the m vector of retained modes. Since $\Phi\ \Phi^T = I$ (as formulated in Eq. (20)), the full mode vector $\underline{q}$ is given by

$$\begin{bmatrix} \underline{q}_1 \\ \underline{q}_2 \end{bmatrix} = \Phi^T \underline{x} = \begin{bmatrix} \Phi_{11}^T & \Phi_{21}^T \\ \Phi_{12}^T & \Phi_{22}^T \end{bmatrix} \begin{bmatrix} \underline{x}_1 \\ \underline{x}_2 \end{bmatrix} \tag{46}$$

where $\underline{x}_1$ is an arbitrary subdivision of the node degrees of freedom whose dimension is the same as $\underline{q}_1$. Then, since our assumption for the order reduction was that $\ddot{\underline{q}}_2 \equiv 0$, which implies $\underline{q}_2 = (\Omega_2^2)^{-1}[\phi_{12}^T \phi_{22}^T]\ \underline{f} = U\underline{f}$

$$\Phi_{12}^T \underline{x}_1 + \Phi_{22}^T \underline{x}_2 = U\underline{f} \tag{47}$$

or

$$\underline{x}_2 = -(\Phi_{22}^T)^{-1}[\Phi_{12}^T \underline{x}_1 - U\underline{f}]$$

therefore

$$\underline{q}_1 = [\Phi_{11}^T - \Phi_{21}^T(\Phi_{22}^T)^{-1}\Phi_{12}^T]\ \underline{x}_1 + \Phi_{21}^T(\Phi_{22}^T)^{-1}U\underline{f} \tag{48}$$

Thus, if $\underline{x}_1$ is the measured degrees of freedom $\underline{x}^m$, L_m and F_m are given by

$$\begin{aligned} L_m &= \Phi_{11}^T - \Phi_{21}^T(\Phi_{22}^T)^{-1}\ \Phi_{12}^T \\ F_m &= \Phi_{21}^T(\Phi_{22}^T)^{-1}U \end{aligned} \tag{49}$$

The optimal control design for the structure defined above was developed in a sequence of four different designs, as follows:

- Rigid body control only; the resulting controller is then tested using the complete structural dynamic model to verify the rigid body control stability
- A continuous optimal control using only the momentum storage devices for control
- A discrete optimal control as in case 2
- A control design as in cases 2 and 3 which uses only a reduced order model; the resulting controller is again verified using the full dynamic model.

The table below summarizes the results for each of the designs.

RESULTS OF OPTIMAL CONTROL DESIGNS

	MODE NO.	OPEN LOOP		RIGID BODY		FULL STATE	
		ω(Hz)	ζ	ω	ζ	ω	ζ
RIGID MODES	YAW	2 REAL POLES-STABLE		.001	.715	.0008	.707
	ROLL	2 REAL POLES-UNSTABLE		.0018	.716	.0013	.712
	PITCH	.0001	0	.0019	.706	.0014	.714
FLEXIBLE MODES	1	.048	10^{-3}	RIGID BODY CONTROL ONLY – STABILITY OF STRUCTURAL MODES IS FUNCTION OF SENSOR LOCATIONS		.06	.425
	2	.055				.068	.342
	3	.06				.069	.048
	4	.084				.084	.02
	5	.092				.104	.002
	6	.103				.113	.435
	7	.109				.117	.309
	8	.113				.118	.01
	9	.116				.127	.02
	10	.123				.13	.29
	11	.131				.135	.002
	12	.148				.148	.003
	13	.152				.152	.004
	14	.154				.154	.2
	15	.174				.175	.05
	16	.2				.2	.006
	17	.226				.226	.05
	18	.26				.260	.047
	19	.269				.269	.006
	20	.271				.271	.021
	21	.306				.31	.004
	22	.308				.31	.030
	23	.324				.32	.014

As can be seen the gravity gradient is unstable in roll. To achieve the level of damping shown (critically damped rigid body and from 2×10^{-3} to 0.4 on various flexible modes) the control forces were not excessively large. For a typical response (the same as the open loop conditions shown in Figs. 9, 10, 11, and 12, where an impulsive force is applied to the solar array) the control torques are as shown in Fig. 13 (continuous control) and Fig. 16 (discrete control). As can be seen, no more than 8 ft. lbs of torque are required to control the vehicle and to damp the flexible mode vibrations created by the 20 ft. lb. aeroydnamic torque. The time response using both the continuous and discrete control at .2 second sample time are shown in Figs. 14 through 15 and Figs. 17 through 18. The time histories of the complete structure are shown in Figs. 19 and 20 for continuous (Fig. 19) and discrete control at 1 second sampling time (Fig. 20).*

The assumption that full state feedback is available is not overly restrictive. It is quite easy to implement this concept using strain gauges or an optical system for sensing the motion of the structural nodes. Since, for most applications, the noise equivalent strain is so low filtering is not necessary which eliminates the sensitivity of the control to the modal parameters introduced by a Kalman filter or an observer. A Kalman filter, by introducing notches at the modal frequencies, causes a sensitivity to the mode frequencies that outweighs its beneficial effects for the spillover of measurements from the truncated modes (see Section III-3).

7. EFFECT OF STRUCTURAL SIZE CHANGES ON CONTROL

We have investigated the stability of the OCDA space structure control system as its dimensions are rescaled while the feedback control matrix is held fixed, which corresponds to a spacecraft with increasing dimension using a fixed gain controller. The feedback matrix D is first calculated so that the system $\dot{\underline{x}} = A\underline{x} + B\underline{u}$, ($\underline{u} = D\underline{x}$) is optimal where $\underline{x}$ is the 52 vector of modal displacements, rates and rigid body angles, and rates. Then A, B are replaced by matrices corresponding to a structure all of whose linear dimensions are scaled by a factor L. We seek the value of L at which the system becomes unstable.

*These figures are frames from a 16mm sound movie that was produced during this contract. Copies of this film are available. Interested parties should contact the authors.

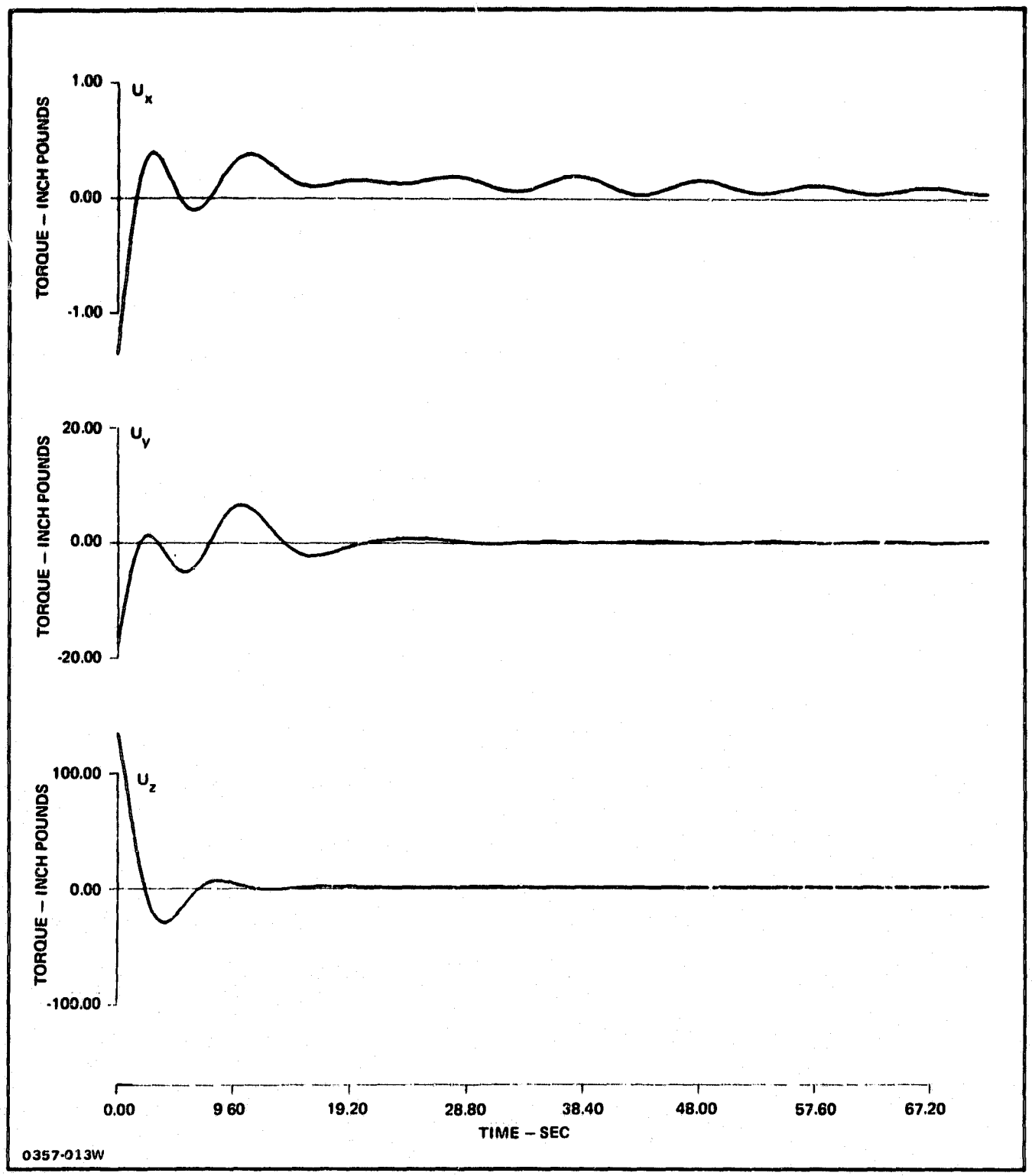

Fig. 13 Orbiting Constant Base – Closed Loop Continuous Control – Control Torques

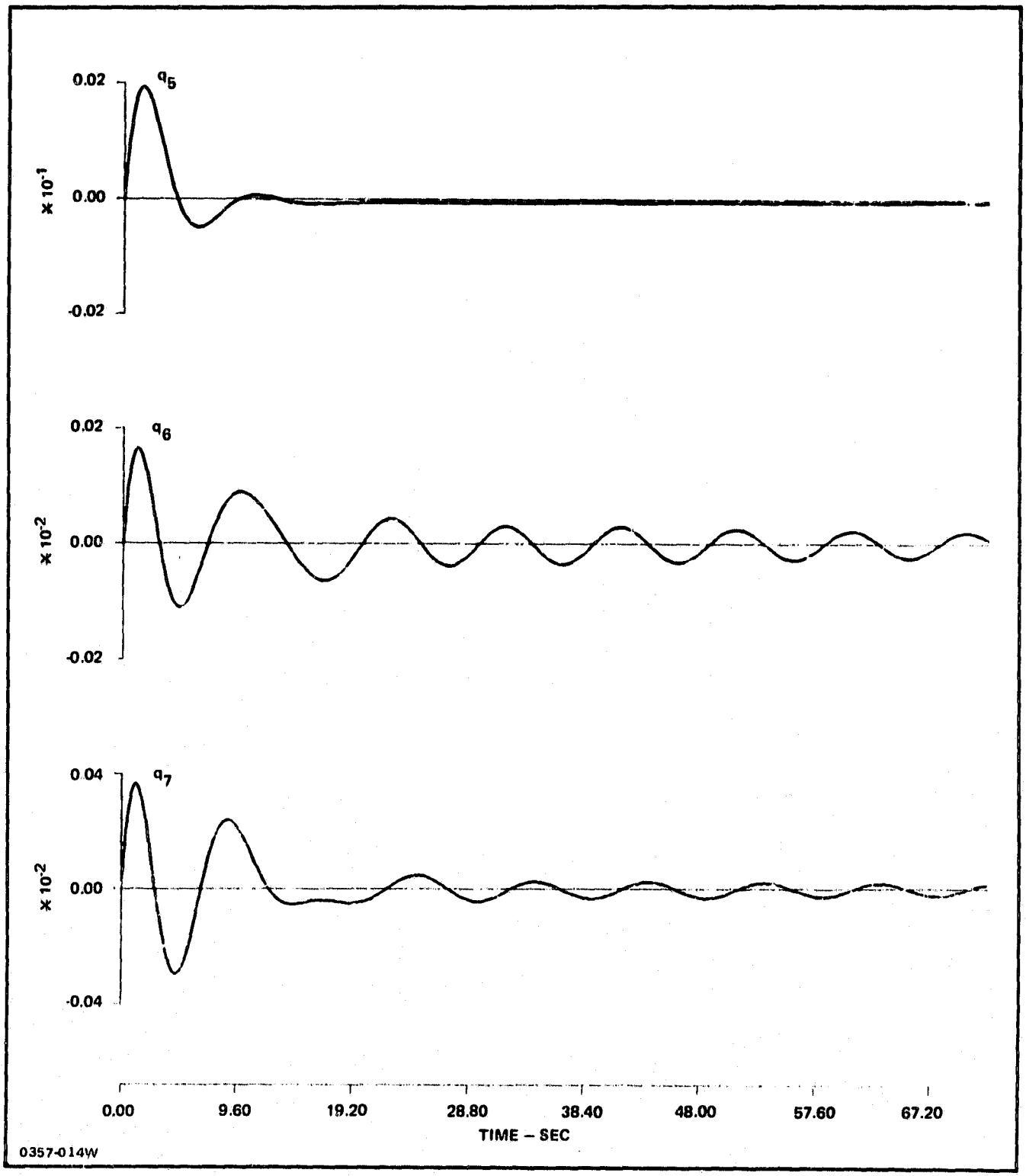

Fig. 14 Orbiting Constant Base – Continuous Control – Modes 5, 6 and 7 (Inches)

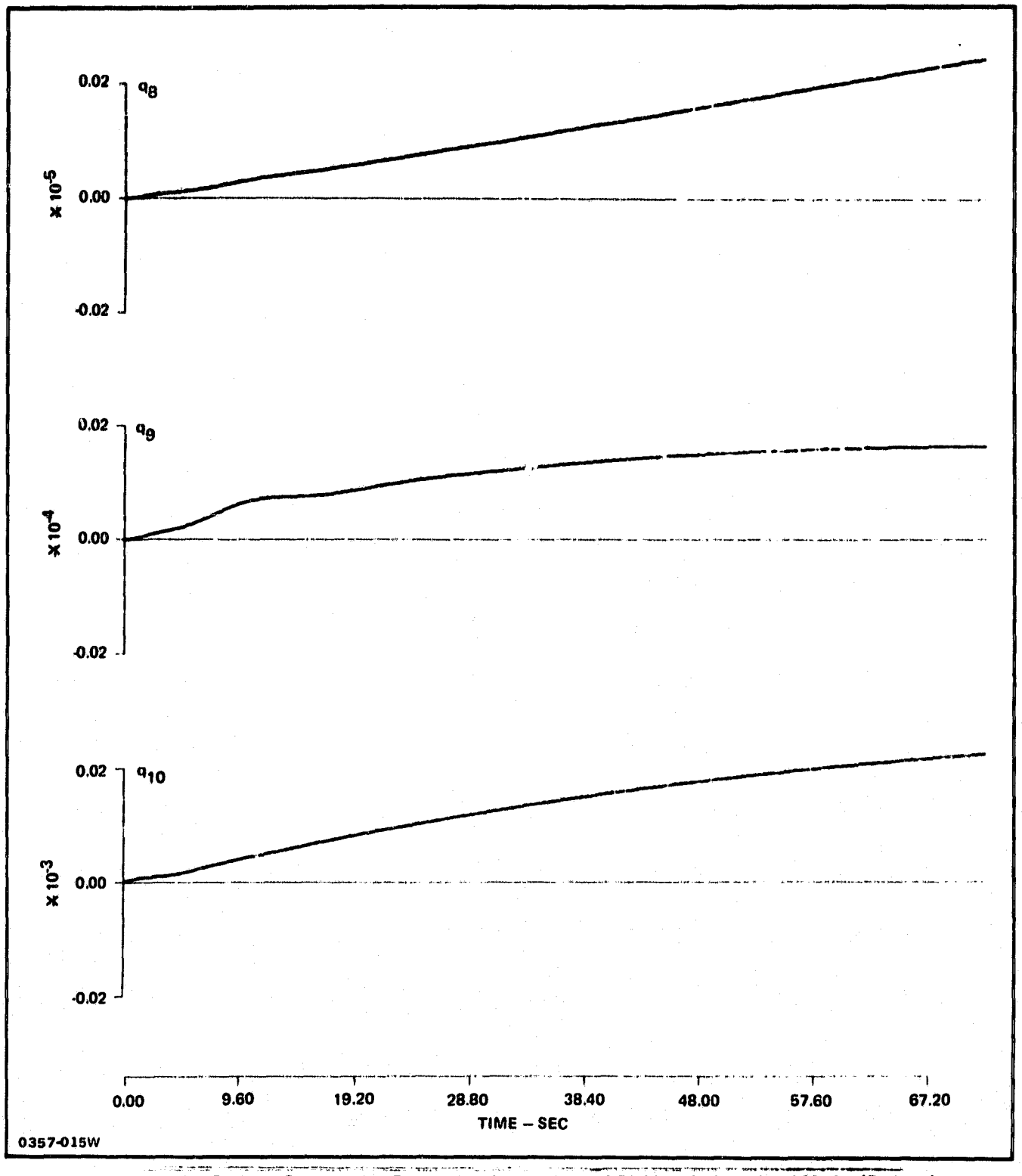

Fig. 15 Orbiting Construction Base – Continuous Control Rigid Body Rotational Modes (Radians)

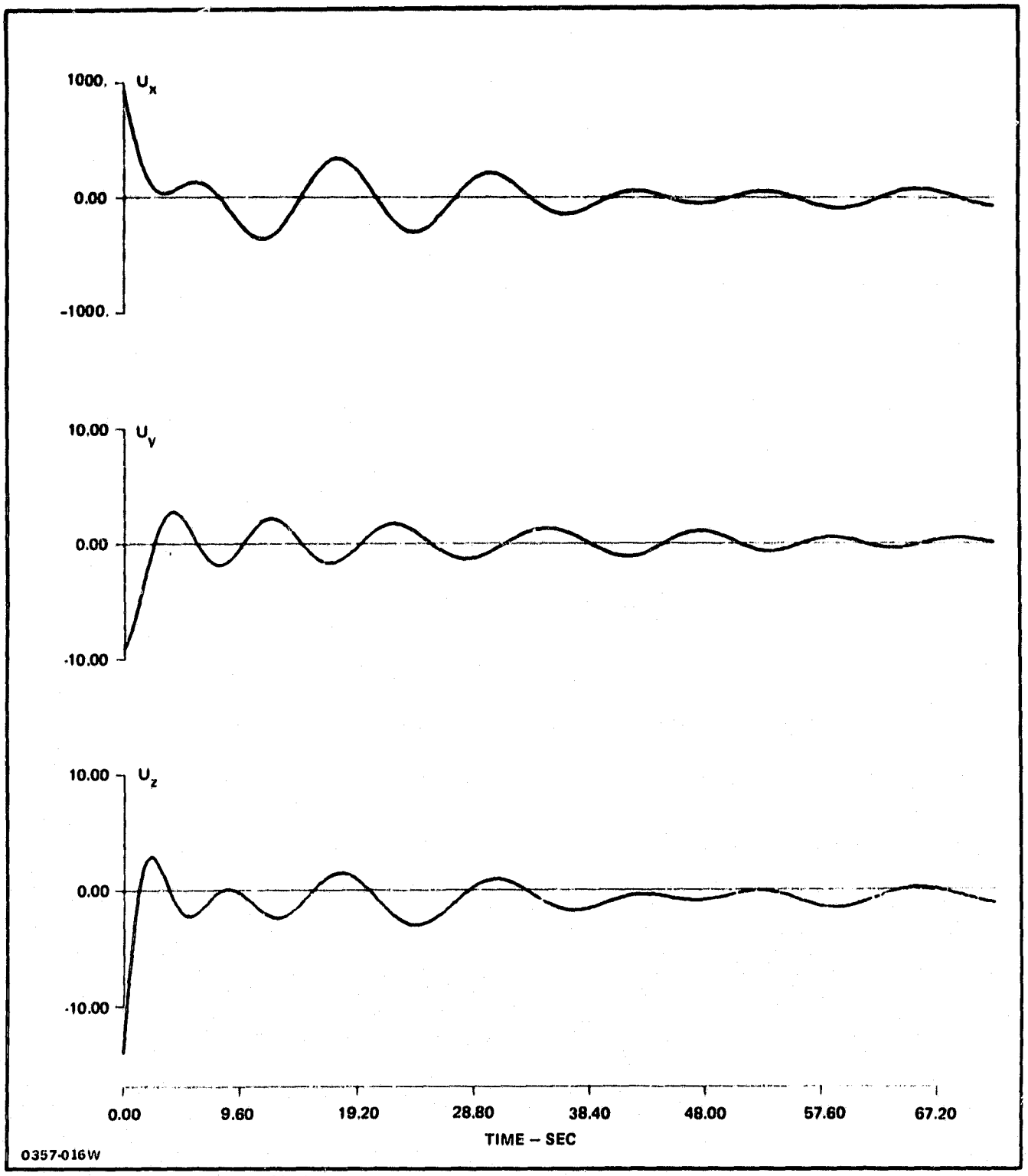

Fig. 16 Orbiting Construction Base – Closed Loop Discrete (0.2 Sec Sample Time) – Control Torques (Inch Lbs.)

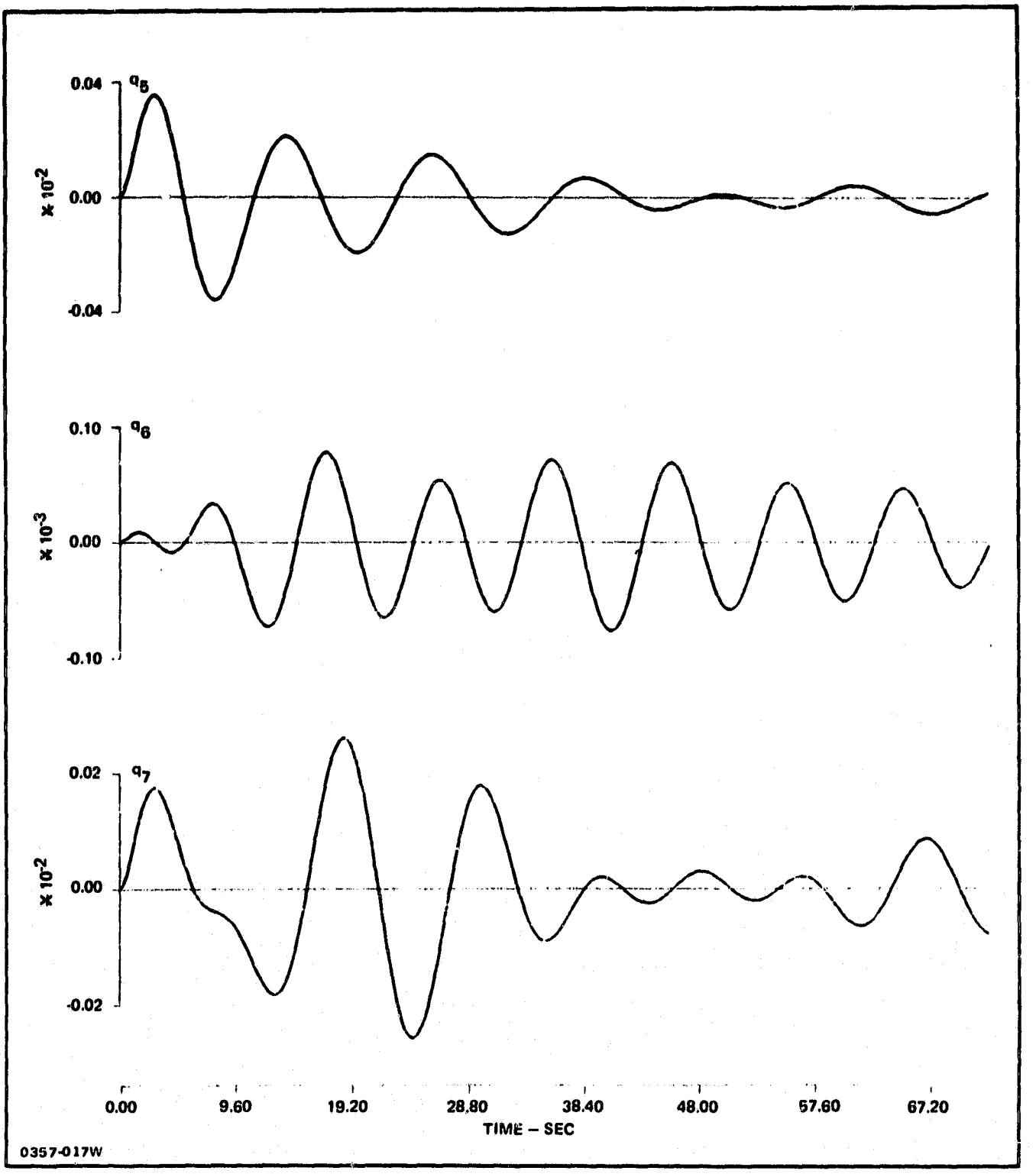

Fig. 17 Orbiting Constant Base – Sample Time 0.20 – Mode 5, 6 and 7 (Inches)

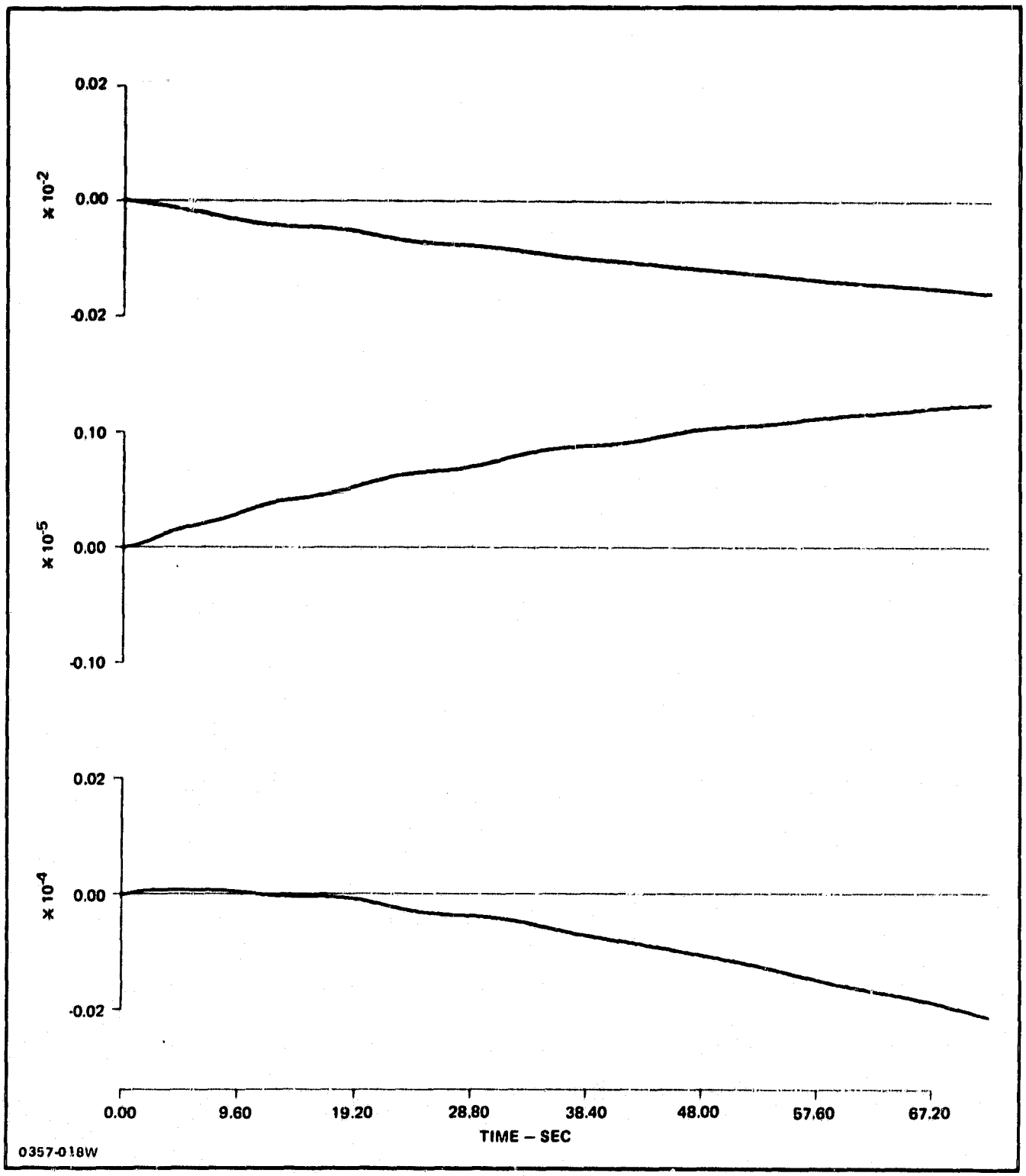

Fig. 18 Orbiting Construction Base – Sample Time 0.20 – Rigid Body Rotational Modes (Radians)

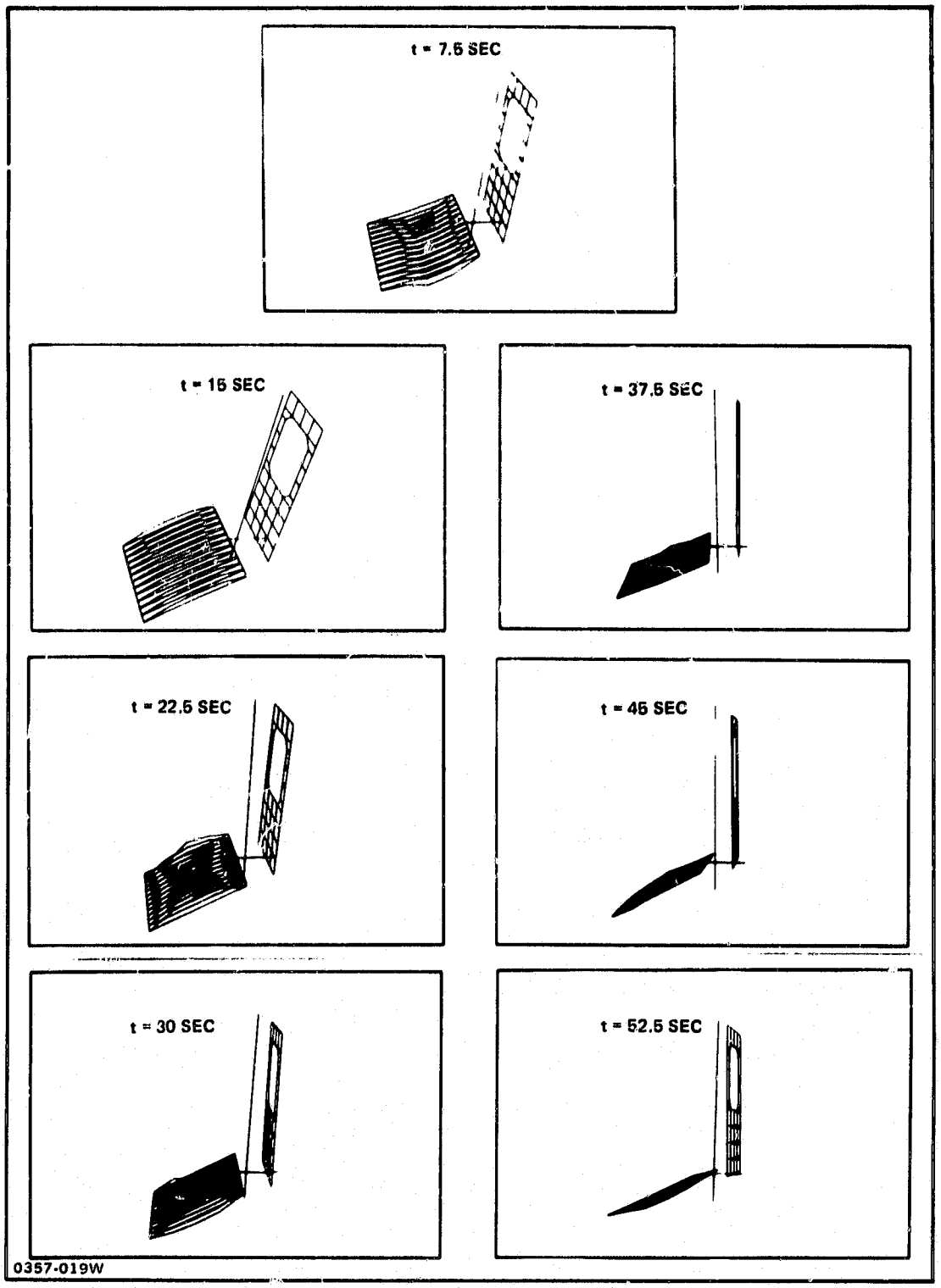

Fig. 19 Controlled, Continuous, Response of the OCDA

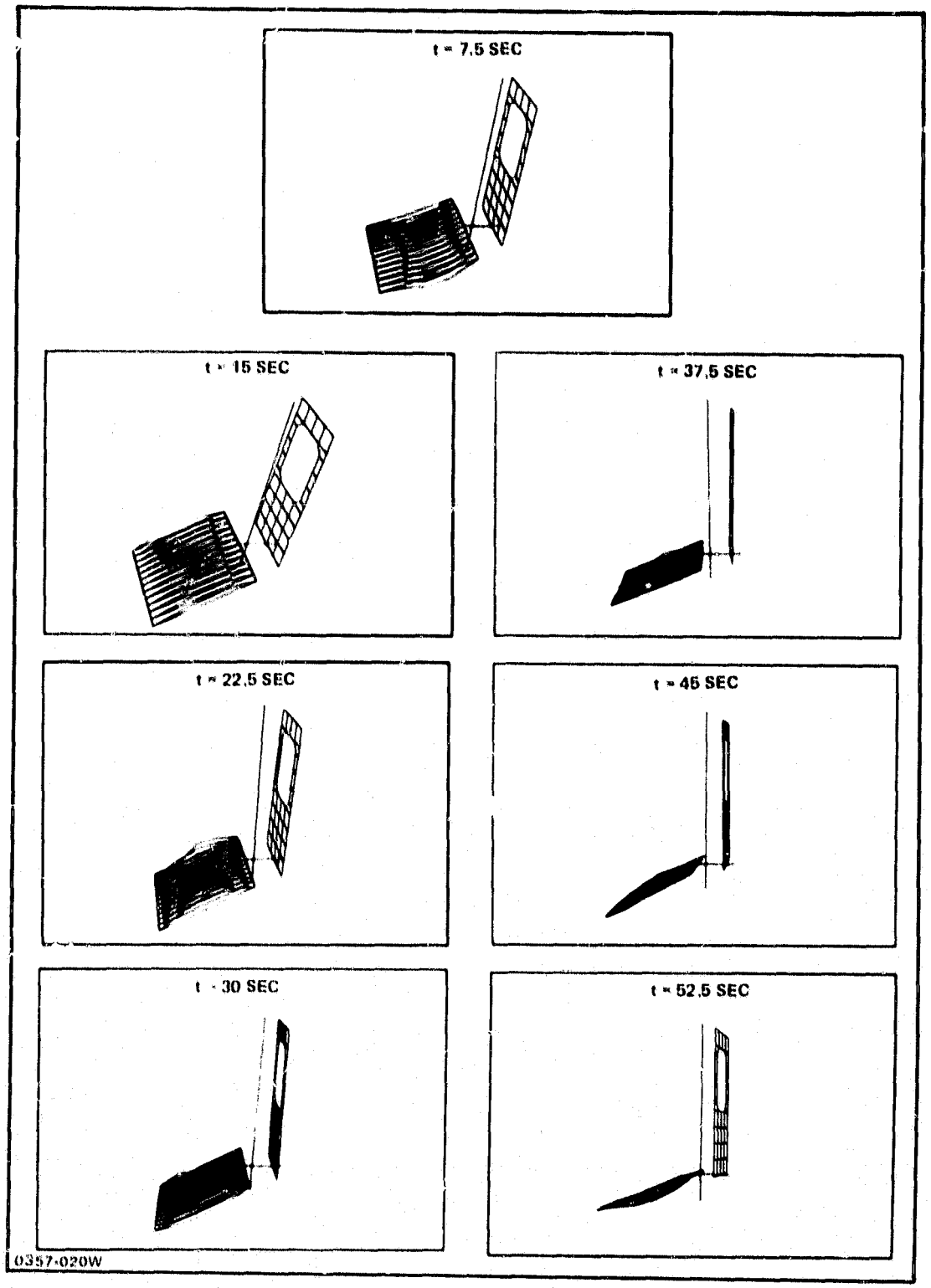

Fig. 20 Controlled, Discrete Time, 1 SEC Sample Time, Response of the OCDA

Recall that the OCDA is gravity gradient unstable and that D is determined by the rotations at the center of mass. The aerodynamic disturbance was assumed to be an impulse rather than a step. Our analysis employs 23 flexible modes. There are 18 translational modes whose generalized masses are scaled by a factor of L^3 as though they were true masses. The five remaining modes are rotations and their generalized masses correspond to torsion and are scaled by a factor of L^5, as though they were moments of inertia. This is also true of the rigid body rotation modes. The elements of the stiffness matrix are similarly multiplied by either L (bending) or L^3 (torsion). The three vectors of the mode matrix Φ that correspond to rigid body translations do not change because their nonzero elements are dimensionless. (We have been deleting these from our analyses in any case.) The linear nodes of the flexibility and rigid body rotation modes are scaled by L while the angular nodes are kept fixed. Note that although the impulsive aerodynamic drag increases by L^2, it plays no role in this analysis since it affects only the initial conditions for the state x. The gravity gradient torque is also affected by the scaling, but since these terms appear in the stiffness matrix they are automatically scaled by L^3.

Some root loci are shown in Fig. 21. It can be seen that instability occurs at L = 2.4 (Fig. 21a) and for the design which ignores the flexible motion (rigid body only), the system is stable for L up to 5.2 (Fig. 21b). In both cases the instability is caused first by the rigid body/gravity gradient going unstable. The structural mode that goes unstable is the same in each case but occurs at a larger L for the case of full state feedback. Thus we can conclude that the optimal designs are reasonably insensitive to variations in the structural size.

8. RIGID BODY CONTROL FOR PRECISION POINTING

The problem of precise control of the vibration of a system and the control of the rigid body are incompatible problems. To control vibration requires a wide band system while the usually high noise on the attitude sensor relative to the rate sensor tends to make the bandwidth of the attitude loop very small. This suggests that a hierarchy of control loops should be designed - the first loop a narrow band attitude loop, the second loop a wider band rate loop that controls the rigid body rate and the final loop a rapid moving (wide band) loop that achieves vibration control. We describe in this section how the first of

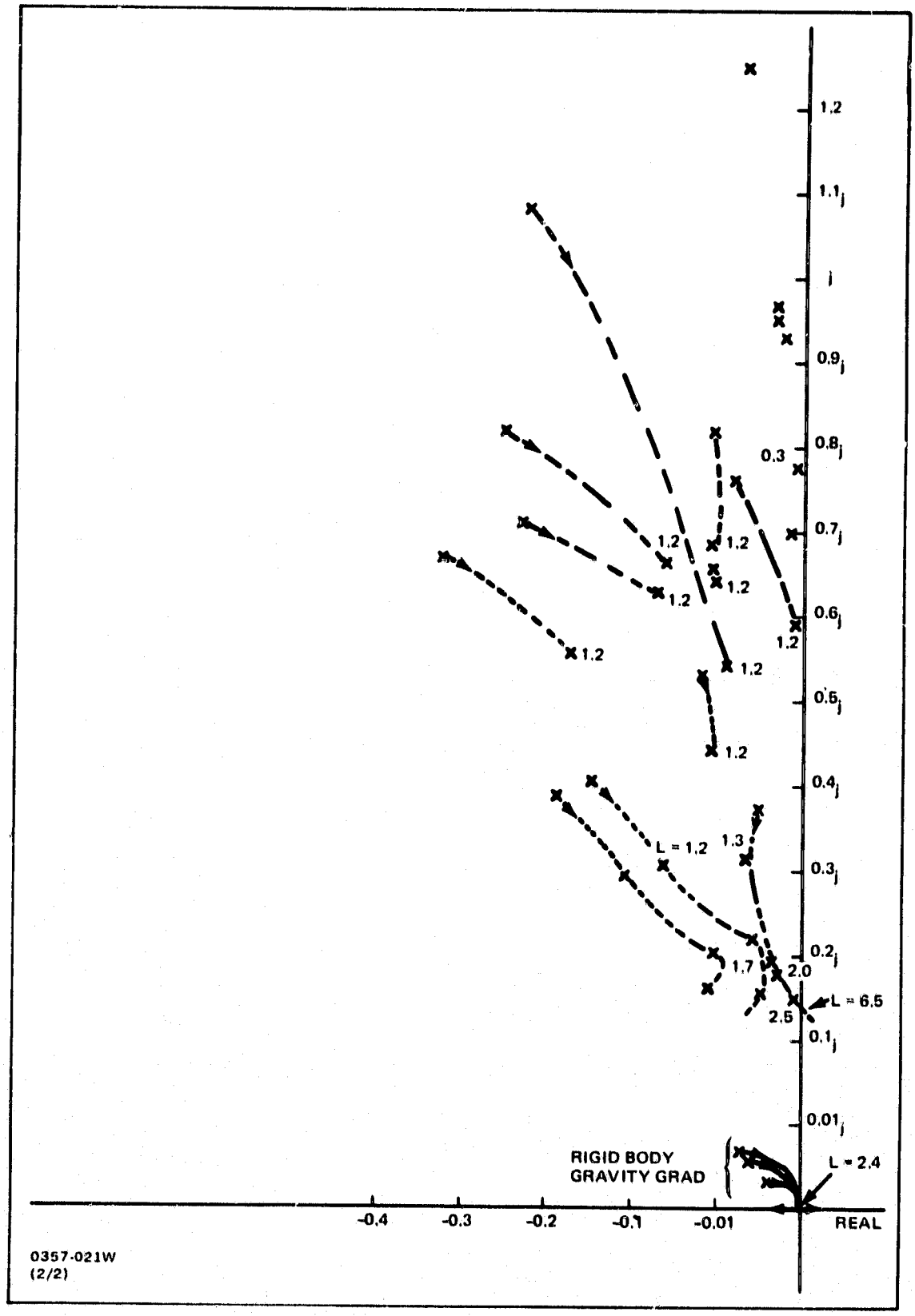

Fig. 21(a) Root Locus Plot For Optimal Control (Full State) As Size (L) Varies

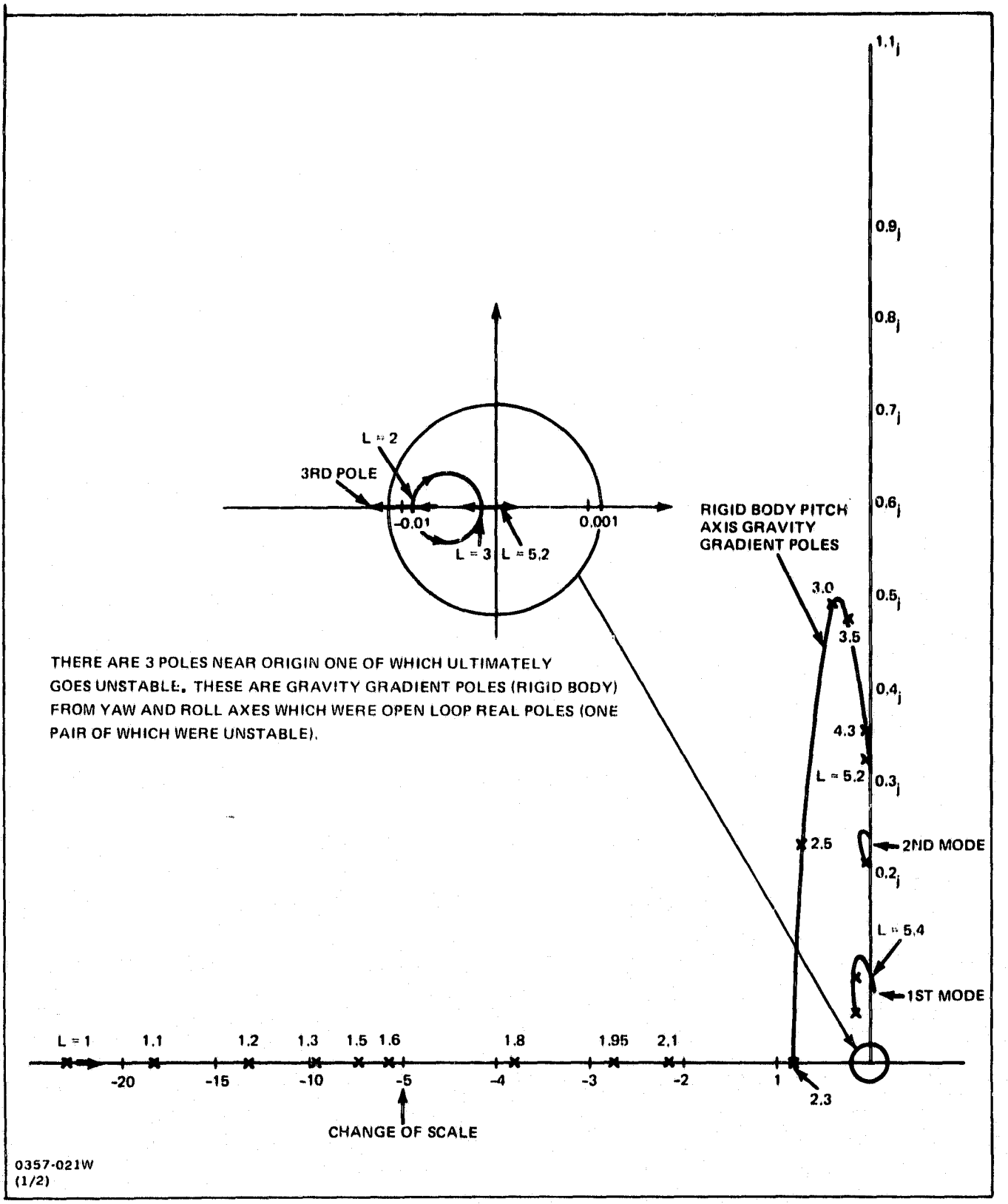

Fig. 21(b) Optimal Rigid Body Control Design – Root Locus As Size (L) Increases

these loops - the attitude control loop can be designed around the second rate control loop. First, however, we show that the rate sensor noise relative to the attitude sensor noise determines the bandwidth of the attitude loop.

When sensor noise and external system noise are both exciting the control loop, the design of the control system requires that an estimator (a Kalman filter) be designed to provide the best estimate of the rotational rigid body states. Consider the rigid body dynamics given by

$$\dot{\underline{x}} = \begin{bmatrix} 0 & 1 \\ 0 & 0 \end{bmatrix} \underline{x} + \begin{bmatrix} 0 \\ \sigma_w/I \end{bmatrix} w \qquad (50)$$

$$\underline{y} = \underline{x} + \underline{n}$$

that is, the rigid body dynamics are $I\ddot{\theta}$ = noise where in Eq. (50) $x_1 = \theta$, $x_2 = \dot{\theta}$, I is the inertia of the rigid body axis and the measurement $\underline{y}$ is a measurement of attitude and rate with additive noise $\underline{n}$. We assume that the noises w, n_1 and n_2 are white with variances σ_w^2, σ_1^2 and σ_2^2, respectively.

The continuous time Kalman filter is given by

$$\dot{\hat{\underline{x}}} = \begin{bmatrix} 0 & 1 \\ 0 & 0 \end{bmatrix} \hat{\underline{x}} + K(\underline{y} - \hat{\underline{x}}) \qquad (51)$$

where $K = P M^T R^{-1}$

and

$$\dot{P} = \begin{bmatrix} 0 & 1 \\ 0 & 0 \end{bmatrix} P + P \begin{bmatrix} 0 & 0 \\ 1 & 0 \end{bmatrix} + \begin{bmatrix} 0 & 0 \\ 0 & \sigma_w^2/I \end{bmatrix}$$

$$-P \begin{bmatrix} 1/\sigma_1^2 & 0 \\ 0 & 1/\sigma_2^2 \end{bmatrix} P$$

The significant aspect of the filter is what it does to the control system when it is inserted in the control loop. It is well known (See Ref. 7) that the closed loop system with a filter in the loop has closed loop poles which are those of the optimal system cascaded with those of the filter. Thus, the bandwidth of

the closed loop system will be that of the optimal control if the filter bandwidth is greater than the control. If the filter bandwidth is smaller than the optimal control, then the closed loop response is dominated by the filter. To determine the poles of the filter (Eq. (51)), we use Potters method on Eq. (50). Thus, the filter poles are the left hand plane eigenvalues of the 4 x 4 matrix

$$\begin{vmatrix} 0 & 0 & +1/\sigma_1^2 & 0 \\ +1 & 0 & 0 & +1/\sigma_2^2 \\ 0 & 0 & 0 & +1 \\ 0 & \sigma_w^2/I & 0 & 0 \end{vmatrix} \tag{52}$$

These eigenvalues may be determined analytically as the solutions of the characteristic polynomial of Eq. (52). This polynomial is

$$\lambda^4 - \lambda^2 \left(\frac{\sigma_n}{I\sigma_2} \right)^2 + \left(\frac{\sigma_w}{I\sigma_1} \right)^2 = 0$$

which has roots

$$\lambda_{1,3} = \pm \frac{\sigma_w \sqrt{2}}{2I\sigma_2} \left\{ 1 + \sqrt{1 - 4\left(\frac{I\sigma_2^2}{\sigma_1 \sigma_w} \right)^2} \right\}^{1/2}$$

$$\lambda_{2,4} = \pm \frac{\sigma_w \sqrt{2}}{2I\sigma_2} \left\{ 1 - \sqrt{1 - 4\left(\frac{I\sigma_2^2}{\sigma_1 \sigma_w} \right)^2} \right\}^{1/2} \tag{53}$$

where λ_1 and λ_2 are the left half plane poles (with the minus sign). To characterize the bandwidth of the filter, the following parameters are introduced. Let S_r (the signal to noise ratio for the rate sensor) be $\sigma_w/I/\sigma_2$ and let ρ (the ratio of the attitude sensor noise to the rate sensor noise) be σ_1/σ_2. Then

$$\lambda_1 = -\sqrt{2}/2 \; S_r \left\{ 1 + \sqrt{1 - 4/(S_r\rho)^2} \right\}^{1/2}$$

$$\lambda_2 = -\sqrt{2}/2 \; S_r \left\{ 1 - \sqrt{1 - 4/(S_r\rho)^2} \right\}^{1/2} \tag{54}$$

Figure 22 shows the root locations for various conditions of S_r and ρ. The situation in Fig. 22a is the critical one. It describes the case when ρ is large, i.e., when the attitude noise is larger than the rate sensor noise. For a typical precision rate gyro and star tracker, the ratio ρ is on the order of 100 which is clearly the case of Fig. 22a. Thus, the bandwidth for the attitude control loop is determined by the filter pole near the origin. In other words, the settling time for the attitude loop is determined by the time it takes to determine the attitude from the rate measurement. Since this is the case, an attitude control system should be designed that uses rate sensors for the basic control and the attitude control loop should provide rate commands. When this is done it becomes possible to also estimate some of the rate gyro parameters.

The basic function of any onboard attitude control system is to maintain constant LOS of the spacecraft axes. Ideally, it should be free of long-term drifts and jitter, and steerable by ground command. To determine the degree to which these ideal characteristics can be achieved, and by what techniques, a baseline approach to the control, determination, and parameter calibration problem is proposed and analyzed. By considering a generic design such as the one proposed, it is possible to identify the specific sources of LOS error and to propose and evaluate techniques for their compensation.

The proposed design utilizes rate stabilization with a three-axis strapdown gyro package coupled with a set of coarse and fine reaction wheels. The stabilization loop recieves ground commands of the required rates it must hold constant, with respect to inertial space, and the period over which they must be held. This system is an onboard velocity feedback loop which can respond rapidly and the position loop is closed through the ground, using an onboard star sensor. The position loop can be closed through a ground loop because of its very low bandwidth as described above. Figure 23 depicts the essential elements of the proposed approach. The dashed portion represents the onboard stabilization loop, the remaining portion represents the ground-based position loop.

Four reference frames are used to characterize the system's operation. The inertial frame, I, is fixed with respect to inertial space. The orbital frame, O, is defined to have axes which are local vertical, orbit tangential, and normal to the orbital plane. The computational frame, C, is defined in terms of the orbital frame and represents the desired location of the vehicle's

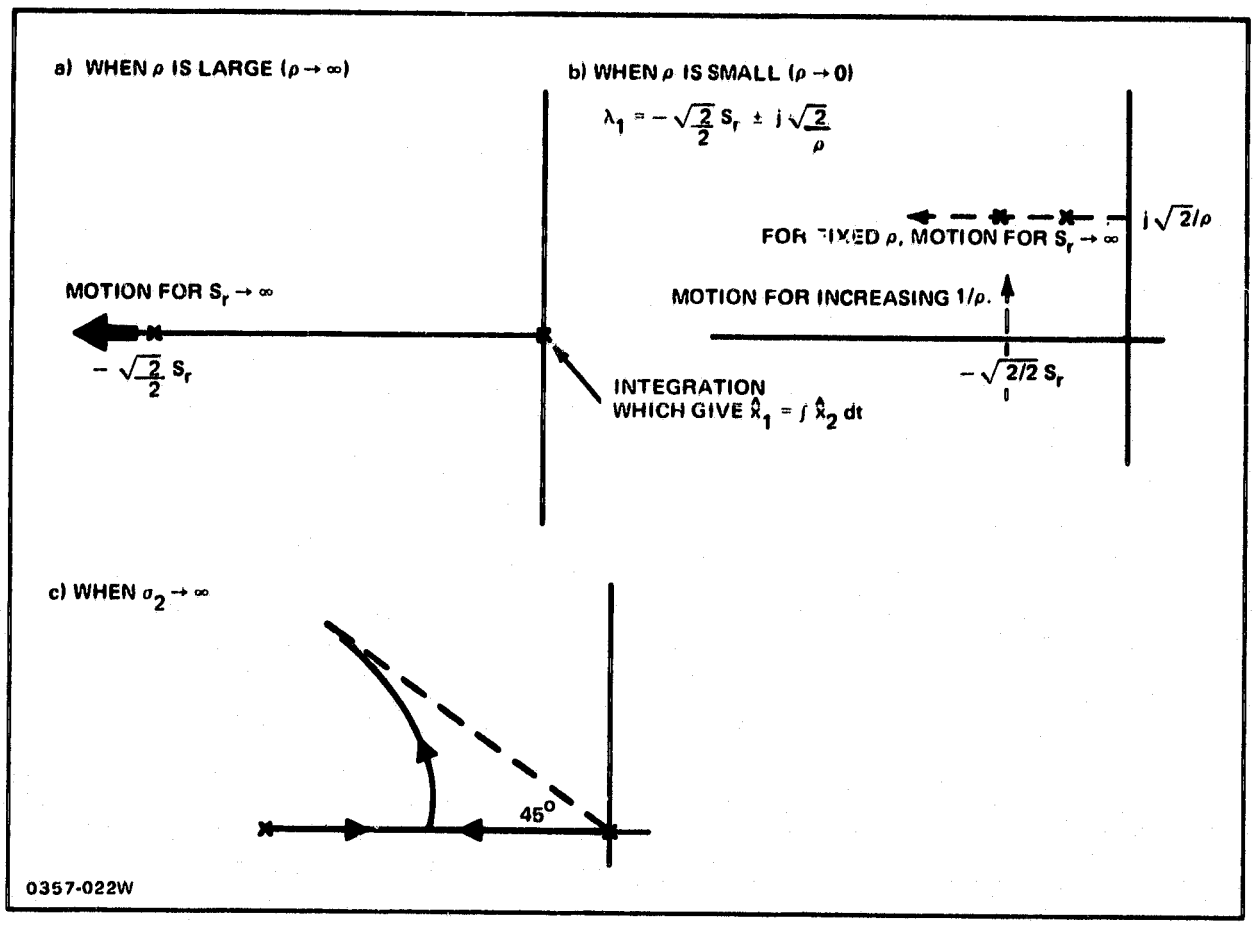

Fig. 22 Pole Locations of Kalman Filter as Function of Sensor Noise and System Noise

body frame, B. Ideally, the B and C frames should be coincident. Attitude misalignment is measured by the small angle misalignment vector, Ψ, between B and C frames (Ψ is the three-vector about which a rotation of $|\Psi|$ radians by computational frame C will bring the B and C frames into coincidence).

In Fig. 23 a commanded rate to the computational frame is generated, ω_{IC}^{C} (for an earth pointing mission this will be earth rate). This command is sent to the stabilization loop and held. The star data, while the rate is held by the stabilization loop, are transmitted to the ground via a radio link, and sent to the star-track preprocessor. The star-track preprocessor collects data from a known star for one stabilization loop sample time (on the order of 30 seconds) and estimates the position $S^{B}(t^{*})$ of that star in the star tracker at time t^{*}. The star-position generator also computes the nominal position for the same star, assuming perfect alignment of the B and C frames.

Any difference between the two star positions is a measure of the misalignment between the two frames. This information is fed to a Kalman filter, which estimates the misalignment between the two frames, $\Psi(t)$, and at the same time, updates the values of any observable system biases.

The misalignment information serves a dual purpose. It is sent to the ground mission processor to update current LOS information, and it is also used, when desired, to provide a correction rate command, which is added to the nominal command transmitted to the spacecraft. The corrective rate will drive the current misalignment to zero in a fixed amount of time.

There are three categories of errors which, if uncompensated, will cause the LOS to diverge; they are all of the bias or slowly varying parameter variety; errors in the gyro package, such as bias, scale factors, and input-axis misalignment; errors in the sensor system alignment; and errors in orbit determination and star position. These can all be included in the state of the Kalman estimator. The more-stable errors can be estimated infrequently in a batch mode; the more unstable ones, such as gyro bias, are estimated on-line along with the misalignment vector, Ψ. The results of a detailed covariance analysis of the star-track preprocessor and Kalman filter estimator for a six-state implementation that predicts the achievable level of performance are described below.

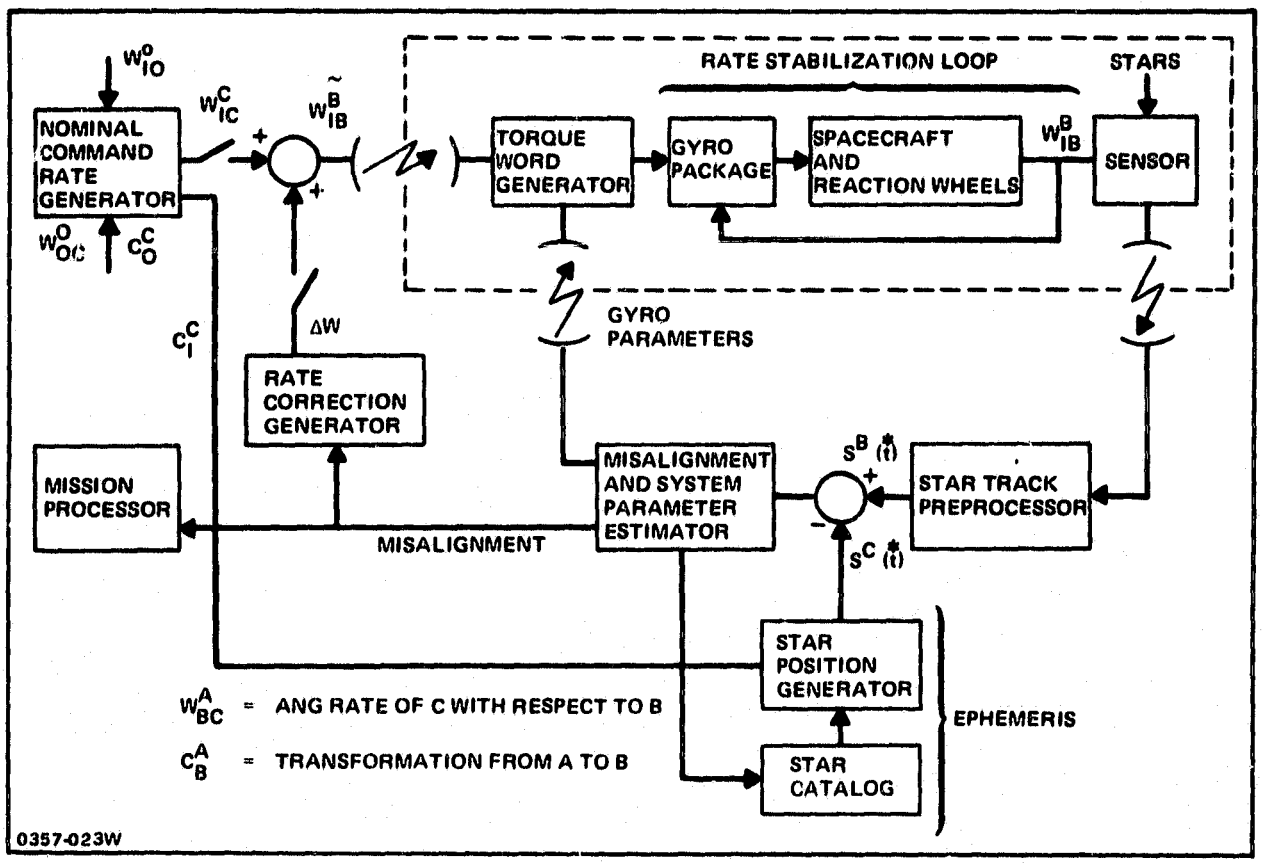

Fig. 23 Attitude Determination and Control

The jitter portion of the LOS has its source in the onboard stabilization portion of the system. The main noise sources are the gyro output noise, stabilization loop electronic noise, and reaction wheel torque noise. These noise sources must be suppressed through the wide band stabilization loop control system and the dynamics of the spacecraft.

A covariance analysis was performed with all of the above noise sources as the excitation. In this analysis, we took advantage of the fact that the shape of the output time history from a star detector depends only on the path of the star point-spread function as it traverses the star sensor detectors, since the intensity remains constant throughout the traversal. In the analysis, we assumed that the star track is completely characterized by a straight line at a known velocity with known point-spread function. Hence, an initial x_o, z_o coordinate pair and a reference angle measured from a line defined by the locus of the star completely determine the output signal. Assuming the electrical characteristics are known, and the point-spread function is an azimuthally symmetric gaussian function, the estimate of the initial star position (and angle) is a recursive update using successive sensor outputs. The covariance analysis results tend to be insensitive to slight modeling inaccuracies.

Given a single voltage measurement at specified location on the sensor (a sensor node), $\{\bar{v}_i\}$, from the previous a priori knowledge we know the least-squares linearized solution for the corrections of the track parameters to be given by

$$\begin{pmatrix} \Delta x \\ \Delta z \\ \Delta\theta \end{pmatrix} = CH^T R^{-1}(\Delta V) \tag{55}$$

where H^T is a 3 by n matrix given by the transpose of the n by 3 measurement sensitivity matrix, H,

R is the n by n covariance matrix of n voltage measurements, assumed diagonal and proportional to the identity matrix, and

(ΔV) is a column vector composed of the n measurement differences, $(v_i - \bar{v}_i)$:

$$H = \begin{bmatrix} \frac{\partial V_1}{\partial x_o} & \frac{\partial V_1}{\partial z_o} & \frac{\partial V_1}{\partial \theta_o} \\ \vdots & \vdots & \\ \frac{\partial V_n}{\partial x_o} & \frac{\partial V_n}{\partial z_o} & \frac{\partial V_n}{\partial \theta_o} \end{bmatrix} \tag{56}$$

$$C = (H^T R^{-1} H)^{-1}$$

where C is also the covariance matrix for the estimate of the three-component state vector. The square roots of the diagonal elements of C, then, give the uncertainties of the x_o, z_o and ϕ_o parameters of the star track.

It can be shown that when each additional node measurement is combined with the current estimate to obtain a better state estimate, the covariance matrix relation is given by the recursive equation

$$C_{k+1}^{-1} = C_k^{-1} + H^T R^{-1} H \tag{57}$$

where C_k^{-1} is the inverse of the previous covariance matrix obtained before the new measurements are used.

Computer analyses have been performed to determine the dependence of the covariance matrix on the relative star-track geometry. As might be expected, the worst uncertainty in position occurs in the z_o estimate, the direction nearly perpendicular to the star track. If the star image continues to traverse successive sensor nodes with near-zero inclination angle, the z_o coordinate becomes nearly unobservable. In this geometry, all of the output signals will be nearly the same for all paths slightly displaced in z from the nominal path. By tilting the star tracker slightly this unobservability quickly disappears as can be seen in Fig. 24.

For a relative star tracker angle of 7 deg, the final standard deviation in the estimate of z_o for a 30-second star-track traversal is on the order of 0.05 mil, and somewhat smaller for x_o. This result assumes a peak signal-to-rms-noise ratio of 10:1. Hence, it seems that the nominal 30-second-duration collections of data will provide sufficient high-fidelity pseudo measurements

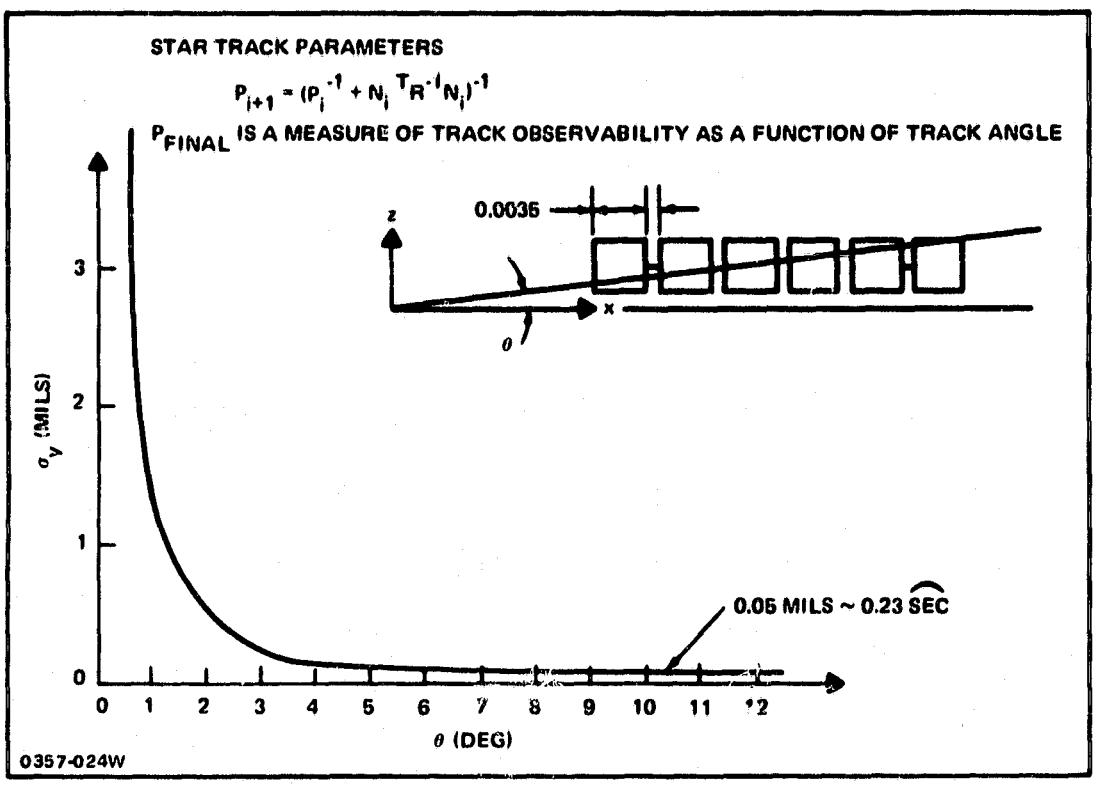

Fig. 24 Pseudomeasurement Performance

to the Kalman filter processing stage for the more time consuming attitude determination/bias parameter estimation function.

The function of the processing segment described above is to determine a measurement that can be used to precisely determine the attitude of the spacecraft and provide the necessary information for any subsequent attitude control corrections of unwanted drifts. A natural byproduct, which is necessary to achieve high-precision results, will also be the estimation ("learning") of at least three different types of system biases. This set of parameters consists of (1) the three-gyro drift rate biases, (2) the misalignments between the rate gyro package axes and the nominal body coordinate system axes (each axis misalignment being characterized by two direction cosines) and (3) the three torquer biases, which will effectively characterize the biases in the onboard rate stabilization segment.

If we define the three vector, ω_{IB}^{B}, to be the angular velocity of the body frame with respect to the inertial frame, expressed in the body-frame coordinates (hence, the superscript), we can write the continuous state equation expressing how the misalignment vector, Ψ behaves with time. Before writing the equation, it should be emphasized that the misalignments are infintessimal. Hence, the state equation will always have at least one error source, even if the system model were perfect. Furthermore, it is assumed that the differences between the actual and nominal rates remain small. The state equation, then, for the misalignment vector becomes

$$\dot{\Psi} = F(\omega_{IC}^{C}) \quad \Psi + \omega_{IB}^{B} - \omega_{IC}^{C} + \text{noise} \tag{58}$$

where F is the skew-symmetric matrix

$$F(\omega) = \begin{bmatrix} 0 & \omega_3 & -\omega_2 \\ -\omega_3 & 0 & \omega_1 \\ \omega_2 & -\omega_1 & 0 \end{bmatrix} \tag{59}$$

When the relation between ω_{IB}^{B} and the commanded (nominal) rates to the onboard gyro package is modeled with unknown biases, the expanded state equations can be shown to assume the following form:

$$
\begin{aligned}
\dot{\Psi} &= F(\omega_{IC}^{C})\ \Psi + B + \Gamma_{\gamma}\gamma + \Gamma_{s}\, s + \text{noise} \\
\dot{B} &= 0 + \text{noise} \\
\dot{\gamma} &= 0 + \text{noise} \\
\dot{s} &= 0 + \text{noise}
\end{aligned}
\tag{60}
$$

where B is the three-vector of gyro biases, γ is a six-component state vector expressing the gyro misalignments, and s is a three-vector expressing the torquer biases, and Γ_{γ}, Γ_{s} are the effect of these on the misalignment vector.

To construct the Kalman filter, it is also necessary to define the relationship between the observable star position pseudomeausrements and the state to be estimated. This equation can be given by

$$\Delta X = M\Psi + n$$

where ΔX is the error in the pseudomeasurement two-vector, and is due only to the first three components of the state vector, i.e., the misalignment vector, Ψ, and n is the pseudomeasurement noise whose covariance is provided by least squares inverse above. The measurement sensitivity matrix, M, is given by

$$M = \begin{bmatrix} 0 & -z_{o} & f \\ -f & x_{o} & 0 \end{bmatrix} \tag{61}$$

where x_{o}, z_{o} is the star pseudomeasurement position and f is the effective focal length of the star sensor.

We performed a preliminary covariance analysis, assuming that only the gyro bias three-vector is to be estimated with the Kalman filter. For the six-component state vector, consisting of the misalignment vector and the gyro biases, the discrete solution for the covariance propagation is given by

$$
\begin{aligned}
M_{n+1} &= \phi P_{n} \phi^{T} + Q \\
P_{n+1} &= (I - K_{n}H_{n})M_{n}(I - K_{n}H_{n})^{T} + K_{n}R_{n}K_{n}^{T}
\end{aligned}
\tag{62}
$$

where $K_{n} = M_{n}H_{n}^{T}(H_{n}M_{n}H_{n}^{T} + R_{n})^{-1}$

Here ϕ is the transition matrix given by:

$$\phi = e^{A_2 \Delta t_2}$$

where

$$A = \left[\begin{array}{c|c} F(\omega_{IC}^{C}) & I \\ \hline 0 & 0 \end{array}\right] \qquad (63)$$

and Δt is the filter cycle time, nominally 30 seconds. Note that ϕ does not change with each update since ω_{IC}^{C} is assumed to be held at some constant value during all mission maneuvers. Returning to the above equations, Q is the six by six covariance matrix expressing the plant uncertainties, P_n is the previous updated covariance matrix, M_{n+1} is the extrapolated covariance matrix before updating with the current pseudomeasurements, and P_{n+1} is the current updated covariance matrix after accounting for the current pseudomeasurements, whose covariances are given by R. The H_n matrix is the same function of the current pseudomeasurements defined above.

The main features of the results of our preliminary analysis are shown in Fig. 25. For the analysis, a gyro drift rate of 0.01-deg-per-hour-per-day was assumed, not an unreasonably demanding requirement. Using only a single star in the FOV of the star tracker at any given time, the upper graph of Fig. 25 shows an excellent transient response for the two sensitive coordinate axes misalignments. The third axis will require about 6-hours before comaprable performance is achieved. In the lower graph of Fig. 25, the drift rate error is seen to achieve 0.01-deg-per-hour within an initial 15-minute time interval.

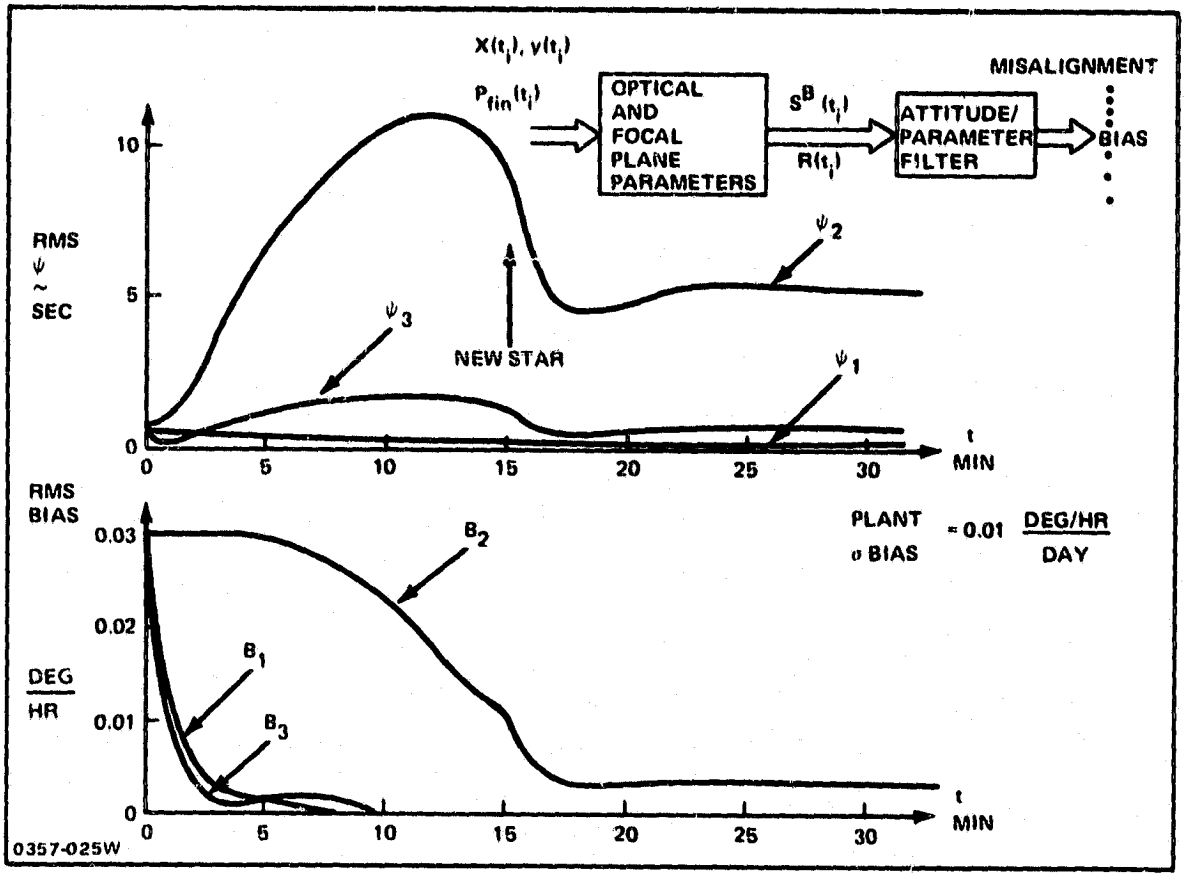

Fig. 25 Attitude-Determination-Filter Performance

III. THEORETICAL QUESTIONS FOR CONTROL OF LARGE SPACE STRUCTURES

1. ORDER REDUCTION PROBLEMS

The fact that the differential equation that result from finite element modeling represents undamped harmonic oscillators means that Eq. (7) is never exactly satisfied at any time.* This is quite distinct from the normal singular perturbation approach which we formally used above where the reduced solution matches the actual solution to the full set of differential equations for times t which are away from the boundary. The reason this convergence is not valid for the finite element method is that there is no damping. A simple 2 mass model can be used to illustrate this point. Figure 26 shows the model for a simplified 2 mass example. With the parameters given, the "finite element" model becomes

$$\begin{bmatrix} 100 & 0 \\ 0 & 343.8 \end{bmatrix} \begin{bmatrix} \ddot{x}_1 \\ \ddot{x}_2 \end{bmatrix} = - \begin{bmatrix} 1780 & -1780 \\ -1780 & 4194.4 \end{bmatrix} \begin{bmatrix} x_1 \\ x_2 \end{bmatrix} + \begin{bmatrix} f_1 \\ f_2 \end{bmatrix} \tag{64}$$

The result of transforming via the Cholesky factor of M (since M is diagonal $L = \begin{bmatrix} 10 & 0 \\ 0 & 18.54 \end{bmatrix}$) is (see Eq. (20))

$$\begin{bmatrix} \ddot{z}_1 \\ \ddot{z}_2 \end{bmatrix} = - \begin{bmatrix} 17.8 & -9.6 \\ -9.6 & 12.2 \end{bmatrix} \begin{bmatrix} z_1 \\ z_2 \end{bmatrix} + \begin{bmatrix} 0.1 & 0 \\ 0 & 0.054 \end{bmatrix} \begin{bmatrix} f_1 \\ f_2 \end{bmatrix} \tag{65}$$

*The matrix Φ in Eq. (7) is a transformation that supposedly gives all of the components of $\underline{x}$ in terms of the modes $\underline{q}$. When $\underline{q}$ is truncated, the harmonic motion of the ignored modes never damps, so $\underline{x}$ is never correct.

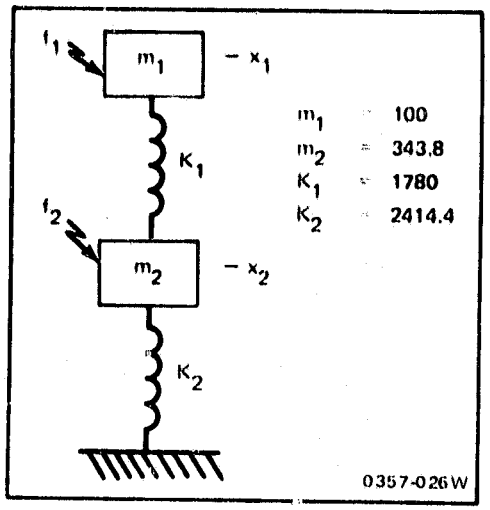

Fig. 26 Simple Example

and if

$$\underline{q} = \begin{bmatrix} 0.6 & 0.8 \\ 0.8 & -0.6 \end{bmatrix} \qquad \underline{z} = \Phi \underline{z}$$

then Eq. (65) becomes

$$\ddot{\underline{q}} = \begin{bmatrix} -5 & 0 \\ 0 & -25 \end{bmatrix} \underline{q} + \begin{bmatrix} 0.06 & 0.043 \\ 0.08 & -0.032 \end{bmatrix} \begin{bmatrix} f_1 \\ f_2 \end{bmatrix} \tag{66}$$

If the second state (the fast state) is eliminated from Eq. (66) then the reduced model is

$$\begin{aligned} \ddot{q}_1 &= 5\, q_1 + .06\, f_1 + 0.043\, f_2 \\ q_2 &= .0032\, f_1 - .00128\, f_2 \end{aligned} \tag{67}$$

Assuming $f_1 = f_2 = 0$ and $q_{1,2}(0)$ are the only initial conditions on the mode state ($\dot{q}_1(0) = \dot{q}_2(0) = 0$) then since $\underline{x} = L^{-1}\Phi\underline{q}$ the solution to Eq. (67) gives $x_1(t)$ as

$$x_1(t) = .06\, q_1(0) \cos \sqrt{5}\, t \tag{68}$$

whereas the solution to Eq. (66) gives $x_1(t)$ as

$$x_1(t) = .06\, q_1(0) \cos \sqrt{5t} + .08\, q_2(0) \cos 5t \tag{69}$$

If $x_1(0) = 1$ then Eq. (68) and Eq. (69) can be compared. Figure 27 shows such a comparison, and as can be seen the reduced solution Eq. (68) never converges to the actual solution Eq. (69).

The solution to this problem is to formulate the order reduction as a "weak" convergence. The best way to achieve this is to use the control performance measure as the criteria. Thus, if the performance measure for the original system is

$$J = \int_0^\infty \left\{ \begin{bmatrix} \underline{x} \\ \dot{\underline{x}} \end{bmatrix}^T Q \begin{bmatrix} \underline{x} \\ \dot{\underline{x}} \end{bmatrix} + \underline{u}^T \underline{u} \right\} dt \tag{70}$$

then an approximate J is obtained by using a transformation based on diagonalization of the cost matrix associated with Eq. (70). The benefit of such a weak

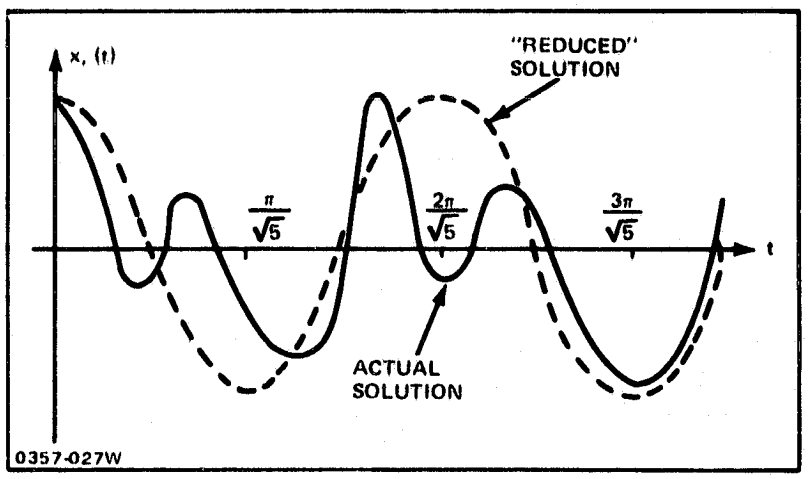

Fig. 27 Comparison of Solutions to Reduced and Full State Dynamic Models

order reduction is two fold:

1. Periodicity in discarded modes may be handled.
2. The closed loop dynamics are used as a criteria for reduction in order.

The first use of this form of order reduction was by Meier in Ref. 10.

2. ORDER REDUCTION IN THE WEAK SENSE

The procedure we have developed for reducing the order of a dynamic system accounts for all of the objections that were raised in Section III-1. Firstly, the reduction in order utilizes the performance index as a criteria for determining the order reduction so that periodic motions in any particular discarded state do not cause problems in the singular perturbation. Second, the procedure uses the closed loop dynamics. Thus if a high gain system is required the order reduction will account for that fact by retaining the "faster" modes in the open loop dynamics that are normally discarded. This second step is a significant departure from the order reduction described in Refs. 11 and 12.

The procedure for order reduction differs from singular perturbation techniques based on the dynamics of the system where the highest derivatives of the fastest states are permitted to go to zero (Refs. 2, 13 and 14). In that case, convergence of the reduced model solution to the solution of the full order system occurs in an absolute sense. In our case the quadratic performance measure is used to determine the order reduction so that convergence is in the "weak sense".

To develop the reduction procedure, we start with the open loop dynamics (i.e., $\underline{u} = 0$)

$$\dot{\underline{x}} = A\,\underline{x} \quad ; \quad \underline{x}(0) = \underline{x}_o \tag{71}$$

and

$$J = \int_{t_o}^{T} \underline{x}^T Q\,\underline{x}\; dt \tag{72}$$

Since $\underline{x}(t) = \Phi(t-t_o)\ \underline{x}(t_o)$

$$J = \underline{x}^T(t_o) \int_{t_o}^{T} \Phi^T(t-t_o)\ Q\ \Phi(t-t_o)\ dt\ \underline{x}(t_o) \tag{73}$$

or

$$J = \underline{x}_o^T\ P(T-t_o)\ \underline{x}_o$$

where $P(T-t_o)$ satisfies the differential equation

$$\frac{dP(t)}{dt} = A^TP + PA + Q \tag{74}$$

which is simply obtained from differentiating Eq. (73) and using the fact that Φ and A commute. If $T \to \infty$, then the steady state solution, P_∞, of Eq. (74) satisfies

$$A^TP_\infty + P_\infty A + Q = 0 \tag{75}$$

The solution to the equation (75) is best developed by diagonalizing A (assuming A can be diagonalized). Thus, if T is the matrix of right eigenvectors, then

$$T^{-1}\ A\ T = \Lambda$$

and if we premultiply Eq. (75) by T^T and postmultiply by T, then

$$T^TAT^{-T}T^TP_\infty T + T^TP_\infty T\ T^{-1}AT + T^TQT = 0$$

or

$$\Lambda T^TP_\infty T + T^TP_\infty T\Lambda + T^TQT = 0$$

and if $\tilde{P} = T^TP_\infty T$ and $\tilde{Q} = T^TQT$, then $\tilde{P}$ is easily seen to be given by

$$\tilde{p}_{ij} = \tilde{q}_{ij}/(\lambda_i + \lambda_j)$$

Thus, $P_\infty = T^{-T}\ \tilde{P}\ T^{-1}$ can be determined by using the eigenvalues and eigenvectors of the matrix A.

The matrix P_∞ is symmetric, hence it is diagonalized by an orthonormal matrix S, i.e.,

$$\Delta = \begin{bmatrix} \delta_1 & 0 & \cdots & 0 \\ 0 & \delta_2 & \cdots & 0 \\ \vdots & \vdots & & \vdots \\ 0 & 0 & \cdots & \delta_n \end{bmatrix} = SP_\infty S^T \tag{76}$$

where $\delta_1 \geq \delta_2 \geq \cdots \geq \delta_n$

The order reduction that is now proposed is based on the eigenvalues of the matrix developed in Eq. (76). The reasoning is that the eigenvalues of Eq. (76) specify the amount of control that is important as each of the initial conditions $\underline{x}_o$ are perturbed, and are therefore a good measure of the effect of the control in terms of the desired performance. Obviously the above derivation depends only on the initial conditions, since the control was assumed to be zero. When the control is non zero, the same analysis may be used if one assumes that the control is linear.

$$\dot{\underline{x}} = (A + B K)\, \underline{x} \quad ; \quad \underline{x}(0) = \underline{x}_o \tag{77}$$

The last piece we need before the order reduction algorithm is derived is the fact that the closed loop dynamics, when the gain is known, can be put into the form of Eq. (71) and Eq. (72).

As the first step in the order reduction procedure, assume that the desired performance has been translated into the quadratic perforamnce measure

$$J = \int_o^\infty (\underline{x}^T Q \underline{x} + \underline{u}^T R \underline{u})\, dt \tag{78}$$

and that the control is known and given by $\underline{u} = K\underline{x}$. Then Eq. (78) becomes

$$J = \int_o^\infty \underline{x}^T (Q + K^T R K)\, \underline{x}\, dt \tag{79}$$

If K is a stable gain in the full state system ($\underline{x}$ is a dimension n, which is large, and we desire to find a reduced order model), then the goal is to find a smaller dimension approximation such that the value of Eq. (79) is approximately the same for both the full state and reduced state system.

Following Eq. (75), the value of the cost matrix P_∞ for Eq. (79) is given by $T^{-T}\tilde{P}T^{-1}$ where

$$\tilde{P}_{ij} = [\tilde{q}_{ij}/(\lambda_i + \lambda_j)] \tag{80}$$

and where

$$\tilde{Q} = T^T(Q + K^TRK)T$$

T is the matrix which diagonalizes A + BK

λ_i are the closed loop eigenvalues i = 1, ..., n.

This matrix is symmetric and hence can be diagonalized as in Eq. (76) so

$$P_\infty = S \Delta S^T \tag{81}$$

where

$$SS^T = S^TS = I$$

In Eq. (81) let us partition P_∞ in blocks of dimension m and n-m as follows:

$$P_\infty = \begin{bmatrix} P_{11} & P_{12} \\ P_{12}^T & P_{22} \end{bmatrix}$$

where P_{11} is m x m

P_{12} is m x n-m

P_{22} is n-m x n-m

m is the order of the reduced model which is specified based on the error introduced by the order reduction.

Thus, from Eq. (81) we get

$$\begin{bmatrix} S_{11} & S_{12} \\ S_{21} & S_{22} \end{bmatrix}^T \begin{bmatrix} P_{11} & P_{12} \\ P_{12}^T & P_{22} \end{bmatrix} = \begin{bmatrix} \Delta_{11} & 0 \\ 0 & \Delta_{22} \end{bmatrix} \begin{bmatrix} S_{11} & S_{12} \\ S_{12}^T & S_{22} \end{bmatrix} \tag{82}$$

or $S_{11}^T P_{11} + S_{21}^T P_{12}^T = \Delta_{11} S_{11}^T$; $S_{11}^T P_{12} + S_{21}^T P_{22} = \Delta_{11} S_{21}^T$

and $S_{12}^T P_{12} + S_{22}^T P_{22} = \Delta_{22} S_{22}^T$; $S_{12}^T P_{11} + S_{22}^T P_{12}^T = \Delta_{22} S_{12}^T$

By the way in which the eignevalues δ_i were ordered in Δ, the eignevalues in Δ_{22} are small compared to those in Δ_{11}. If these eigenvalues are of order ε then from Eq. (82) as $\varepsilon \to 0$ (the magnitude of ε that is "considered small" in fact will determine m)

$$S_{12}^T P_{12} + S_{22}^T P_{22} = 0$$

or

$$P_{22} = -S_{22}^{-T} S_{12}^T P_{12} \tag{83a}$$

and

$$S_{12}^T P_{11} + S_{22}^T P_{12}^T = 0$$

so

$$P_{12} = -P_{11}^T S_{12} S_{22}^{-1} \tag{83b}$$

which gives

$$P_{22} = S_{22}^{-T} S_{12}^T P_{11} S_{12} S_{22}^{-1} \tag{83c}$$

since P_{11} is symmetric.

The cost matrix P, from Eq. (83) is therefore

$$P = \begin{bmatrix} P_{11} & -P_{11} S_{12} S_{22}^{-1} \\ -S_{22}^{-T} S_{12}^T P_{11} & S_{22}^{-T} S_{12}^T P_{11} S_{12} S_{22}^{-1} \end{bmatrix} \tag{84}$$

$$P = \begin{bmatrix} I \\ -S_{22}^{-T} S_{12}^{T} \end{bmatrix}^{T} P_{11} \begin{bmatrix} I \\ -S_{22}^{-T} S_{12}^{T} \end{bmatrix}^{T} \qquad (84) \text{ (con't)}$$

When the initial conditions are Gaussian zero mean with covariance Q_o, then

$$E\{J\} = tr\{PQ_o\}$$

$$= tr\{P_{11} Q_{o_{11}} + P_{12} Q_{o_{21}} + P_{21} Q_{o_{12}} + P_{22} Q_{o_{22}}\}$$

Thus, we assume that $\underline{x}_2 = -S_{22}^{-T} S_{12}^{T} \underline{x}_1$, where $(\underline{x}_1, \underline{x}_2)$ is a partition of the state $\underline{x}$ into an m dimensional reduced order subset $(\underline{x}_1)$ and an n-m dimensional "residual" subset which are now a linear combination of $\underline{x}_1$. Using this definition,

$$\underline{x} = \begin{bmatrix} \underline{x}_1 \\ -S_{22}^{-T} S_{12}^{T} \underline{x}_1 \end{bmatrix} = \begin{bmatrix} I \\ -S_{22}^{-T} S_{12}^{T} \end{bmatrix} \underline{x}_1 \qquad (85)$$

so when $\underline{x}$ is used in Eq. (79),

$$J = \int_o^\infty \underline{x}^T (Q + K^T R K) \underline{x} \, dt =$$

$$\int_o^\infty \underline{x}_1^T \begin{bmatrix} I \\ -S_{22}^{-T} S_{12}^{T} \end{bmatrix}^{T} (Q + K^T R K) \begin{bmatrix} I \\ -S_{22}^{-T} S_{12}^{T} \end{bmatrix} \underline{x}_1 \, dt \qquad (86)$$

The state variable model for $\underline{x}_1$ is given by substituting Eq. (85) into Eq. (79), thus if we call the closed loop state matrix F and partition it as:

$$(A + BK) = \begin{bmatrix} F_{11} & F_{12} \\ F_{21} & F_{22} \end{bmatrix}$$

where F_{11} is m x m

F_{22} is n-m x n-m

then

$$\dot{\underline{x}}_1 = F_{11}\,\underline{x}_1 - F_{12}S_{22}^{-T}S_{12}^{T}\underline{x}_1 \quad ; \qquad \underline{x}_1(0) \quad \text{as before} \tag{87a}$$

and

$$\dot{\underline{x}}_2 = (F_{21} - F_{22}S_{22}^{-T}S_{12}^{T})\underline{x}_1 \quad ; \qquad \underline{x}_2(0) = -S_{22}^{-T}S_{12}^{T}\,\underline{x}_1(0) \tag{87b}$$

are the reduced order state variable models. Since we have assumed $\underline{x}_2(0) = -S_{22}^{-T}S_{12}^{T}\underline{x}_1(0)$, the performance measure becomes

$$J = \int_0^\infty \underline{x}^T (Q + K^T R K)\underline{x} \quad dt$$

$$= \underline{x}_o^T P\, \underline{x}_o$$

$$= \underline{x}_1^T(0) \begin{bmatrix} I \\ -S_{22}^{-T}S_{12}^{T} \end{bmatrix}^T P \begin{bmatrix} I \\ -S_{22}^{-T}S_{12}^{T} \end{bmatrix} \underline{x}_1(0) \tag{88}$$

which, if $\varepsilon \to 0$ becomes:

$$\underline{x}_1(0)^T[I + S_{12}S_{22}^{-1}S_{22}^{-T}S_{12}^{T}]\, P_{11}[I + S_{12}S_{22}^{-1}S_{22}^{-T}S_{12}^{T}]\underline{x}_1(0) \tag{89}$$

Comparing Eq. (89) with Eq. (84), the order reduction implied by Eq. (85) gives the same performance measure as results when the small terms in the cost matrix are zero ($\varepsilon \to 0$).

To develop the series expansion in ε for the cost measure requires an expansion of Eq. (86) as a function of ε. The result of such an expansion will give an indication of the error introduced by the truncation. This was not done during this contract and is one of the issues that should be pursued.

The reduced model Eq. (87a) where $\underline{u}$ is not $K\underline{x}$ is given by

$$\dot{\underline{x}}_1 = (A_{11} - A_{12}S_{12}S_{22}^{-1})\,\underline{x}_1 + B_1\,\underline{u}$$

$$J = \int_0^\infty \{\underline{x}_1^T \begin{pmatrix} I \\ -S_{22}^{-T}S_{12}^{T} \end{pmatrix}^T [Q] \begin{pmatrix} I \\ -S_{22}^{-T}S_{12}^{T} \end{pmatrix} \underline{x}_1 + \underline{u}^T R\, \underline{u}\ \}\ dt \tag{90}$$

which gives the reduced order optimal control problem. The control $\underline{u}$ is given by $u = K_r \underline{x}_1$ where K_r is the reduced order gain given by

$$K_r = - R^{-1} B_1^T P_\infty \quad ; \quad \underline{u} = K_r \underline{x}_1 \quad ; \tag{91}$$

and

$$0 = (A_{11} - A_{12} S_{22}^{-T} S_{12}^T)^T P_\infty + P_\infty (A_{11} - A_{12} S_{22}^{-T} S_{12}^T) + \begin{bmatrix} I \\ -S_{22}^{-T} S_{12}^T \end{bmatrix}^T Q \begin{bmatrix} I \\ -S_{22}^{-T} S_{12}^T \end{bmatrix} + P_\infty B R^{-1} B^T P_\infty \tag{92}$$

The gain Eq. (91) is an m x p matrix, which may be used in Eq. (79) to evaluate the performance of the complete n state system as follows:

Let E_m be the n x m matrix given by

$$E_m = \begin{bmatrix} I_m \\ 0_{n-m \times m} \end{bmatrix}$$

then

$\underline{x}_1 = E_m^T \underline{x}$ so Eq. (79), with the gain K_r becomes

$$J = \int_0^\infty \underline{x}^T \{Q + E_m K_r^T R K_r E_m^T\} \underline{x} \, dt \tag{93}$$

Obviously, all of the steps leading to the reduced model Eq. (87) can be performed using Eq. (93) instead of Eq. (79) with $\underline{u} = K_{r-1} x_1 = K_r E_m^T \underline{x}$. There is no reason, on the first iteration, that the resulting state matrix F in Eq. (87) will be the same. Thus, we must iterate on the gain K_r and the reduced model $(F_{11} - F_{12} S_{12} S_{22}^{-1})$ until the result of two iterations gives the same F. When this occurs, the reduced model will have been determined along with the optimal gain that accompanies the dynamic model.

Figure 28 shows the iteration that is described above for the case where $M\ddot{x} + Kx = f$ are the dynamics (corresponding to the finite element model). The matrix A is then (formally) given by

$$\frac{d}{dt}\begin{bmatrix} x \\ \dot{x} \end{bmatrix} = \begin{bmatrix} 0 & I \\ -M^{-1}K & 0 \end{bmatrix}\begin{bmatrix} x \\ \dot{x} \end{bmatrix} + \begin{bmatrix} 0 \\ M^{-1}B \end{bmatrix} f \tag{94}$$

3. MODE SPILLOVER

Mode spillover of the control (Ref. 15) refers to the problem that when an actuator is placed on a physical structure, it excites all of the structural modes. This can be minimized if the actuator is constrained to move slowly relative to some defined high frequency. The problem is how to limit the control bandwidth without adversely affecting the response.

Because an optimal control design has a $1/\omega$ characteristic (see Ref. 7) for large frequencies, the fundamental theorem due to Bode is satisfied (the requirement of at least 20 db/decade roll-off at the zero decibel crossover). However this 20 db roll-off continues to the higher modal frequencies where an additional $1/\omega$ roll-off in each control channel for high frequencies would be desirable. To achieve an additional 20 db roll-off, an observer is introduced into each control channel. We assume the state to be observed is the feedback gains times the state $[q_1, \dot{q}_1]$. Thus, z the observer state will become the control

$$z \to K \begin{bmatrix} q_1 \\ \dot{q}_1 \end{bmatrix}; \quad z \text{ of dim. } p \tag{95}$$

The observer equation is (where the state variable model here comes from Eq. (42))

$$\dot{z} = F z + G \begin{bmatrix} q_1 \\ \dot{q}_1 \end{bmatrix} + K \begin{bmatrix} 0 \\ 0 \\ I_p \end{bmatrix} u \tag{96}$$

where from the observer constraint equation (the matrix K is the observed linear combination of states)

$$G = K \begin{bmatrix} 0 & I & 0 \\ -\Omega_1^2 & 0 & (\phi_{11}^T \phi_{21}^T) L^{-1} B \\ 0 & 0 & 0 \end{bmatrix} - FK$$

and L is defined in Eq. (17).

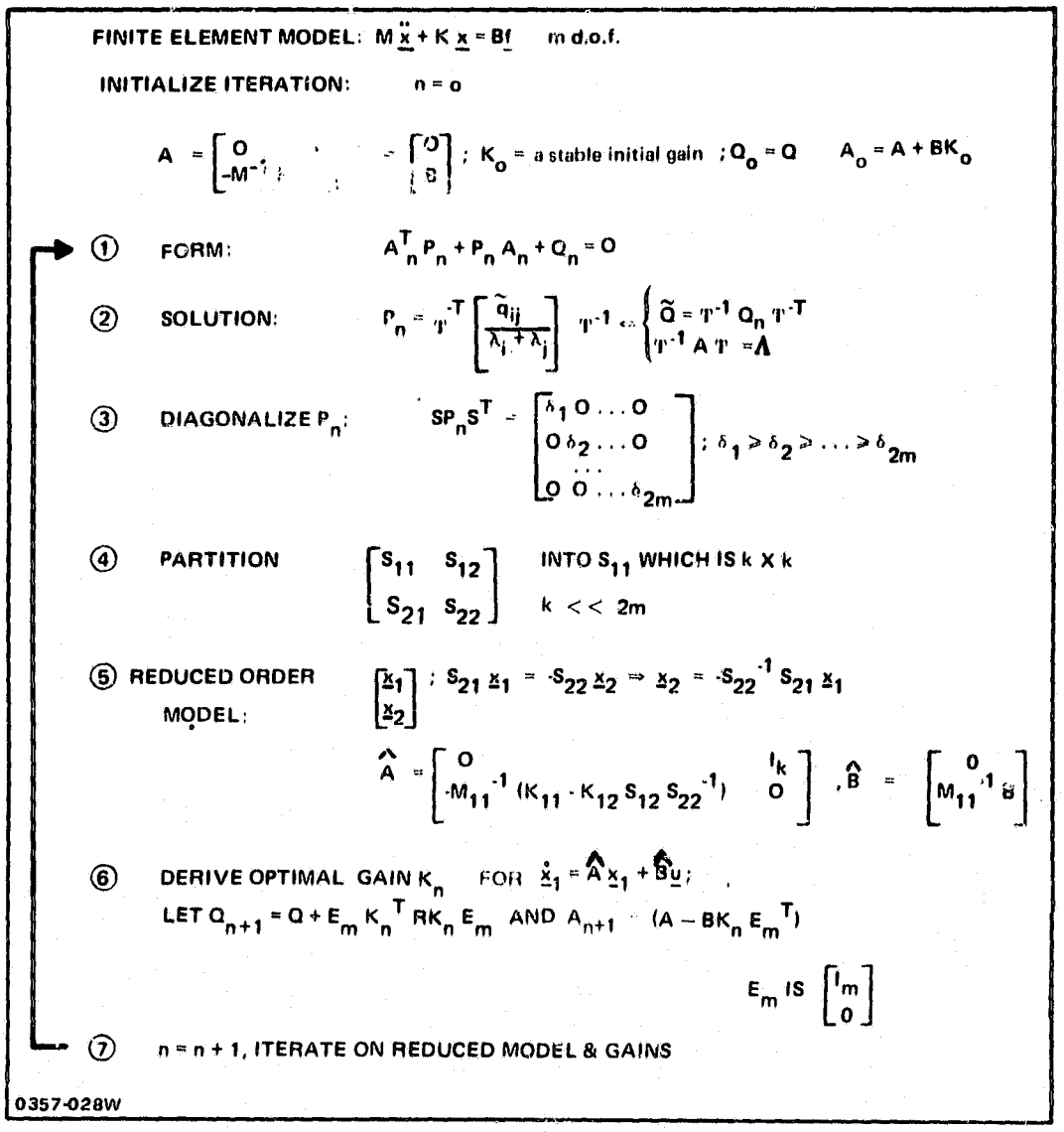

Fig. 28 Order Reduction Algorithm

The selection of the "poles" of the observer (eigenvalues of F) is made in such a way that the Bode criteria is satisfied at the frequency which is the highest frequency retained in the reduced order model and for frequencies beyond that, an additional pole is introduced. The resulting control system appears as shown in Fig. 29. The same transformation used in Section II.6 is used here to provide the modal measurements $\begin{bmatrix} q_1 \\ \dot{q}_1 \end{bmatrix}$ in terms of m coordinates of the structure and their rates.

4. COMMAND GENERATORS FOR SLEWING AND SHAPE CONTROL

The problem of moving a system from one orientation to another may be formulated as a control problem as follows:

> "Given an initial condition $\underline{x}_o$ and a terminal condition $\underline{x}_f$, determine the control $\underline{u}$ such that some performance measure is minimized (such as minimum time, etc.) that also causes the system $\dot{\underline{x}} = A\underline{x} + B\underline{u}$ to move from $\underline{x}_o$ to $\underline{x}_f$."

Most of the problems formulated this way lead to nonlinear control laws which are difficult to compute - particularly when the dimension of $\underline{x}$ is large as it is in the structural control problem. Thus, we have formulated the slew problem in a different way - an approach that allows the use of linear optimal control techniques.

The assumption is made that the command is the output of a linear system with an input that is a step function. Since it is important that slew commands be smooth, the command generator should be such that as many derivatives as possible are zero at $t = 0$ and that near the terminal time of the command ($t = t_f$) the derivatives of the command should all be assymptoically approaching zero. Thus, the command time duration t_f may be selected based on the degree of steady state performance desired (how much motion is tolerable at t_f). A linear system which achieves this level of performance is the approximation to an ideal delay network (Ref. 16) whose transfer function is e^{-sT} where T is the delay time. The transfer function of the approximate system of order N (even) is given by

$$T(s) = \frac{a_o}{a_N s^N + \ldots + a_1 s + a_o}$$

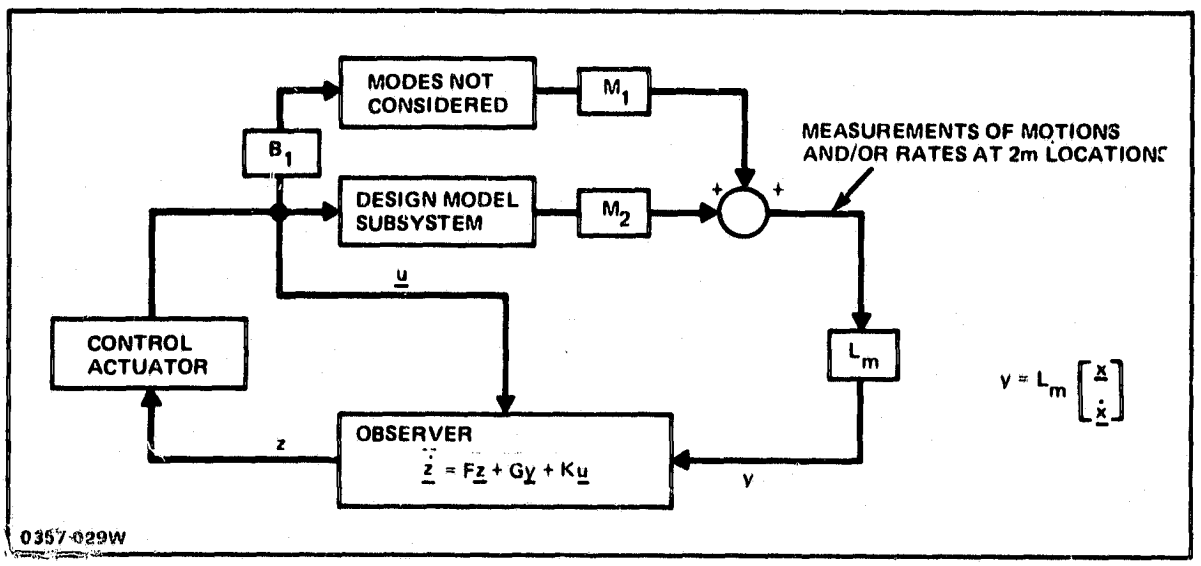

Fig. 29 Control System with Observer to Reduce Spillover of Control

where

$$a_i = \frac{\binom{2N-i}{i}}{2^{N-1}} \qquad \text{and} \qquad \binom{j}{k} = \frac{j!}{(j-k)!k!}$$

By using a partial fraction expansion on T(s), the transfer function becomes

$$T(s) = \frac{b_1}{s-p_1} + \frac{b_1^*}{s-p_1^*} + \ldots + \frac{b_{N/2}}{s-p_{N/2}} + \frac{b_{N/2}^*}{s-p_{N/2}^*} \tag{98}$$

where * denotes complex conjugate, and the state variable form of Eq. (98) is trivially given by ($\underline{x}_c$ is an N vector)

$$\dot{\underline{x}}_c = \begin{bmatrix} p_1 & 0 & 0 \ldots & 0 \\ 0 & p_1^* & 0 \ldots & 0 \\ & \ldots & & \\ 0 & 0 & 0 \ldots & p_{N/2}^* \end{bmatrix} \underline{x}_c + \begin{bmatrix} b_1 \\ b_1^* \\ \vdots \\ b_{N/2}^* \end{bmatrix} u \tag{99}$$

$$y = x_{c_1} + x_{c_2} + \ldots + x_{c_N}$$

The roots of the denominator polynomial in T(s) ($p_1, \ldots, p_{N/2}$ and their conjugates) are not simply described. They are all complex when N is even and they are not clustered along any path in the complex plane (unlike the Butterworth and Tchebyshev filter poles). We rely on the control design calculation to formulate Eq. (99) and calculate p_i, i = 1, ... , N/2. The step response of Eq. (99) (u = 1) is computed by the addition of an N + 1st state variable in Eq. (99). This variable becomes u and since a step has a derivative that is zero, the new form of Eq. (99) is

$$\dot{\underline{x}}_c = \begin{bmatrix} p_1 & 0 & 0 & \ldots & 0 & 0 & b_1 \\ 0 & p_1^* & 0 & \ldots & 0 & 0 & b_1^* \\ & & & \ldots & & & \\ 0 & 0 & 0 & \ldots & p_{N/2} & 0 & b_{N/2} \\ 0 & 0 & 0 & \ldots & 0 & p_{N/2}^* & b_{N/2}^* \\ 0 & 0 & 0 & \ldots & 0 & 0 & 0 \end{bmatrix} \underline{x}_c \quad ; \quad y = [11 \ \ldots \ 10]\underline{x}_c \tag{100}$$

with $\underline{x}_c(0) = [0, 0, \ldots, 0, 1]^T$.

Our computer codes do not use complex arithmetic, so a transformation P is applied to Eq. (100) to make all of the elements real, where P^{-1} is given by

$$P^{-1} = \left[\begin{array}{cc|cc|c|cc|c} 1 & -i & -1 & 0 & & -1 & 0 & 0 \\ 1 & i & -1 & 0 & \cdots & -1 & 0 & 0 \\ \hline & & 1 & -i & & & & 0 \\ \multicolumn{2}{c|}{0} & 1 & i & \cdots & \multicolumn{2}{c|}{0} & 0 \\ \hline \multicolumn{2}{c|}{\cdots} & \multicolumn{2}{c|}{\cdots} & \cdots & \multicolumn{2}{c|}{\cdots} & \cdots \\ \hline \multicolumn{2}{c|}{0} & \multicolumn{2}{c|}{0} & \cdots & 1 & -i & 0 \\ \multicolumn{2}{c|}{} & \multicolumn{2}{c|}{} & & 1 & i & 0 \\ \hline 0 & 0 & 0 & 0 & \cdots & 0 & 0 & 1 \end{array}\right]$$

It is readily verified that P is given by

$$P = \frac{1}{2}\left[\begin{array}{cc|cc|cc|c} 1 & 1 & 1 & 1 & 1 & 1 & \\ i & -i & 0 & 0 & 0 & 0 & \cdots \\ \hline & & 1 & 1 & & & \\ \multicolumn{2}{c|}{0} & & & \multicolumn{2}{c|}{0} & \cdots \\ & & i & -i & & & \\ \hline & & \multicolumn{2}{c}{\cdots} & & & \end{array}\right]$$

In the new coordinate system (through the transformation P), the state equation becomes (where in this equation $p_j = \alpha_j + i\beta_j$; $j = 1, \ldots, N/2$)

$$\dot{\underline{x}}_c = \left[\begin{array}{cc|c|c|c|cc|c} \multicolumn{8}{c}{\overbrace{\qquad\qquad\qquad\qquad\qquad\qquad\qquad\qquad}^{A_c}} \\ \alpha_1 & \beta_1 & (\alpha_2-\alpha_1) & \beta_2 & \cdots & (\alpha_{N/2}-\alpha_{N/2}^{-1}) & \beta_{N/2} & \sum_{j=1}^{N/2} \frac{b_j+b_j^*}{2} \\ -\beta_1 & \alpha_1 & \beta_1 & 0 & \cdots & \beta_1 & 0 & \frac{b_1^*-b_1}{2i} \\ \hline \multicolumn{2}{c|}{\cdots} & \multicolumn{2}{c|}{\cdots} & \cdots & \multicolumn{2}{c|}{\cdots} & \cdots \\ \hline & & & & & \alpha_{N/2} & \beta_{N/2} & \frac{b_{N/2}^*-b_{N/2}}{2i} \\ \multicolumn{2}{c|}{0} & \multicolumn{2}{c|}{0} & \cdots & & & \\ & & & & & -\beta_{N/2} & \alpha_{N/2} & \frac{b_{N/2}^*+b_{N/2}}{2} \\ \hline 0 & 0 & 0 & 0 & \cdots & 0 & 0 & 0 \end{array}\right]$$

and the output is

$$y = [1 \quad 0 \quad 0 \ldots \quad 0] \quad \underline{x}_c \tag{101}$$

A typical set of plots of x_1, x_2, ... x_N when N = 10 is shown in Fig. 4.

The next step in using Eq. (101) to design the control system is the determination of what in the structure is to be commanded. If the rigid body coordinates are the only coordinates to be rotated, then the structural model in the rigid body modes are commanded to follow y in Eq. (101). This is achieved by applying a torque that is the double integral of y since the rigid body motion in modal coordinates is $I\ddot{\theta} = T$. If the rigid body rotational modes in the vector $\underline{q}$ (as introduced in Eq. (20)) are the last three components of $\underline{q}$, then the actual motion of the physical degrees of freedom are given by

$$\underline{x}_D(t) = L^{-T}\Phi^T \begin{bmatrix} 0 \\ \vdots \\ 0 \\ 1 \\ 1 \\ 1 \end{bmatrix} y(t)$$

} three rigid body coordinates are only non zero terms.

where:

$\underline{x}_D(t)$ are the desired motions of physical coordinates in the finite element model ($\underline{x}(t)$ is the original finite element model coordinates)

L and Φ are as in Eq. (20)

y(t) is the output of the command generators above.

The optimal control problem is now modified to cause the actual nodes $\underline{x}$ to follow $\underline{x}_D$ as follows

$$J = \int_0^\infty \{(\underline{x}-\underline{x}_D)^T Q(\underline{x}-\underline{x}_D) + \underline{u}^T R\underline{u}\} \ dt \tag{102}$$

where

$$\underline{x}_D = L^{-1}\Phi^T \begin{bmatrix} 0 \\ \vdots \\ 0 \\ 1 \\ 1 \\ 1 \end{bmatrix} [1 \quad 0 \ldots 0] \quad \underline{x}_c$$

$$\dot{\underline{x}}_c = A_c \underline{x}_c$$

and

$$M\ddot{\underline{x}} + K\underline{x} = B\ u$$

As can be seen, the control solution will consist of a gain matrix multiplying the states $\underline{x}_D$ and $\underline{x}$. Thus the actuator command will be a linear combination of feedbacks from $\underline{x}$ and feed forwards from the command generator $\underline{x}_c$.

5. ON ORBIT TESTING FOR LARGE SPACE STRUCTURES

One of the difficulties encountered when controlling large space structures is that the structural dynamics are not known well enough. If a finite element model of the structure is used to develop the control system, then the typical errors in the mode frequencies and mode shapes that result will lead to a control system that at best does not perform as well as possible and at worst could be unstable. The dilemma is that large space structures cannot be built and tested on the ground -- one must wait until the structure is designed and built in orbit before reasonable testing may begin. The problems of this "on-orbit" dynamic testing is discussed here in terms of a phase locked loop adaptive spectrum analyzer that could provide mode frequencies and mode shapes for control design during the initial orbital operations of a large space structure.

The determination of the structural parameters of a large space structure is almost impossible using ground testing. The influences of gravity, aerodynamic forces and the difficulty in establishing the thermal gradient that will be encountered in orbit all contribute to uncertainties (even when these effects are analytically extracted from the test data). Added to these problems is the impossibility of even assembling the actual structure on the ground so that it maintains its intended shape. Thus it becomes important to consider testing the structure when it is in orbit.

The use of modern control theory to develop control systems for large structures requires that a detailed model of the structure exist. Due to the difficulty with testing the structure on the ground, the control design must be deferred until the system is in orbit and the structural model becomes available. Use of a digital control system is then ideal, because a rigid body low bandwidth controller may be used initially (during dynamic testing). After the control

algorithm is developed using the test data, the original low bandwidth controller may be easily stripped out of memory and replaced with the control system designed using the structural data. Thus, the question becomes one of developing a structural model.

Since the structural frequencies are discrete, a Fourier transform of the output of a sensor mounted on the structure will show discrete lines at the modal frequencies. The use of a spectrum analyzer is thus a possible way of developing a structural model. The problem with this approach is that a decision process must be appended to the output of the spectrum analyzer to allow the discrete mode frequencies to be selected. This decision process must be automated since one would expect to do the dynamic testing periodically to update structural mode data as the structure's properties change.

A natural device for automatically selecting the mode frequencies is a Phase Locked Loop (PLL). This device suffers from some problems when the frequencies of two modes are close together because it will alternately pick out one or the other frequency. In addition, the loops are sensitive to certain noise processes. The characteristics of a PLL are described and a method is introduced that will allow the loop to be better tuned to the characteristics of structural dynamics. The theory for identification of structural parameters that are built into the new phase locked loop, and some results from a simple computer simulation of the loop are also shown below.

The technique we are describing here uses an optimal filter in the loop to tie the loop operation to the known characteritcs of the structural dynamics. Reference 1 is the closest application of such an approach in the literature. There, a Weiner filter is developed to give an optimum filter for a single sinusoid, whereas here a Kalman filter with a frequency identifier is used.

Figure 30 shows a phase lock loop as it is normally configured. The operation of the loop relies on the fact that the result of multiplying two sinusoids is sinusoids at the sum and difference frequency of the two sine waves. Thus if the input sinusoid is $\sin(\omega_i t + \phi)$ and the output of the voltage controlled oscillator (VCO) is $\sin(\omega_o t + \theta)$ the input to the low pass filter is given by

$$E(t) = \sin(\omega_o t+\phi)\cos(\omega_o t+\theta) =$$

$$\tfrac{1}{2}\sin((\omega_o-\omega_o)t+\phi-\theta) + \tfrac{1}{2}\sin((\omega_o+\omega_o)t+\phi+\theta) \qquad (103)$$

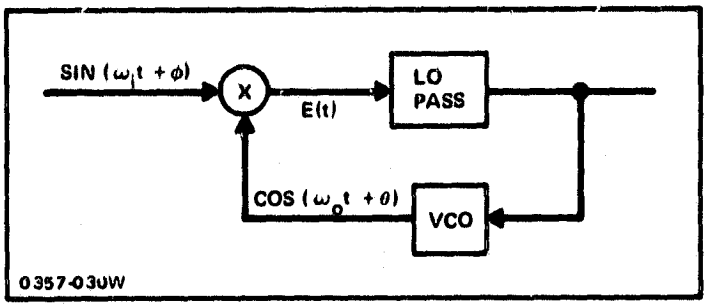

Fig. 30 Phase Lock Loop Block Diagram

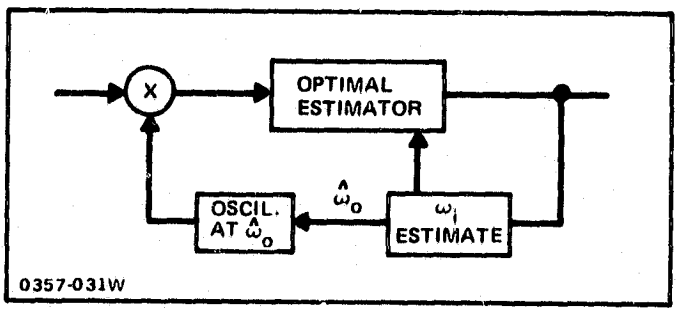

Fig. 31 Modification to Phase Lock Loop to Allow Estimation of Mode Frequencies

and the output of the low pass filter will be the difference frequency component of Eq. (103). The VCO will change frequency following the low frequency term until $\sin\{(\omega_i-\omega_o)t+\phi-\theta\} = 0$ at which point the loop is locked where $\omega_i = \omega_o$ and $\phi = \theta$. The assumption that the input signal is a single sinusoid is crucial to the operation of the phase locked loop. If a second sinusoid with a frequency close to the primary sinusoid exists in the input then the VCO will not stay locked on the primary frequency and will alternate between the two frequencies in a random way.

Figure 31 shows the modification to the basic phase lock loop that was first shown in Ref. 9. The fundamental feature of this loop is that the optimal filter will have a variable bandwidth with multiple notches. The variable bandwidth is a consequence of the convergence of the loop frequency, $\hat{\omega}_o$, to the frequency contained in the signal ω_i. The multiple notches in the estimator comes from the apriori assumption of multiple frequencies in the signal. These two properties overcome the major objections to the use of a PLL for structural frequency determination.

The problem of identification of the coefficients of a linear differential equation may be formulated as a nonlinear filtering problem since the unknown constants may be assumed to satisfy a differential equation where the constant's derivative are zero (Refs. 18 and 19).

For the phase lock loop used to identify the structural mode parameters, the assumption is made that the underlying structural systems is modeled by a finite element model of the form

$$M\ddot{\underline{x}} + K\underline{x} = \underline{f} \tag{104}$$

A series of transformations are used on Eq. (104) to obtain the modal form of Eq. (104) as follows

- Transform from $\underline{x}$ to $\underline{z}$ using the Cholesky factor of the mass matrix M. Thus if L is lower triangular and $LL^T = M$, then defining $\underline{z} = L^T \underline{x}$ and substituting in Eq. (104) gives

$$\ddot{\underline{z}} = - L^{-1}KL^{-T}\,\underline{z} + L^{-1}\,\underline{f} \tag{105}$$

- Transform Eq. (105) to diagonal form using the orthogonal transformation $\underline{q} = \phi^T \underline{z}$ to give

$$\ddot{\underline{q}} = -\Omega^2 \underline{q} + \Phi^T L^{-1} \underline{f} \tag{106}$$

where Ω^2 is a diagonal matrix which has the square of the mode frequencies along its diagonal.

In Eq. (106), each mode satisfies an independent differential equation of the form

$$\ddot{q}_i = -\omega_i^2 q_i + b_{i1} f_1 + \ldots + b_{ip} f_p \tag{107}$$

where the b_{ij} are the terms in the matrix $\Phi^T L^{-1}$.

Let us consider a single mode with p = 1 (i.e., only a single force is applied to the system). Since we are postulating a dynamic test mode, we can use the actuators on the spacecraft to excite the structure one at a time. The unknowns in Eq. (107) then are ω_i^2 and b_{ij}. Since the solution to Eq. (107) is of the form of the sum of sinusoids multiplied by the modal initial condition plus the forcing term, the b_{i1} is a scale factor on the amplitude of the steady state oscillation induced by the force f_1. By adjusting the amplitude of f_1, the coefficient b_{i1} may be made unity. Thus, the only unknown parameter is ω_i^2.

If we write the equation (107) in state variable form, where we further assume ω_i^2 is also a solution of a differential equation we get

$$\frac{d}{dt}\begin{bmatrix} q_i \\ \dot{q}_i \\ \omega_i^2 \end{bmatrix} = \begin{bmatrix} 0 & 1 & 0 \\ -\omega_i^2 & 0 & 0 \\ 0 & 0 & 0 \end{bmatrix} \begin{bmatrix} q_i \\ \dot{q}_i \\ \omega_i^2 \end{bmatrix} + \begin{bmatrix} 0 \\ 1 \\ 0 \end{bmatrix} f_1 + \begin{bmatrix} 0 & 0 \\ \sigma_1 & 0 \\ 0 & \sigma_2 \end{bmatrix} \begin{bmatrix} w_1 \\ w_2 \end{bmatrix} \tag{108}$$

where in Eq. (108) the white noise terms w_1 and w_2 represent the uncertainty in the problem. w_1 is the vibration noise that is exciting the structure and w_2 is used to change the rate of convergence of the estimator (σ_1 and σ_2 are the standard deviations of these noises and is assumed known).

In Eq. (108), since ω_1^2 is a state (the 3rd component of the state vector), the equation is nonlinear. To linearize Eq. (108) and estimate the coefficient ω_i^2, an approximate nonlinear filter described in Ref. 19 is used. This filter, closely related to the extended Kalman filter used in inertial navigators uses terms up to second order in the Taylor series linearization of Eq. (108). The filter uses as a measurement the standard phase lock loop measurement (as in Eq. (103)) thus

$$y_f(t) = \cos \hat{\omega}_i t \; y_j(t) \tag{109}$$

where

$\hat{\omega}_i$ is the estimate of the mode frequency

$y_j(t)$ is the measurement at the physical degree of freedom on the actual structure labeled x_j and is given by

$$y_j(t) = \sum_{i=1}^{\infty} \phi_{ji} \; q_i(t).$$

Since f_1 was adjusted to give unity mode motion, ϕ_{ji} will be the actual amplitude at the frequency ω_i contained in the measurement $y_j(t)$. This means that once the frequency $\hat{\omega}_i$ is at the modal frequency ω_i, the output of the phase loop will be ϕ_{ji}, the mode influence matrix. Thus if a full set of m modes are desired, altogether m measurements with m loops at each measurement point are required (a total of m^2 phase lock loops connected through a single filter) as shown in Fig. 32.

The resulting nonlinear filter is given by

$$\frac{d}{dt}\begin{bmatrix} \hat{q}_i \\ \dot{\hat{q}}_i \\ \hat{\omega}_i^2 \end{bmatrix} = \begin{bmatrix} 0 & 1 & 0 \\ -\hat{\omega}_i^2 & 0 & 0 \\ 0 & 0 & 0 \end{bmatrix} \begin{bmatrix} \hat{q}_i \\ \dot{\hat{q}}_i \\ \hat{\omega}_i^2 \end{bmatrix} + \begin{bmatrix} 0 \\ P_{23} \\ 0 \end{bmatrix} + K\{\cos\hat{\omega}_i t \; y_j(t) - \cos\hat{\omega}_i t \phi_{ji} \hat{q}_i\} \tag{110}$$

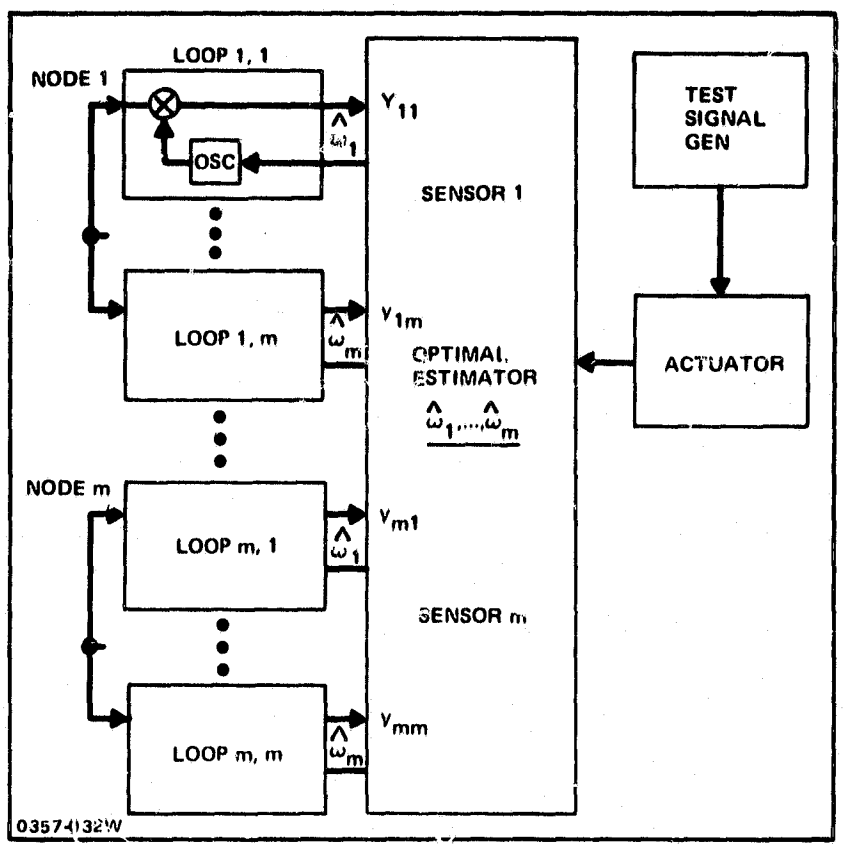

Fig. 32 Multiple Modes Estimated with m^2 Phase Loops and a Single Estimator

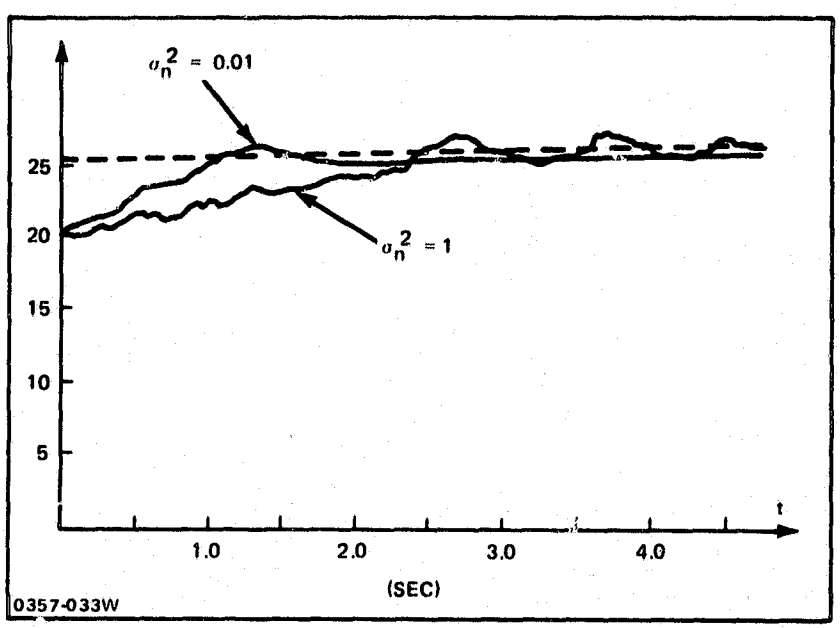

Fig. 33 Estimate of Mode Frequency for a Single Mode. Effect of Noise Variance Assumed for the Measurements (σ_n^2) on the Rate of Convergence.

where P_{23} is the 2,3 element of the estimation error covariance matrix P and K is the "optimal gain" given by

$$K = P \left[\frac{\cos\hat{\omega}_i t}{\sigma_n^2} \quad 0 \quad 0 \right] \tag{111}$$

$$\dot{P} = \begin{bmatrix} 0 & 1 & 0 \\ -\hat{\omega}_i^2 & 0 & 0 \\ 0 & 0 & 0 \end{bmatrix} P + P \begin{bmatrix} 0 & -\hat{\omega}_i^2 & 0 \\ 1 & 0 & 0 \\ 0 & 0 & 0 \end{bmatrix}$$

$$+ \begin{bmatrix} 0 & 0 & 0 \\ 0 & \sigma_1^2 & 0 \\ 0 & 0 & \sigma_2^2 \end{bmatrix} - P \begin{bmatrix} \frac{\cos^2\hat{\omega}_i t}{\sigma_n^2} & 0 & 0 \\ 0 & 0 & 0 \\ 0 & 0 & 0 \end{bmatrix} P \tag{112}$$

where σ_n^2 is the variance of the measurement noise on the sensor that is measuring the physical motion $y_j(t)$.

A single mode system (m = 1 in Eq. (106)) was simulated to determine the operation of the optimal loop filter. The result of estimating the loop frequency is shown in Fig. 33. One of the unique characteristics of this system is the time varying dynamics of the loop filter. As a function of time, the loop filter tends to start out with a high bandwidth which gradually gets smaller as the loop frequency estimate gets better. In the absence of a noise on the coefficient ω_i^2 (i.e., when $\sigma_2 \to 0$) the loop filter bandwidth goes to zero in steady state. Thus the parameter σ_2 can be used to adjust the steady state filter bandwidth.

In practical application each filter will have a variable bandwidth and will have multiple notches (at the frequency of the modes not being estimated). Furthermore, the actual loop frequency, once estimated, will not be changed unless there is some reason to believe the estimates are incorrect. We are currently building a large simulation code that will estimate multiple modes to test the method on a relatively large problem.

6. STRUCTURAL DAMPING IN FINITE ELEMENT MODELING

The finite element model is an approximation to the underlying partial differential equation of the structure it models. As such the full order finite element model is the only vehicle available for verifying the stability and performance of the control system design. Since the low order design model usually has some damping assumed, there actually is a measure of stability imposed on the full order design. This stability is a consequence of the way the damping is introduced, and as such it is important that the control designer understand this modeling.

In order to preserve the mode transformation developed where the damping is assumed zero, the damping matrix that is used to model the damping on the structural degrees of freedom is assumed to be (Ref. 20)

$$C = M \sum_{i=1}^{m} \alpha_i (M^{-1}K)^i \qquad (1'^3)$$

where

- C is the damping matrix (see Eq. (3) in Section III-1)
- M is the mass matrix
- K is the stiffness matrix
- α_i are coefficients which are determined by the amount of damping desired on the various modes
- m is the number of modes in the reduced order model

Using the notation of Section II-3 the diagonalization of the matrix C uses the same transformation that diagonalized K and M. Thus if

$$\underline{q} = \Phi^T L^T \underline{x}$$

where

$$M = LL^T$$

then

$$\phi^T L^{-1} C L^{-T} \phi =$$

$$\sum_{i=1}^{m} \alpha_i \phi^T L^{-1} M \underbrace{(M^{-1}K) \ldots (M^{-1}K)}_{i \text{ terms}} L^{-T} \phi =$$

$$\sum_{i=1}^{m} \alpha_i (\phi^T L^{-1} K L^{-T} \phi) \ldots (\phi^T L^{-1} K L^{-T} \phi) =$$

$$\sum_{i=1}^{m} \alpha_i (\Omega^2)^i =$$

$$\begin{bmatrix} \alpha_1\omega_1^2 + \alpha_2\omega_2^4 + \ldots + \alpha_m\omega^{2m} & 0 & 0 \ldots 0 \\ 0 & \alpha_1\omega_2^2 + \alpha_2\omega_2^4 + \ldots + \alpha_m\omega^{2m} & \ldots 0 \\ \ldots & & \\ 0 & 0 & 0 \ldots \alpha_1\omega_m^2 + \alpha_2\omega_m^2 + \ldots + \alpha_m\omega^{2m} \end{bmatrix} \quad (114)$$

Thus, the transformation $\phi^T L^T$ diagonalizes M and K and therefore also C. To determine $\alpha_1, \alpha_2, \ldots, \alpha_m$, the levels of damping in each mode is determined (i.e., the terms ξ_i $i = 1, \ldots, m$)

Then the equations

$$\xi_i = \frac{\alpha_1\omega_i^2 + \alpha_2\omega_i^4 + \ldots + \alpha_m\omega_i^{2m}}{2\omega_i} \quad i = 1, 2, \ldots, m \quad (115)$$

are solved for $\alpha_1, \ldots, \alpha_m$. This set of equations may be written as

$$\begin{bmatrix} \omega_1^2 & \omega_1^4 & \ldots & \omega_1^{2m} \\ \ldots & & & \\ \omega_m^2 & \omega_m^4 & \ldots & \omega_m^{2m} \end{bmatrix} \begin{bmatrix} \alpha_1 \\ \alpha_2 \\ \vdots \\ \alpha_m \end{bmatrix} = \begin{bmatrix} 2\omega_1\xi_1 \\ 2\omega_2\xi_2 \\ \vdots \\ 2\omega_m\xi_m \end{bmatrix} \quad (116)$$

and hence

$$\begin{bmatrix} \alpha_1 \\ \vdots \\ \alpha_m \end{bmatrix} = V^{-1} \begin{bmatrix} 2\omega_1\xi_1 \\ \vdots \\ 2\omega_m\xi_m \end{bmatrix}$$

where V is the vandemonde matrix of Eq. (116).

Notice that there is now an implicit damping for all of the higher frequency modes, m + 1 to n. These damping coefficients grow with frequency. Since the same transformation applies to the full nth order system, the damping of the higher frequency modes is also given by Eq. (115) where i = m+1, ..., n. Obviously as the frequencies ω get larger, $\xi_1 \to \infty$ which means that these higher frequencies are no longer going to be oscillatory. Thus, if this model is used to verify stability of the control design, an unrealistic damping is actually being used on the modes which are expected to be problems.

IV. SIMPLIFIED DESIGN EXAMPLES

The two mass system of Fig. 26 will be used here to describe the linear discrete time optimal control techniques that were used to develop the control for the OCDA in Section I. This example has most of the features that were needed for the understanding of the larger problem, but it is sufficiently simple that all of the matrices etc., may be written explicitly.

The problem is to control the two mass system using the force f_1 only. Thus, the "finite element" model is

$$\begin{bmatrix} 100 & 0 \\ 0 & 343.8 \end{bmatrix} \begin{bmatrix} \ddot{x}_1 \\ \ddot{x}_2 \end{bmatrix} = - \begin{bmatrix} 1780 & -1780 \\ -1780 & 4194.4 \end{bmatrix} \begin{bmatrix} x_1 \\ x_2 \end{bmatrix} + \begin{bmatrix} f_1 \\ 0 \end{bmatrix} \qquad (117)$$

STEP 1: COMMAND INPUT

Let us assume that the desired response of Eq. (117) is such that the position of the dominant generalized coordinates follows the profile shown below

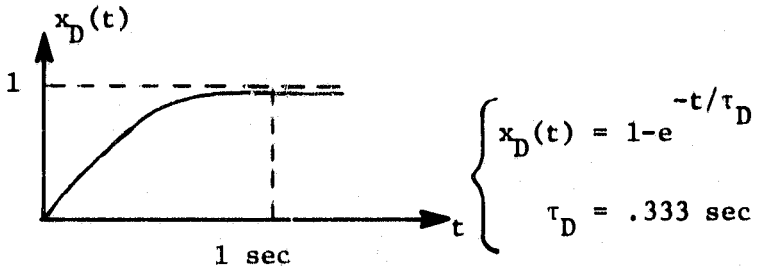

where $x_D(t)$ denotes the desired position of both x_1 and x_2. Clearly, with only one force alplied to mass 1, the positions of masses one and two cannot both be increased from their initial values by 1 unit since, in steady state, if $x_1 = 1$ and $\begin{bmatrix} f_1 \\ 0 \end{bmatrix} = \begin{bmatrix} 1780 & -1780 \\ -1780 & 4194.4 \end{bmatrix} \begin{bmatrix} 1 \\ x_2 \end{bmatrix}$

from Eq. (117) gives $x_2 = \frac{1780}{4194.4}$ and $f_1 = 1780\ (1 - \frac{1780}{4194.4})$. The procedure we described in Section III solves for x_1 and x_2 using a weighted least squares approach so that x_1 and x_2 are both moved approximately the desired one unit.

The motion $x_D(t)$ is imparted to the dominant mode, that is, from Eq. (117)

$$\dot{q}_1 = -5q_1 + .06\, f_1 \tag{118}$$

and since

$$\underline{x} = L^{-T}\underline{z} = L^{-T}\Phi^T q =$$

$$\begin{bmatrix} 0.1 & 0 \\ 0 & 0.054 \end{bmatrix} \begin{bmatrix} 0.6 & 0.8 \\ 0.8 & -0.6 \end{bmatrix} q = \begin{bmatrix} 0.06 & 0.08 \\ .0432 & -.0324 \end{bmatrix} q$$

which gives

$$x_1 = 0.06q_1 \text{ and } x_2 = .0324\, q_1$$

If $q_1(t) = \alpha x_D(t)$, then Eq. (118) gives

$$f_1(t) = \{-\frac{1}{\tau_D^2} e^{-t/\tau_D} + 5(1-e^{-t/\tau_D})\} \alpha/.06$$

$$= \frac{\alpha}{.06} \{5 - (5 + \frac{1}{\tau_D^2}) e^{-t/\tau_D}\} = \{5-14e^{-t/\tau_D}\} \alpha/.06 \tag{119}$$

now the amplitude α of the command x_D can be determined by solving for α such that x_1 and x_2 are as close to 1 (in steady state) as possible. Thus we want to solve

$$[0.06 \quad .0324] \frac{5\alpha}{.06} = [1 \quad 1] \tag{120}$$

which can only be solved in the least squares sense (this is two equations in one unknown) to give (following Section III-4)

$$\frac{5\alpha}{.06} = [0.06 \quad 0.0324] \begin{bmatrix} 1 \\ 1 \end{bmatrix} \Big/ (.06)^2 + (.0324)^2$$

$$= \frac{.06 + .0324}{.0046} = 19.872$$

$$\therefore \alpha = .238 \tag{121}$$

Therefore, the desired motion is

$$x_D(t) = .238\ (1-e^{-t/\tau_D})$$

which may be modeled as the differential equations

$$\dot{x}_D = -1/\tau_D\ x_D + \frac{.238}{\tau_D}$$

$$= -3\ x_D + \varepsilon \tag{122a}$$

$$\dot{s} = 0 \tag{122b}$$

with

$s(o) = .714$

$x_D(o) = 0$

STEP 2: CONTROL AND COMMAND MODEL IN STATE VARIABLE FORM

The combined slew and reduced order model in state variable form can be written in terms of an augmented state variable $\underline{\rho}$ defined as

$$\underline{\rho} = \begin{bmatrix} q_1 \\ \dot{q}_1 \\ x_o \\ s \end{bmatrix} \quad \text{so that} \quad \dot{\underline{\rho}} = \begin{bmatrix} 0 & 1 & 0 & 0 \\ -5 & 0 & 0 & 0 \\ 0 & 0 & -3 & 1 \\ 0 & 0 & 0 & 0 \end{bmatrix} \underline{\rho} + \begin{bmatrix} 0 \\ .06 \\ 0 \\ 0 \end{bmatrix} f_1 \tag{123}$$

where

$$\underline{\rho}(0) = \begin{bmatrix} q_1(0) \\ \dot{q}_1(0) \\ x_o(0) \\ s(0) \end{bmatrix} = \begin{bmatrix} 6\ x_1(0) + 14.81\ \ x_2(0) \\ 6\ \dot{x}_1(0) + 14.81\ \ \dot{x}_2(0) \\ 0 \\ .714 \end{bmatrix}$$

The initial condition on $\underline{\rho}$ is obtained from the fact that $\underline{q} = \Phi^T L^T \underline{x}$.

STEP 3: PERFORMANCE INDEX

The optimal control is required to minimize the difference between the actual response $x_1(t)$, $x_2(t)$ and the desired response $x_{1_D}(t)$ and $x_{2_D}(t)$. Thus, let us assume that we want to minimize

$$J = \int_0^\infty \{[x_1(t) - x_{1_D}(t)]^2 + q[x_2(t) - x_{2_D}(t)]^2 + rf_1^2(t)\}\, dt \qquad (124)$$

The reason this performance measure is over an infinite time interval is that a constant gain system is desired. The only parameters in J are q and r since any multiplier on the first term can be factored out of J (q and r are used to adjust the relative match of x_1 and x_2 with x_{1_D} and x_{2_D} and to adjust the maximum force applied). Since x_1 and x_2 as well as x_{1_D} and x_{2_D} are modeled by the order reduction as functions of q_1, $\dot{q}_1$ and x_D, the performance measure Eq. (124) may be written in terms of ϱ as follows

The vector $\begin{bmatrix} x_1 \\ x_2 \\ x_{1_D} \\ x_{2_D} \end{bmatrix}$ can be written in terms of ϱ using Eq. (118) as

$$\begin{bmatrix} x_1 \\ x_2 \\ x_{1_D} \\ x_{2_D} \end{bmatrix} = \begin{bmatrix} .06 & 0 & 0 & 0 \\ .0324 & 0 & 0 & 0 \\ 0 & 0 & .06 & 0 \\ 0 & 0 & .0324 & 0 \end{bmatrix} \begin{bmatrix} q_1 \\ \dot{q}_2 \\ x_D \\ S \end{bmatrix}$$

But the integrand in Eq. (124) is

$$\begin{bmatrix} x_1 \\ x_2 \\ x_{1_D} \\ x_{2_D} \end{bmatrix}^T \begin{bmatrix} 1 & 0 & -1 & 0 \\ 0 & q & 0 & -q \\ -1 & 0 & 1 & 0 \\ 0 & -q & 0 & q \end{bmatrix} \begin{bmatrix} x_1 \\ x_2 \\ x_{1_D} \\ x_{2_D} \end{bmatrix} + rf_1^2$$

Hence, in terms of the reduced state vector $\underline{\rho}$, J becomes

$$J = \int_0^\infty \left\{ \begin{bmatrix} q_1 \\ \dot{q}_1 \\ x_D \\ S \end{bmatrix}^T \begin{bmatrix} .06 & .0324 & 0 & 0 \\ 0 & 0 & 0 & 0 \\ 0 & 0 & .06 & .0324 \\ 0 & 0 & 0 & 0 \end{bmatrix} \begin{bmatrix} 1 & 0 & -1 & 0 \\ 0 & q & 0 & -q \\ -1 & 0 & 1 & 0 \\ 0 & -q & 0 & q \end{bmatrix} \right.$$

$$\left. \begin{bmatrix} .06 & 0 & 0 & 0 \\ .0324 & 0 & 0 & 0 \\ 0 & 0 & .06 & 0 \\ 0 & 0 & .0324 & 0 \end{bmatrix} \begin{bmatrix} q_1 \\ \dot{q}_1 \\ x_D \\ S \end{bmatrix} + rf_1^2 \right\} dt$$

$$= \int_0^\infty \left\{ \begin{bmatrix} q_1 \\ \dot{q}_1 \\ x_D \\ S \end{bmatrix}^T \begin{bmatrix} (.06)^2+(.0324)^2q & 0 & -(.06)^2-(.0324)^2q & 0 \\ 0 & 0 & 0 & 0 \\ -(.06)^2-(.0324)^2q & 0 & (.06)^2+(.0324)^2q & 0 \\ 0 & 0 & 0 & 0 \end{bmatrix} \right.$$

$$\left. + rf_1^2 \right\} dt \qquad (125)$$

This performance measure, when applied to the reduced order system described in Eq. (118) will cause the control system to be structured as shown in the block diagram on the following page, where K_1, K_2, K_3, K_4 are the gains that are derived to make $f_1 = \underline{K}^T\underline{\rho}$ via the optimal control derivation.

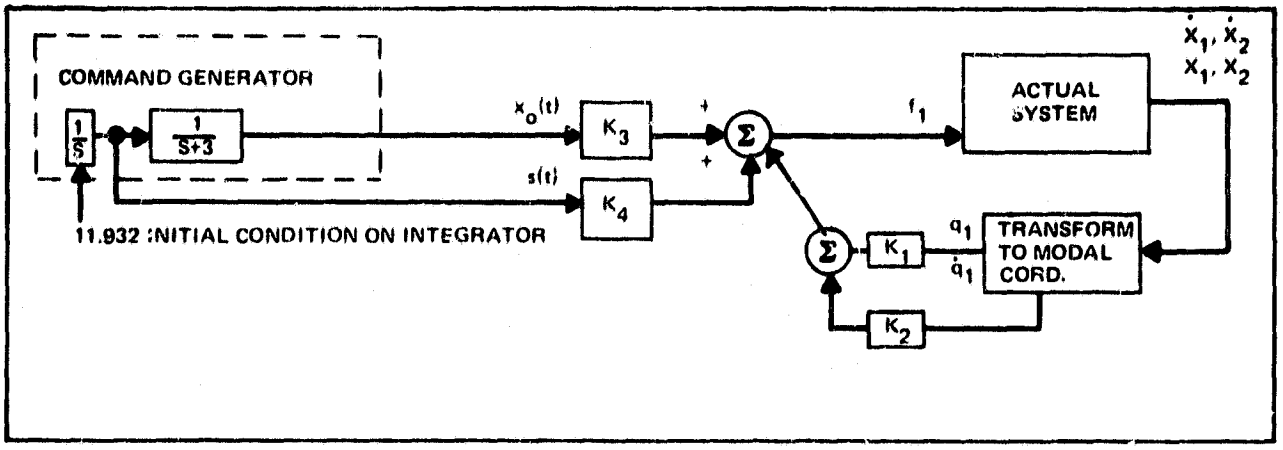

STEP 4: OPTIMAL CONTROL

The steady state optimal control comes from the Riccatti equation

$$\dot{P} = 0 = \underbrace{\begin{bmatrix} P_{11} & P_{12} & P_{13} & P_{14} \\ & & \cdots & \\ P_{14} & P_{24} & P_{34} & P_{44} \end{bmatrix}}_{\gamma} \begin{bmatrix} 0 & 1 & 0 & 0 \\ -5 & 0 & 0 & 0 \\ 0 & 0 & -3 & 0 \\ 0 & 0 & 0 & 0 \end{bmatrix} + \begin{bmatrix} 0 & -5 & 0 & 0 \\ 1 & 0 & 0 & 0 \\ 0 & 0 & -3 & 0 \\ 0 & 0 & 1 & 0 \end{bmatrix} P$$

$$+ \begin{bmatrix} (.06)^2+(.0324)^2 q & 0 & -\gamma & 0 \\ 0 & 0 & 0 & 0 \\ -\gamma & 0 & \gamma & 0 \\ 0 & 0 & 0 & 0 \end{bmatrix}$$

$$- P \begin{bmatrix} 0 & 0 & 0 & 0 \\ 0 & \frac{(.06)^2}{\gamma} & 0 & 0 \\ 0 & 0 & 0 & 0 \\ 0 & 0 & 0 & 0 \end{bmatrix} P \qquad (126)$$

or

$$\left[\begin{array}{cc|cc} (-10p_{12}+\gamma-\beta p_{12}^2) & \cdot & \multicolumn{2}{c}{\multirow{2}{*}{symmetric}} \\ (-5p_{22}+p_{11}-\beta p_{12}p_{22}) & (2p_{12}-\beta p_{22}^2) & & \\ \hline (-5p_{23}-3p_{13}-\gamma-\beta p_{12}p_{23}) & (p_{13}-3p_{23}-\beta p_{22}p_{23}) & (-6p_{33}+\gamma-\beta p_{32}^2) & \cdot \\ (-5p_{24}+p_{13}-\beta p_{12}p_{24}) & p_{14}+p_{23}-\beta p_{22}p_{24} & (-3p_{34}+p_{33}-\beta p_{23}p_{24}) & (2p_{34}+p_{44}^2) \end{array}\right]$$

$$= 0 \qquad (127)$$

where $\gamma = (.06)^2 + (.0348)^2 q$

and $\beta = \dfrac{.06^2}{r}$

This matrix has been partitioned into four 2 x 2 blocks so that the point can be made that the optimal control feedback gains are independent of the feed forward gains. This is obvious in Eq. (127) because the 2 x 2 block in the upper left depends only on p_{11}, p_{12}, and p_{22}, i.e., this block may be determined independent of the other blocks. Since the feedback gains are given by $K = -R^{-1}B^T P_\infty$ and since B is zero everywhere except in those positions corresponding to the upper left most 2 x 2 block of P_∞, the gain also only depends on the elements p_{11}, p_{12}, and p_{22}. Solving Eq. (127) gives the upper 2 x 2 block and the feedback gains as:

$$p_{12} = \frac{-5r^2}{.06^2}\left(1 - \sqrt{1+(.06^2/5r)^2\,[.06^2 + .0348^2 q]}\right)$$

$$p_{22} = \frac{\sqrt{2r\,p_{12}}}{.06} \quad ; \quad p_{11} = 5\sqrt{1+(.06^2/5r)^2\,[.06^2 + .0348^2 q]}$$

the control gains are

$$K_1 = 5/.06\left(1 - \sqrt{1 + (.06^2/5r)^2\,[.06^2 + .0348^2 q]}\right) = 5/.06(1-\Delta)$$

$$K_2 = -\sqrt{\frac{2(-K_1)}{.06}} = -\sqrt{10(\Delta-1)}\,/.06$$

Since the mode we have retained is the differential equation

$$\ddot{q}_1 + 5q_1 = .06f_1$$

and since $f_1 = K_1 q_1 + K_2\dot{q}_1$, the closed loop dynamics are given by

$$\ddot{q}_1 - .06 K_2\dot{q}_1 + (5-.06K_1) q_1 = 0$$

or

$$\ddot{q}_1 + \sqrt{10(\Delta-1)}\ \dot{q}_1 + 5\Delta\ q_1 = 0$$

Hence the new undamped natural frequency and damping of this mode becomes

$$\omega = \sqrt{5\Delta}$$

and

$$\xi = \frac{\sqrt{2}}{2}\ \sqrt{\frac{\Delta-1}{\Delta}}$$

Since

$$\Delta = \sqrt{1 + (.06^2/5r)^2\ [.06^2 + .0348^2 q]}\ ,$$

the mode is damped to .707 when q is large relative to r^2, i.e., whenever the control saturation is not important. On the other hand, as r^2 gets large (less and less control authority is permitted relative to q, the mode is less dampled and in the limit no control at all is exercised. Note that as $\Delta \to \infty$, the closed loop undamped natural frequency (ω) increases as the damping gets closer to .707 which is exactly the problem with the order reduction as it was performed because when $\Delta = 5$, the mode retained (q_1) crosses in frequency with the discarded mode (q_2) whose frequency was 25 rad/sec.

To make these points clear, a root locus plot is shown in Fig. 34 that shows the closed loop pole locations of the design as q and r are varied.

The feed forward gains which determine the optimum response to the command such that x_1 and x_2 are as close to 1 in the least squares sense are given by $K_3 = -.06/r\ p_{23}$ and $K_4 = -.06/r\ p_{24}$. From Eq. (127) p_{23} and p_{24} are given by:

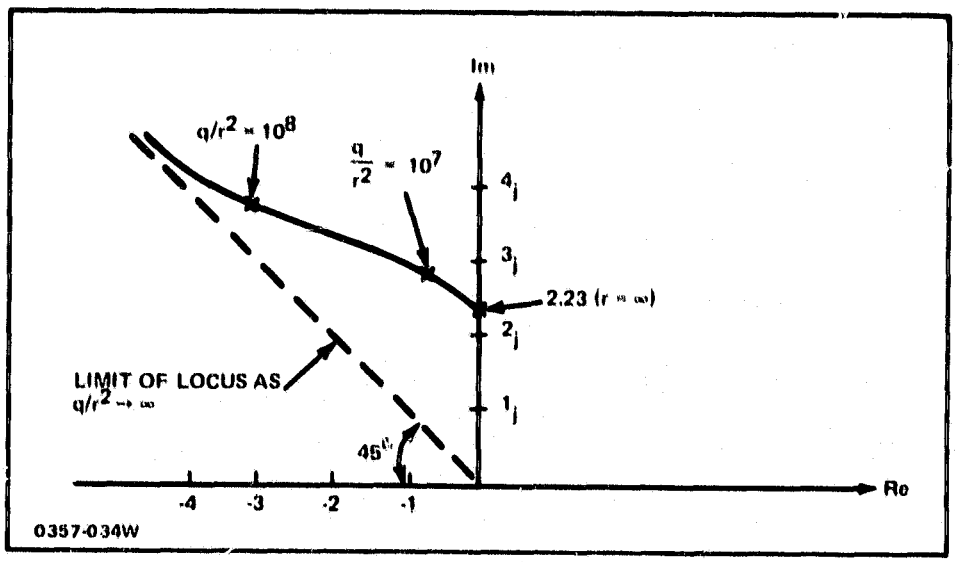

Fig. 34 Root Locus for Mode 1 of Example as Function of q/r^2

$$P_{23} = \frac{-\gamma}{14 + \beta\,(3p_{22} + p_{12})} \qquad K_3 = \frac{\gamma\beta/.06}{14 + \beta\,(3p_{22} + p_{12})}$$

$$P_{24} = \frac{-\gamma(\beta p_{22}+3)}{(\beta p_{12}+5)(14+\,(3p_{22}+p_{12}))} \qquad K_4 = \frac{\gamma\beta/.06\;(\beta p_{22} + 3)}{(\beta p_{12}+5)(3\beta p_{22}+\beta p_{12}+14)}$$

The reuslt of combining the command generator whose block diagram is given by

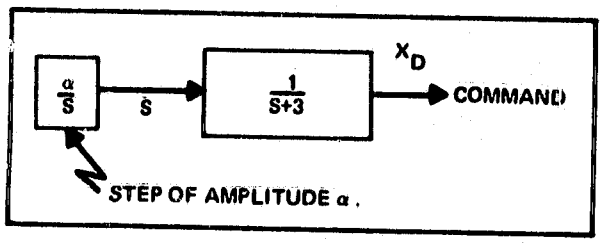

with the feed forward control gains which give a force equal to $K_3x_D + K_4s$ is the following block diagram

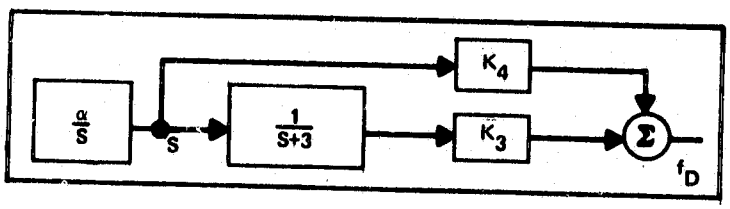

Hence, the transfer function from s to f_D is given by

$$\frac{f_D}{S}(s) = \frac{K_3}{S+3} + K_4 = \frac{K_4\{S+(K_3/K_4+3)\}}{S+3}$$

The last point that must be made is that in implementing the feedback control derived above, the measurements will be on x_1 and x_2, hence since the feedback force is given by

$$f_1 = K\begin{bmatrix} q_1 \\ \dot{q}_1 \end{bmatrix} = [K_1 \quad K_2]\begin{bmatrix} q_1 \\ \dot{q}_1 \end{bmatrix} \tag{128}$$

but since $q_1 = 6x_1 + 14.83\,x_2$ the implementation of this control seems to require four measurements (x_1, $\dot{x}_1$, x_2, and $\dot{x}_2$). Actually, the measurements need only be x_1 and $\dot{x}_1$ as in Eq. (49).

Via a series of simple block diagram manipulations, the above closed loop system becomes

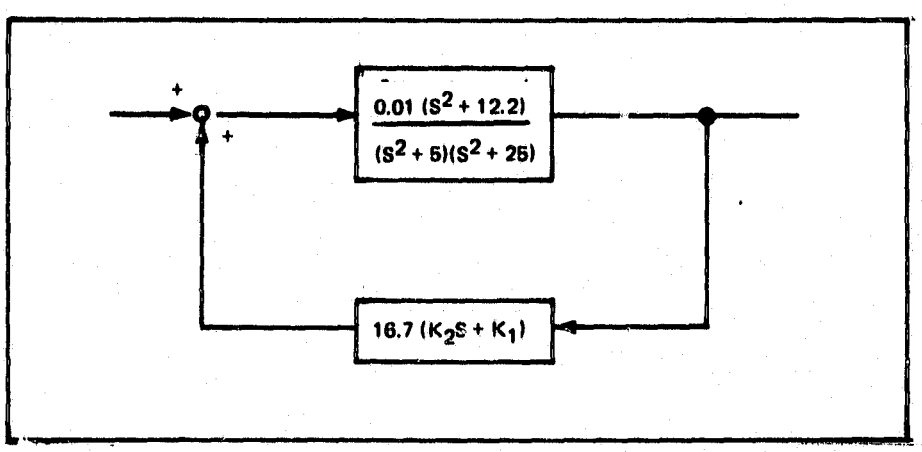

which has a closed loop root locus that is always stable so that, for this problem, no additional stabilization need be done and the problem may be considered complete.

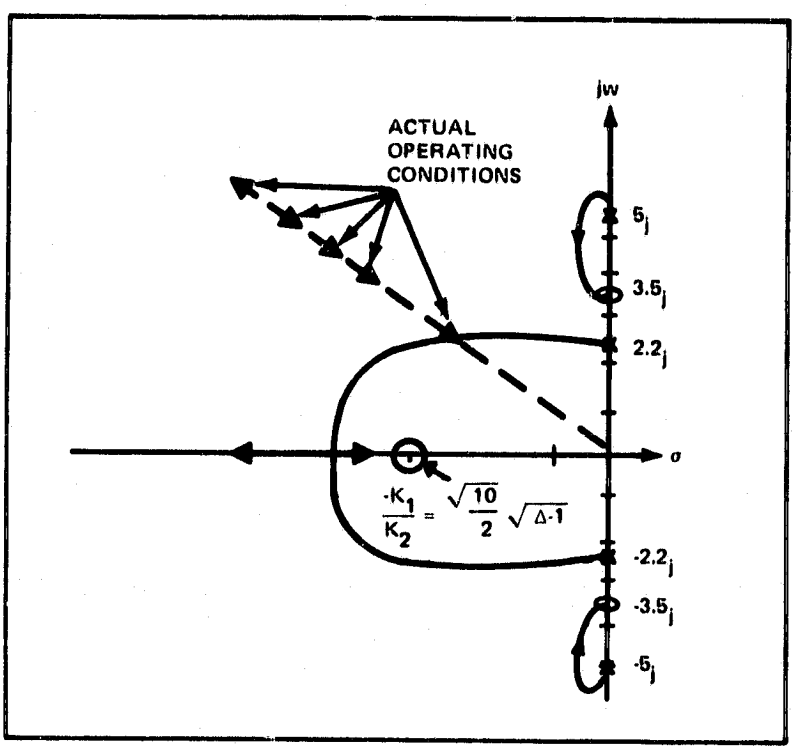

STEP 5: DIGITAL CONTROL

The state variable model Eq. (123) is used to derive a discrete model. Since

$$\underline{x}(t) = \Phi(t-t_o)\ \underline{x}(t_o) + \int_{t_o}^{t} \Phi(t-\tau)\ \underline{b}\ f_1(\tau)\ d\tau$$

if $t = (k+1)\Delta t$ and $t_o = k\Delta t$, then from Eq. (35) the discrete system becomes:

$$\underline{x}_{k+1} = \Phi(\Delta t)\ \underline{x}_k + \int_{o}^{\Delta t} \Phi(x)\ dx\ \underline{b}\ f_1(k\Delta t)$$

where

$$\Phi(\Delta t) = \begin{bmatrix} \cos\sqrt{5}\Delta t & 1/\sqrt{5}\sin\sqrt{5}\Delta t & 0 & 0 \\ -\sqrt{5}\sin\Delta t & \cos\sqrt{5}\Delta t & 0 & 0 \\ 0 & 0 & e^{-3\Delta t} & \frac{1-e^{-3\Delta t}}{3} \\ 0 & 0 & 0 & 1 \end{bmatrix}$$

and

$$\int_0^{\Delta t} \Phi(x)dx\, \underline{b} = \begin{bmatrix} .012(1-\cos\sqrt{5}\Delta t) \\ .027(\sin\sqrt{5}\Delta t) \\ 0 \\ 0 \end{bmatrix} .$$

If the sample time Δt is 1 sec., then

$$\underline{x}_{k+1} = \begin{bmatrix} -.617 & .352 & 0 & 0 \\ -1.76 & -.617 & 0 & 0 \\ 0 & 0 & .0497 & .317 \\ 0 & 0 & 0 & 1 \end{bmatrix} \underline{x}_k + \begin{bmatrix} .019 \\ .021 \\ 0 \\ 0 \end{bmatrix} f_{1_k}$$

This model is used with the discretized performance index to design the optimal digital control.

V. CONCLUSIONS AND RECOMMENDATIONS

This report represents one step on a relatively long road that will provide the technology for designing control systems for large space structures. This technology is of extreme importance for without it, the schemes, ideas and dreams for a large number of space missions will never reach fruition. The work here has demonstrated that control systems may be designed that provide structural and attitude control when the control specifications are not severe. It has also been shown that many of the technology items: structural modeling, modeling of damping, determination of the structural dynamics in orbit, slew command and control spillover, all have an effect on the control solution. One of the significant contributions of this effort is the realization that a control system should exploit the ability to "play" one disturbance off against another. This synoptic design approach can pay very great dividends in the use of actuator fuel and performance. Also a synoptic design is best developed using linear optimal control techniques because of the natural incorporation of disturbances, dynamics of the structures, rigid body torques and command generator dynamics in the design model. If there is one feature that we believe is important in this work it is that the linear optimal control design philosophy has been used throughout the work. The design incorporates the concepts of stability margin, phase margin and in general the robustness properties that are usually considered "classical" but using the terminology and theory of linear optimal control.

Many of the steps taken here are tentative. In particular the "on orbit dynamics test" procedure must be developed so that multiple mode frequencies may be estimated. The order reduction in the weak sense should be attempted on a large problem to demonstrate its effectiveness. Finally, the whole question of Kalman filter sensitivity vs. the gain margin achieved by the introduction of an observer must be resolved.

In the course of this effort, three technical papers were presented. These papers are Refs. 9, 21, and 22.

VI. REFERENCES

1. "Orbital Construction Demonstration Study," Final Report on Contract NAS 9-14916, prepared for Lyndon B. Johnson Space Center, Grumman Aerospace Corporation, June 1977.

2. Kokotvic, P.V., O'Malley, R.C., and Sannuti, P., "Singular Perturbations and Order Reduction in Control Theory - An Overview," Automatica , Vol. 12, pp. 123-132, 1976.

3. Noble, B., Applied Linear Algebra, Wiley, 1972.

4. Kaplan, M.H., Modern Spacecraft Dynamics and Control, Wiley, 1976.

5. Likens, P.W., "A Study of Altitude Control Concepts for Precision Pointing Nonrigid Spacecraft," NASA Report CR-2619, October 1975.

6. Dorato, P. and Levis, A., "Optimal Linear Regulators: The Discrete-Time Case," IEEE Trans. on Automatic Control, Vol. AC-16, No. 6, pp. 613-620, December 1971.

7. Kwakernaak and Sivan, Linear Optimal Control Systems, Wiley, 1972.

8. Berman, H. and Gran, R., "Design Principles for Digital Synthesis," Journal of Aircraft, Vol. 11, pp. 414-422, July 1974.

9. Gran, R., Rossi, M., Moyer, H.G., "Optimal Digital Control of Large Space Structures," AAS Rocky Mountain Conference, March 1978, (also J. of Astr. Sciences , Vol. XXVII, No. 2, April-June 1979, pp. 115-130.)

10. Meier, L. et. al., "Design of Guidance and Control Systems for Optimum Utilization of Information," NASA Contractor Report CR-897, May 1968.

11. Likens, P. and Skelton, R., "Dynamics and Control of Flexible Spacecraft," Notebook for short course given in Los Angeles as AIAA Professional Study Series.

12. Skelton, R., "Some Limitations of Model Reduction and Controller Design Methods for Large Uncertain Dynamical Systems," AAS Rocky Mountain Conference, Keystone, Colorado, March 1978 (to appear in AAS J. op. cit.).

13. Kokotovic, P.V., and Yackel, R.A., "Singular Perturbations of Linear Regulators," IEEE Trans on Automatic Control Vol. AC-17, February 1972, pp. 29-37.

14. Jennings, A., "Mass Condensation and Simultaneous Iteration for Vibration Problems," National J. for Numerical Methods in Eng., Vol. 6, pp. 543-552, 1973.

15. Balas, M., "Active Control of Flexible Systems," AIAA Symposium on Dynamics and Control of Large Flexible Spacecraft, Blacksburg, Virginia, June 1977.

16. Storch, L., "An Application of Modern Network Systhesis to the Design of Constant Time Delay Networks," IRE Convention Record Part 2, pp. 105-117, 1954.

17. Jaffe, R. and Rechtin, E.,"Design and Performance of Phase Lock Circuits Capable of Optimum Perforamnce," IRE Tans. on Inf. Thy., Vol. IT-1, pp. 66-76, March 1955. Also in Phase Locked Loops and Their Applications, IEEE Press, 1977.

18. Koop, R. and Orford, R., "Linear Regression Applied to System Identification for Adaptive Control Systems," AIAA Journal, 1963, pp. 2300-2306.

19. Gran, R., "System Identification Using Approximate Nonlinear Filters," Proceedings of 3rd Symp. on Nonlinear Estimation, San Diego, Calif., 1972.

20. Clough, R.W. and Penzion, J., Dynamics of Structures, McGraw-Hill, p. 336, 1975.

21. Gran, R. and Rossi, M., "Large Space Structures Control: What are the Problems" What are the Solutions?", AIAA Conf. on Large Space Platforms, L.A., Calif., Sept. 1978, Paper No. 78-1688.

22. Gran, R. and Rossi, M., "On-Orbit Testing for Large Space Structures," AIAA 17th Aerospace Sciences Meeting, New Orleans, La., Paper No. 79-0406, Jan. 15-17, 1979.

APPENDIX A

INTRODUCTION OF GRAVITY-GRADIENT AND ROTATION TERMS INTO STRUCTURAL MODELS

As indicated in Figure A-1, the analyzed satellite is represented by a number of lump masses. A typical mass m_k, has a moment-of-inertia matrix $[I_i]$ in the local body axes $\underset{\sim}{x}^{(i)}$. Point 0 is the location of the cm of the satellite, assuming that it traveled in the nominal orbit. This orbit is specified by the user. The user also specifies the initial position of the $\underset{\sim}{Z}$ axes and their constant angular velocity $\{\Omega\}$. These axes rotate at the nominal angular velocity of the satellite (e.g., the orbital rate for earth-pointing satellites) so that motions of the satellite relative to the $\underset{\sim}{Z}$ axes are small. $\{a_i\}$ is the undeformed location of m_i in the $\underset{\sim}{Z}$ axes, and $\{v_i\}$ and $\{\psi_i\}$ are the translational and rotational deformation, respectively, of m_i as observed in the $\underset{\sim}{Z}$ axes. In the undeformed system, all of the $\underset{\sim}{x}^{(i)}$ axes are parallel to the $\underset{\sim}{Z}$ axes.

The equations of motion are

$$[m]\{\ddot{x}\} + [k]\{x\} = \{f\} + \{f_g\} - \{g\} \ , \tag{A-1}$$

where [m] is the system mass matrix,

$$[m] = \begin{bmatrix} m_1 \underset{\sim}{\mid}_3 & & \\ & \ddots & \\ & & m_n \underset{\sim}{\mid}_3 \end{bmatrix} \ , \tag{A-2}$$

(with I_1 and $\underset{\sim}{I}_n$ in the corresponding diagonal blocks)*

where $[\underset{\sim}{\mid}_3]$ is the 3 x 3 identity matrix. In Eq. (1), [k] is the system stiffness matrix, {x} is the deformation vector,

*The tilde under a symbol is used to designate a nonscalar quantity such as a vector, a matrix, or a set of Euler angles.

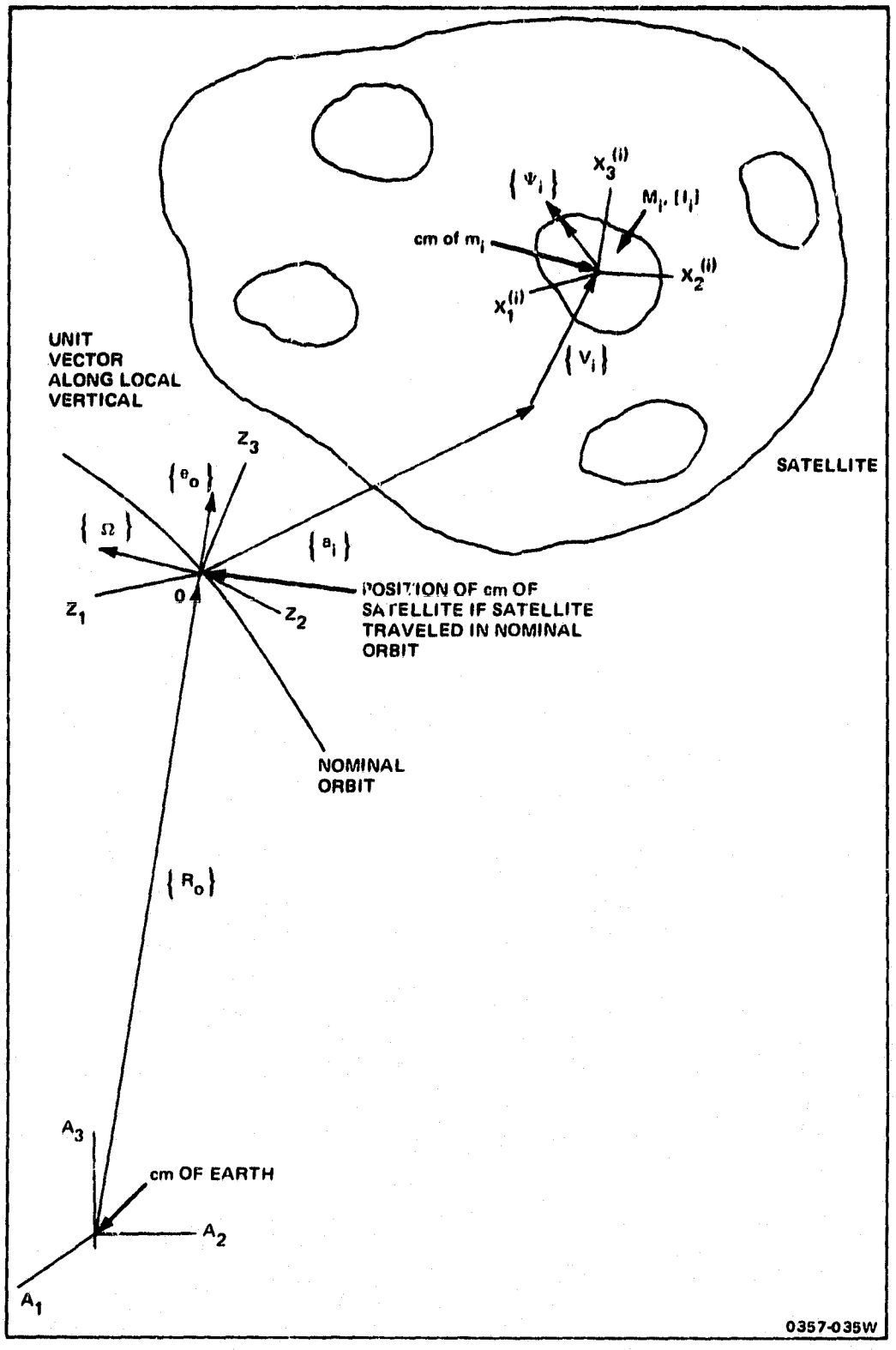

Fig. A-1 Representation of Satellite and Coordinates Used

$$\{x\} = \begin{Bmatrix} \underset{\sim}{v}_1 \\ \underset{\sim}{\psi}_1 \\ \vdots \\ \underset{\sim}{v}_n \\ \underset{\sim}{\psi}_n \end{Bmatrix} , \tag{A-3}$$

{f} contains the forces and torques on the system other than the gravity-gradient and stiffness loads,

$$\{f\} = \begin{Bmatrix} \underset{\sim}{f}_1 \\ \underset{\sim}{t}_1 \\ \vdots \\ \underset{\sim}{f}_n \\ \underset{\sim}{t}_n \end{Bmatrix} , \tag{A-4}$$

$\{f_g\}$ contains the gravity-gradient forces and torques,

$$\{f_g\} = \begin{Bmatrix} \underset{\sim}{F}_{g1} \\ \underset{\sim}{T}_{g1} \\ \vdots \\ \underset{\sim}{F}_{gn} \\ \underset{\sim}{T}_{gn} \end{Bmatrix} , \tag{A-5}$$

and {g} contains the mass times acceleration terms attributable to rotation.

$$\{g\} = \begin{Bmatrix} \underset{\sim}{g}_1 \\ \underset{\sim}{h}_1 \\ \vdots \\ \underset{\sim}{g}_n \\ \underset{\sim}{h}_n \end{Bmatrix} . \tag{A-6}$$

The gravity forces in Eq. (A-5) are expressed in the $\underset{\sim}{Z}$ axes and are

$$\{F_{g_i}\} = - m_i \frac{g_o}{R_o} (\{p_i\} - 3(\{e_o\}^T\{p_i\})\{e_o\}), \qquad (A-7)$$

where g_o is the acceleration of gravity at point 0, and $\{p_i\}$ is the location of m_i in the $\underset{\sim}{Z}$ axes; i.e.,

$$\{p_i\} = \{v_i\} + \{a_i\} \qquad (A-8)$$

The gravity torques in Eq. (A-5) are expressed in the $\underset{\sim}{X}^i$ axes and are

$$\{T_{gi}\} = 3 \frac{g_o}{R_o} [\Gamma(e_i')][I_i]\{e_i'\} \qquad (A-9)$$

where $[\Gamma(\ )]$ is the cross-product function defined in Appendix B, and

$$\{e_i'\} = ([|_3] - [\Gamma(\psi_i)]\{e_o\}) \qquad (A-10)$$

The components in Eq. (A-6) that modify the force equations are expressed in the $\underset{\sim}{Z}$ axes and are

$$\{g_i\} = m_i (2[\Gamma(\Omega)]\{\dot{v}_i\} + [\Gamma(\Omega)]^2\{p_i\}) \qquad (A-11)$$

while the components in Eq. (A-6) that modify the torque equations are expressed in the $x^{(i)}$ axes and are

$$\{h_i\} = [I_i][\Gamma(\Omega)]\{\dot{\psi}_i\} + [\Gamma(\omega_i)][I_i]\{\omega_i\} \qquad (A-12)$$

where $\{\omega_i\}$ is the angular velocity of m_i in the $\underset{\sim}{X}^{(i)}$ axes; i.e.,

$$\{\omega_i\} = \{\dot{\psi}_i\} + ([|_3] - [\Gamma(\psi_i)])\{\Omega\} . \qquad (A-13)$$

Reduction to Modal Form

The modal matrix is arranged as follows:

$$[\phi] = [\underset{\sim}{\phi}^f \ \underset{\sim}{\phi}^t \ \underset{\sim}{\phi}^r] , \qquad (A-14)$$

where $[\phi^f]$ contains the flexible modes, $[\phi^t]$ contains the rigid-body translation modes, viz,

$$[\phi^t] = \begin{bmatrix} \underset{\sim}{I}_3 \\ \underset{\sim}{0}_3 \\ \vdots \\ \underset{\sim}{I}_3 \\ \underset{\sim}{0}_3 \end{bmatrix} , \qquad \text{(A-15)}$$

where $\underset{\sim}{0}_3$ is the 3 x 3 zero matrix. $[\phi^r]$ contains the rigid-body rotation modes, viz,

$$[\underset{\sim}{\phi}^r] = \begin{bmatrix} -\underset{\sim}{\Gamma}(a_1) \\ \underset{\sim}{I}_3 \\ \vdots \\ -\underset{\sim}{\Gamma}(a_n) \\ \underset{\sim}{I}_3 \end{bmatrix} . \qquad \text{(A-16)}$$

With

$$\{x\} = [\phi]\{\xi\} , \qquad \text{(A-17)}$$

the equations of motion in modal form are

$$[M]\{\ddot{\xi}\} + [C]\{\dot{\xi}\} + [K]\{\xi\} = \{\Xi\} . \qquad \text{(A-18)}$$

[M] is the modal-mass matrix,

$$[M] = [\phi]^T[m][\phi] = \begin{bmatrix} \mu_1 & & & & \\ & \mu_2 & & & \\ & & \ddots & & \\ & & & \mu_r & \\ & & & & \underset{\sim}{m}_3 \\ & & & & & \underset{\sim}{I} \end{bmatrix} , \qquad \text{(A-19)}$$

where the μ_i's are the modal masses corresponding to the r flexible modes that are used,

$$\mu_i = \{\phi_i\}^T [m]\{\phi_i\} ; \quad i = 1, \ldots, r, \tag{A-20}$$

m is the total system mass,

$$m = \Sigma\, m_i, \tag{A-21}$$

and [I] is the total moment of inertia of the undeformed vehicle about its cm relative to the $\underset{\sim}{Z}$ axes

$$[I] = \Sigma\, ([I_i] - m_i[\Gamma(a_i)]^2) . \tag{A-22}$$

[K] is the modal-stiffness matrix

$$[K] = [\phi]^T[k][\phi] = \begin{bmatrix} K_1 & & & & \\ & K_2 & & & \\ & & \ddots & & \\ & & & K_r & \\ & & & & \underset{\sim}{0}_6 \end{bmatrix} , \tag{A-23}$$

where

$$K_i = \mu_i\, \omega_i^2 \quad ; \quad i = 1, \ldots, r \tag{A-24}$$

with ω_i equal to the i^{th} flexible frequency. [C] is a modal damping matrix that has been added to the formulation at this step:

$$[C] = \begin{bmatrix} \underset{\sim}{\bar{C}} & \\ & \underset{\sim}{0}_6 \end{bmatrix} . \tag{A-25}$$

$\{\Xi\}$ is the equivalent modal force which contains the coriolis and centrifugal reverse-acceleration forces $-\{g\}$ as well as the physical forces $\{f\} + \{f_g\}$; viz,

$$\{\Xi\} = [\phi]^T(\{f\} + \{f_g\} - \{g\}) \tag{A-26}$$

Motion of Rigid-Body Axes

The modal-displacement vector is partitioned as follows:

$$\{\xi\} = \begin{Bmatrix} \bar{\xi} \\ p \\ \gamma \end{Bmatrix} \tag{A-27}$$

where $\{\bar{\xi}\}$, $\{p\}$, and $\{\gamma\}$ are the flexible, rigid-body translation, and rigid-body rotation coordinates. It can be shown that $\{p\}$ locates the cm of the satellite and satisfies the relations

$$m\{p\} = \Sigma m_i\{p_i\} = \Sigma m_i \{v_i\} = [\phi^t]^T[m]\{x\} \tag{A-28}$$

As indicated in Figure A-2 , $\{p\}$ locates the origin of a set of axes known as the rigid-body (or mean) axes of the satellite, denoted as the x axes, $\{\gamma\}$ orients these axes relative to the z axes. For a given deformed shape of the satellite $\{x\}$,$\{\gamma\}$ may be defined by the relation

$$[I]\{\gamma\} = [\phi^r]^T[m]\{x\} \tag{A-29}$$

The total motion may be decomposed as follows:

$$\{x\} = [\phi^f]\{\bar{\xi}\} + [\phi^t]\{p\} + [\phi^r]\{\gamma\} \tag{A-30}$$

where

$[\phi^f]\{\bar{\xi}\}$ is the flexible motion relative to the rigid-body axes

$[\phi^t]\{p\}$ is the translation of the rigid-body axes

$[\phi^r]\{\gamma\}$ is the rotation of the rigid-body axes

The components of Eq. (A-30) are

$$\{v_i\} = [\phi_i^{ft}]\{\bar{\xi}\} + \{p\} - [\Gamma(a_i)]\{\gamma\} \tag{A-31}$$

$$\{\psi_i\} = [\phi_i^{fr}]\{\bar{\xi}\} + \{\gamma\} \tag{A-32}$$

where $[\phi_i^{ft}]$ is the partition of $[\phi^f]$ corresponding to the translation of m_i, and $[\phi_i^{fr}]$ is the partition of $[\phi^f]$ corresponding to the rotation of m_i. The flexible contributions i. Eq. (A-31) and Eq. (A-32) are called $\{\mu_i\}$ and $\{\theta_i\}$; i.e.,

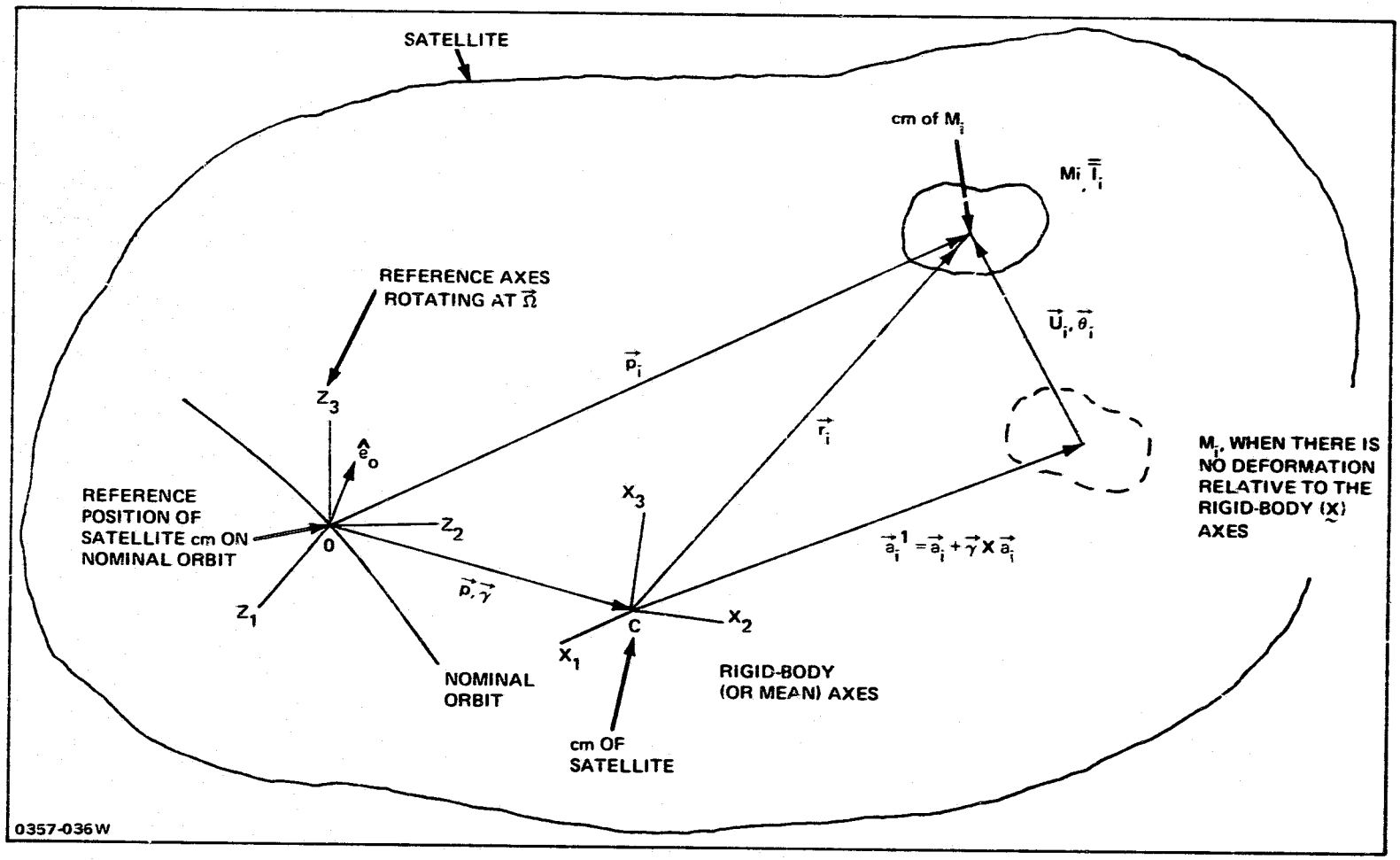

Fig. A-2 Vector Representation of Deformations

$$\{m_i\} = [\phi_i^{ft}]\{\bar{\xi}\} \tag{A-33}$$

$$\{\theta_i\} = [\phi_i^{fr}]\{\bar{\xi}\} \tag{A-34}$$

$\{v_i\}$, $\{\psi_i\}$, $\{p\}$, $\{\gamma\}$, $\{u_i\}$, and $\{\theta_i\}$ are expressed in the $\underset{\sim}{Z}$ axes. Figure A-2 shows the components of the motion in vector form. $\vec{a}_i'$ (which locates the undeformed position of m_i as seen by an observer fixed in the x axes) is the vector $\vec{a}_i$ rotated through the angle $\vec{\gamma}$.

The last six equations of the set Eq. (A-18) are the overall equations of motion for the system, i.e., the equations for $\{p\}$ and $\{\gamma\}$. The first three of these equations are

$$m\{\ddot{p}\} = \Sigma\{f_i\} + \{F_g\} - 2m[\Gamma(\Omega)]\{\dot{p}\} - m[\Gamma(\Omega)]^2\{p\} \tag{A-35}$$

where $\{F_g\}$ is the gravity-gradient contribution to the total load; i.e.,

$$\{F_g\} = -\, m\,\frac{g_o}{R_o}\,(\{p\} - 3\,(\{e_o\}^T\{p\})\,\{e_o\}) \tag{A-36}$$

The last three euqtions of Eq. (A-18) are

$$\begin{aligned}[I]\{\ddot{\gamma}\} = \{T_R\} + \{T_g'\} - \Sigma\,(&2m_i[\Gamma(a_i)][\Gamma(\Omega)]\{\dot{v}_i\} \\ &+ m_i\,[\Gamma(a_i)][\Gamma(\Omega)]^2\{p_i\} + [I_i][\Gamma(\Omega)]\{\dot{\psi}_i\} \\ &+ [\Gamma(\omega_i)][I_i]\{\omega_i\})\end{aligned} \tag{A-37}$$

where $\{T_R\}$ is the resultant torque of all of the external loads, other than gravity loads, about the cm that the system would experience if it were rigid, and $\{T_g'\}$ is the contribution to the equation attributable to gravity, i.e.,

$$\{T_g'\} = [\phi^r]^T\,\{f_g\} \tag{A-38}$$

Total Gravity-Gradient Torque on Satellite

$\{T_g'\}$ is an approximation to the total gravity-gradient torque on the satellite; however, it does not include certain effects attributable to vibration. The total gravity torque can be obtained more accurately from the following equation. This torque is expressed in the rigid-body, or $\underset{\sim}{X}$, coordinate system,

$$\{T_g\} = ([|_3] - [\Gamma(\gamma)])\ \Sigma[\Gamma(r_i)]\{F_{gi}\} + \Sigma\ ([|] + [\Gamma(\theta_i)])\{T_{gi}\} \qquad \text{(A-39)}$$

where

$$\{r_i\} = \{p_i\} - \{p\} \qquad \text{(A-40)}$$

$$\{\theta_i\} = \{\psi_i\} - \{\gamma\} \qquad \text{(A-41)}$$

Gravity Constants

For reference, note that

$$g_o = \frac{K_E}{R_o^2} = \frac{R_E^2}{R_o^2}\ g_E \qquad \text{(A-42)}$$

where K_E is the earth's gravitational constant, R_E is the earth's radius, and g_E is the acceleration of gravity at the earth's surface. Equation (A-42) is useful for calculating g_o and K_E.

Particularization to Nominal Circular Orbit

For a circular orbit

$$g_o = \omega_o^2\ R_o \qquad \text{(A-43)}$$

The components of $\{e_o\}$, the unit vector along the local vertical in the $\underset{\sim}{Z}$ axes, are needed for use in several of the equations. In the $\underset{\sim}{A}$ axes s-own in Figure A-3, $\{e_o\}$is called $\{e_o\}_A$ where

$$\{e_o\}_A = \begin{Bmatrix} 0 \\ \cos(\omega_o\ t + \delta) \\ \sin(\omega_o\ t + \delta) \end{Bmatrix} \qquad \text{(A-44)}$$

Then, $\{e_o\}$ in the $\underset{\sim}{Z}$ axes is

$$\{e_o\} = [T(\sigma)](\pi(\beta)]\{e_o\}_A \qquad \text{(A-45)}$$

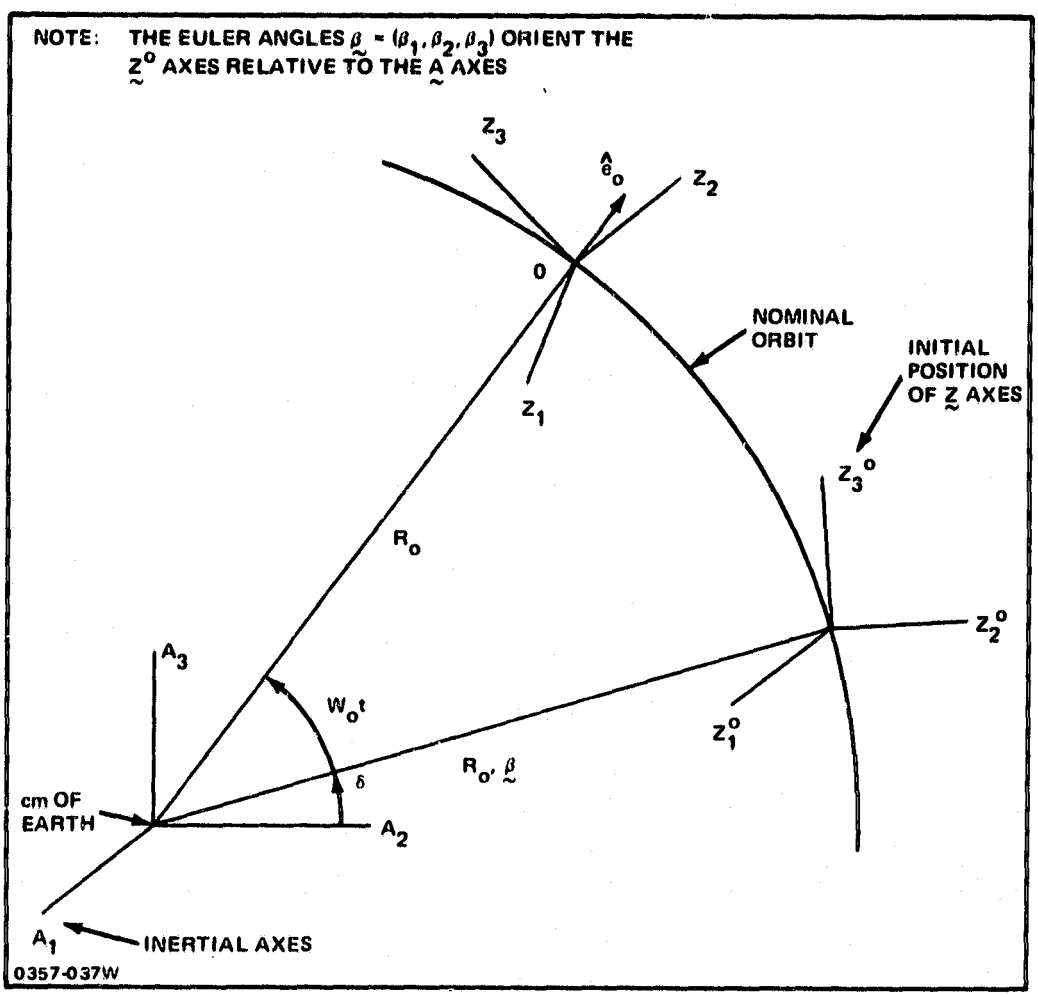

Fig. A-3 Nominal Coordinates Relative to Earth-Centered Coordinates

where $[\pi(\beta)]$ is the coordinate thransformation defined in Appendix B for the Euler angles $\underset{\sim}{\beta} = (\beta_1, \beta_2, \beta_3)$ orienting the $\overset{\circ}{\underset{\sim}{Z}}$ axes relative to the $\underset{\sim}{A}$ axes,

$$\sigma = \Omega\, t \ . \tag{A-46}$$

$\{\Omega\}$ is given in the $\overset{\circ}{\underset{\sim}{Z}}$ axes as

$$\{\Omega\} = \Omega\, \{\eta\}, \tag{A-47}$$

and $[T(\sigma)]$ is the transformation from the $\overset{\circ}{\underset{\sim}{Z}}$ axes to the $\underset{\sim}{Z}$ axes due to a rotation σ about an axis, along $\{\Omega\}$, fixed in space; viz,

$$[T(\sigma)] = \begin{bmatrix} 1-\ell(1-\eta_1^2) & \ell\eta_1\eta_2 + s\eta_3 & \ell\eta_1\eta_3 - s\eta_2 \\ \ell\eta_1\eta_2 - s\eta_3 & 1-\ell(1-\eta_2^2) & \ell\eta_2\eta_3 + s\eta_1 \\ \ell\eta_1\eta_3 + s\eta_2 & \ell\eta_2\eta_3 - s\eta_1 & 1-\ell(1-\eta_3^2) \end{bmatrix} \tag{A-48}$$

where

$$s \equiv \sin\sigma, \quad c \equiv \cos\sigma, \quad \ell \equiv 1-c \tag{A-49}$$

APPENDIX B

DEFINITIONS OF MATRIX FUNCTIONS

Cross-product matrix:

For any vector $x = [x_1\ x_2\ x_3]^T$,

$$[\Gamma(x)] = \begin{bmatrix} 0 & -x_3 & x_2 \\ x_3 & 0 & -x_1 \\ -x_2 & x_1 & 0 \end{bmatrix} \tag{B-1}$$

Euler-angle coordinate transformation:

For any set of ordered rotations $\underset{\sim}{\gamma} = (\gamma_1, \gamma_2, \gamma_3)$ about axes 1, 2, and 3,

$$[A(\gamma)] = \begin{bmatrix} 1 & 0 & 0 \\ 0 & \cos\gamma_1 & \sin\gamma_1 \\ 0 & -\sin\gamma_1 & \cos\gamma_1 \end{bmatrix} \tag{B-2}$$

$$[B(\gamma)] = \begin{bmatrix} \cos\gamma_2 & 0 & -\sin\gamma_2 \\ 0 & 1 & 0 \\ \sin\gamma_2 & 0 & \cos\gamma_2 \end{bmatrix} \tag{B-3}$$

$$[C(\gamma)] = \begin{bmatrix} \cos\gamma_3 & \sin\gamma_3 & 0 \\ -\sin\gamma_3 & \cos\gamma_3 & 0 \\ 0 & 0 & 1 \end{bmatrix} \tag{B-4}$$

The total transformation is

$$[\pi(\gamma)] = [C(\gamma)][B(\gamma)][A(\gamma)] \tag{B-5}$$